EPFL

School of Architecture, Civil and Environmental Engineering (ENAC)
Resilient Steel Structures Laboratory (RESSLab)

Search Commitee, Purdue University
Lausanne, October 29th, 2023

Re: Cover letter for my faculty position application

Dear Search Commitee,

I am delighted to apply for the tenure-track position in structural engineering within the Lyles School of Civil Engineering at Purdue University. Currently, I am a post-doctoral researcher at the Resilient Steel Structures Laboratory (RESSLab) at École Polytechnique Fédérale de Lausanne (EPFL), Switzerland. I successfully defended my PhD thesis in April 2022 under the supervision of Prof. D.Lignos at EPFL, where I received the Outstanding PhD Thesis Distinction in Civil and Environmental Engineering at EPFL. Additionally, I earned my M.Eng in Civil Engineering with summa cum laude honors from National and Technical University of Athens (NTUA).

My research work to date has primarily focused on promoting instability-free design concepts in steel structures under extreme seismic loading. Through advanced computational methods, multi-scale experimentation, and performance-based natural hazards engineering assessment methods, my work has advanced knowledge on the potential use of stable energy dissipation mechanisms for enhanced performance of steel structures. Moreover, I have experience in the reliability of distance-heating piping network via multi-scale experimentation and high-fidelity finite element modeling. In my future academic endeavors, I intend to comprehend the potential damage mechanisms that influence the behavior of materials and structures under extreme loading through physical experimentation across scales. I envision leveraging this knowledge to assess existing deficient structures, aiming to develop solutions to extend their service life and develop innovative low-damage systems that promote the deconstruction and reuse of reclaimed structural elements.

Aside from my research activities, I served as a lecturer of the postgraduate course 'Advanced Steel Design'. I assisted with semester-long projects as part of the graduate courses 'Advanced Steel Design' and 'Structural Stability', while I supervised the research theses of five MSc students. I currently co-supervise a PhD student.

Purdue University offers excellent experimental and computational facilities to conduct research in the general areas of structural and earthquake engineering. I believe that my research background and my teaching and supervising experience, in combination with my eagerness for interdisciplinary and multidisciplinary collaborations with other faculty members at USU, make me a strong candidate for the position.

I would like to take the opportunity to sincerely thank you for considering my application for a faculty position at Purdue University, and I look forward to hearing from you.

Yours sincerely,

Andronikos Skiadopoulos, PhD

École polytecnique fédérale de Lausanne

Dr. Andronikos Skiadopoulos
EPFL ENAC IIC RESSLAB
GC B3 465 (Bâtiment GC)
Station 18
CH–1015 Lausanne

+41 78 751 02 25
andronikos.skiadopoulos@epfl.ch
http://resslab.epfl.ch

Skiadopoulos Andronikos, Ph.D │ Curriculum Vitae

PERSONAL INFORMATION

Date of birth	29.11.1993
Nationality	Greek
Phone	+41 78 751 02 25
E-mail	andronikos.skiadopoulos@epfl.ch
Address	Chemin de l'Ochettaz 16, CH-1025, St-Sulpice, Switzerland
IDs	**Scopus ID**: 57221605864; **ORCHID**: 0000-0002-3813-4325

EDUCATION

05.2022-present	**Postdoctoral Research Fellow, Civil Engineering** École Polytechnique Fédérale de Lausanne (EPFL), Switzerland • Supervisor: Prof. Dimitrios G. Lignos
01.2018-04.2022	**PhD, Civil Engineering** École Polytechnique Fédérale de Lausanne (EPFL), Switzerland • Thesis: Welded Moment Connections with Highly Dissipative Panel Zones for Enhanced Seismic Performance of Steel Moment Frames • Supervisor: Prof. Dimitrios G. Lignos • PhD defense date: 29.04.2022 • Outstanding Ph.D Thesis Distinction in Civil and Environmental Engineering (top 8% of Ph.D thesis at EPFL within all disciplines): https://www.epfl.ch/education/phd/edce-civil-and-environmental-engineering/edce-awards-laureates/
09.2011-10.2016	**Diploma, M.Eng Civil Engineering (5-year joint degree)** National Technical University of Athens (NTUA), Greece • Thesis: Comparison of Alternative Methods for the Analysis and Design of Steel Frames (Grade: 10/10) • Supervisor: Prof. Charis J. Gantes • Specialization: Structural Engineering • GPA: **9.41/10**

HONORS AND AWARDS

EPFL Outstanding Ph.D Thesis Distinction in Civil and Environmental Engineering, 2023
Awarded by École Polytechnique Fédérale de Lausanne (EPFL), Switzerland
Link: https://www.epfl.ch/education/phd/edce-civil-and-environmental-engineering/edce-awards-laureates/

Raymond C. Reese Research Prize, 2022
Awarded by the *American Society of Civil Engineers (ASCE)*
For the paper "Proposed Panel Zone Model for Seismic Design of Steel Moment-Resisting Frames"
Link: https://www.asce.org/career-growth/awards-and-honors/raymond-c-reese-research-prize

17WCEE Early Career and Student Award, 2021
17th World Conference on Earthquake Engineering, Sendai, Japan, 2020-21
For the paper "Improved Panel Zone Model for Seismic Design of Steel Moment Resisting Frames"
Link: https://www.jaee.gr.jp/jp/event/wcee/assets/dl/index/winners_list.pdf

Leventis Foundation Scholarship, 2017
Awarded by *A.G. Leventis Foundation*, Athens, Greece

Limmat Foundation Prize for Academic Excellence (3rd among all graduating students), 2016
Awarded by *Limmat Foundation*, Zürich, Switzerland

Scholarship for Extraordinary Achievement (Highest GPA), 2014-15
Awarded by *Sarafis Foundation*, N.T.U. Athens

Scholarship for Highest Nationwide University Entrance Grade in High School, 2011

Awarded by *Eurobank EFG*, "The big moment for education"

National Mathematics Olympiad Archimedes, 2011
Merits Awarded by the Hellenic Mathematical Society (H.M.S.)

JOURNAL PUBLICATIONS

J.1. **Skiadopoulos, A.**, de Castro e Sousa, A., and Lignos, D. G. (2023). "Experimental investigation and residual stress modeling distributions for hot-rolled wide flange steel members." *Journal of Constructional Steel Research*, 210: 108069. DOI: https://doi.org/10.1016/j.jcsr.2023.108069.

J.2. **Skiadopoulos, A.**, Lignos, D. G., Arita, M., and Hiroshima, S. (2023). "Full-scale experiments of cyclically loaded welded moment connections with highly dissipative panel zones and simplified weld details (in press)." *Journal of Structural Engineering*, American Society of Civil Engineers. DOI: https://doi.org/10.1061/JSENDH/STENG-12128.

J.3. **Skiadopoulos, A.**, and Lignos, D. G. (2022). "Seismic demands of steel moment resisting frames with inelastic beam-to-column web panel zones." *Earthquake Engineering & Structural Dynamics*, Wiley, 51(7), 1591-1609. DOI: https://doi.org/10.1002/eqe.3629.

J.4. **Skiadopoulos, A.**, and Lignos, D. G. (2022). "Proposed backing bar detail in welded beam-to-column connections for seismic applications." *Journal of Structural Engineering*, American Society of Civil Engineers, 148(8), 04022102. DOI: https://doi.org/10.1061/(ASCE)ST.1943-541X.0003374.

J.5. **Skiadopoulos, A.**, Elkady, A., and Lignos, D. G. (2021). "Proposed panel zone model for seismic design of steel moment-resisting frames." *Journal of Structural Engineering*, American Society of Civil Engineers, 147(4), 04021006. DOI: https://doi.org/10.1061/(ASCE)ST.1943-541X.0002935.

J.6. **Skiadopoulos, A.**, and Lignos, D. G. (2021). "Development of inelastic panel zone database." *Journal of Structural Engineering*, American Society of Civil Engineers, 147(4), 04721001. DOI: https://doi.org/10.1061/(ASCE)ST.1943-541X.0002957.

CONFERENCE PUBLICATIONS

C.1. **Skiadopoulos, A.**, Lignos, D. G., Arita, M., and Hiroshima, S. (2023). "Experimental investigation of instability-free welded moment connections with simplified weld details." *10th National Conference on Steel Structures*, Athens, Greece: Steel Structures Research Society.

C.2. **Skiadopoulos, A.**, Elkady, A., and Lignos, D. G. (2023). "Proposed panel zone model for beam-to-column joints in steel moment resisting frames." *10th National Conference on Steel Structures*, Athens, Greece: Steel Structures Research Society.

C.3. **Skiadopoulos, A.**, de Castro e Sousa, A., and Lignos, D. G. (2023). "Experimental evaluation and modeling of residual stress distributions for hot-rolled wide flange steel members." *10th National Conference on Steel Structures*, Athens, Greece: Steel Structures Research Society.

C.4. **Skiadopoulos, A.**, Lignos, D. G., Arita, M., and Hiroshima, S. (2023). "Hysteretic behaviour of welded connections with highly inelastic panel zones." *10th European Conference on Steel and Composite Structures (Eurosteel)*, Amsterdam, Netherlands.

C.5. **Skiadopoulos, A.**, de Castro e Sousa, A., and Lignos, D. G. (2023). "Proposed residual stress model for hot-rolled wide flange steel cross sections." *10th European Conference on Steel and Composite Structures (Eurosteel)*, Amsterdam, Netherlands.

C.6. Wen, C., **Skiadopoulos, A.**, and Lignos, D. G. (2023). "Geometric tolerances of welded connections with inelastic panel zones." *10th European Conference on Steel and Composite Structures (Eurosteel)*, Amsterdam, Netherlands.

C.7. Bijelic, N., **Skiadopoulos, A.**, and Lignos, D. G. (2023). "Surrogate modelling for seismic collapse risk assessment of steel moment resisting frames." *Canadian Conference - Pacific Conference on Earthquake Engineering (CCEE-PCEE)*, Vancouver, British Columbia.

C.8. **Skiadopoulos, A.**, and Lignos, D. G. (2022). "Towards instability-free welded moment connections." *13th International Congress on Mechanics*, Patras, Greece: Hellenic Society for Theoretical and Applied Mechanics.

C.9. **Skiadopoulos, A.**, and Lignos, D. G. (2022). "Seismic stability of steel moment resisting frames with inelastic panel zones." *12th National Conference on Earthquake Engineering (NCEE)*, Salt Lake City, UT, USA: Earthquake Engineering Research Institute.

C.10. **Skiadopoulos, A.**, Elkady, A., and Lignos, D. G. (2021). "Improved panel zone model for seismic design of steel moment resisting frames." *17th World Conference on Earthquake Engineering (WCEE)*, Sendai, Japan: Japan Association for Earthquake Engineering.

PATENTS

P.1. **Skiadopoulos, A.**, Hiroshima, S., Arita, M., Suzuki, Y., Kitaoka, S., and Lignos D. G. "Beam-column joint structure (filled)." EU Patent No.: EP23179922.2, European Patent Office, 2023.

INVITED TALKS

T.1. **Skiadopoulos, A.** "Welded moment connections with highly dissipative panel zones for enhanced seismic performance of steel moment frames." Society for Earthquake and Civil Engineering Dynamics (SECED), UK, June 14, 2023. URL: https://www.youtube.com/watch?v=fS4yvYqlvXY.

T.2. **Skiadopoulos, A.** "Welded moment connections with highly dissipative panel zones for enhanced seismic performance of steel moment frames." Civil Engineering Seminar Series, University of California at Davis, California, USA, June 20, 2022.

TEACHING AND SUPERVISION

Teaching

02.2023- 07.2023	**CIVIL-435, Advanced Steel Design** École Polytechnique Fédérale de Lausanne (EPFL), Switzerland • Graduate course; advanced topics in seismic design of steel structures • Course co-instructed with Prof. D. Lignos

Supervision of Junior Researchers

09.2022- present	**PhD Thesis Co-Supervisor** École Polytechnique Fédérale de Lausanne (EPFL), Switzerland • Student: Wen Ce (co-supervised with Prof. D. Lignos)
02.2023- 07.2023	**Master Thesis Advisor** École Polytechnique Fédérale de Lausanne (EPFL), Switzerland • Student: Balmer Damien • Thesis: Time-history analysis of steel buildings with highly inelastic panel zone
02.2022- 07.2022	**Master Thesis Advisor** École Polytechnique Fédérale de Lausanne (EPFL), Switzerland • Student: Bussat Jeremy • Thesis: Panel Zone Model for the Seismic Design of Beam-to-Column Joints with Hollow Structural Section
09.2021- 01.2022	**Master Thesis Advisor** École Polytechnique Fédérale de Lausanne (EPFL), Switzerland • Student: Schipani Carmine • Thesis: Development of a Python-Based Simulation Tools Library for Composite Steel Concrete Structures
02.2021- 07.2021	**Master Thesis Advisor** École Polytechnique Fédérale de Lausanne (EPFL), Switzerland • Student: Beqiraj Meriton • Thesis: Finite Element Investigation of Stability Bracing Force Demands of Steel Moment Resisting Frame Columns under Cyclic Loading

| 09.2020-
01.2021 | **Master Thesis Advisor** |
| | École Polytechnique Fédérale de Lausanne (EPFL), Switzerland |

- Student: Falconi Gabriele
- Thesis: Influence of Residual Stresses on the Buckling Capacity of Axially Loaded Steel Columns

| 02.2019-
07.2022 | **Master Semester Projects** |
| | École Polytechnique Fédérale de Lausanne (EPFL), Switzerland |

- Fundamental Understanding of Structural Stability Using Educational Tools (1)
- Design of a Typical Earthquake Resilient Two-Story Steel Building (7)
  (the parenthesis number indicates the number of projects supervised per subject)

Outreach Activities

| 11.2019/2021 | **High-School Student Thematic Day** |
| | École Polytechnique Fédérale de Lausanne (EPFL), Switzerland |

- Annual high-school student thematic day to engage students in Civil Engineering
- Hands-on activities involving the design of a building resilient in gravity and seismic loading

EXPERTISE WORK

| 09.2022-
present | **GeniLac Project by Services Industriels de Genève (SIG)** |
| | École Polytechnique Fédérale de Lausanne (EPFL), Switzerland |

- Fracture mechanics and finite element analysis of distance heating welded concrete steel pipes

PROFESSIONAL AND VOLUNTEERING EXPERIENCE

| 11.2016-
08.2017 | **Engineering Arm of Hellenic Army, Greece** |

- Supervision of construction sites of refugee camps

| 06.2015-
09.2015 | **Engineering Intern** |
| | HOCHTIEF Polska S.A., Warsaw |

- Supervision of the following contruction cites: *Residential Houses JK51* and *The Business Garden Warszawa Office Complex*

| 11.2012-
01.2018 | **Founding Member and Website Administrator of the CEE portal of NTUA** |
| | www.mqn.gr, Greece |

- Organized events to promote the CEE portal and ensure funding
- Counting nearly 150.000 posts, 5.000 topics, 10.000 files and 10.000 users

SCIENTIFIC REVIEWS
(Publons: https ://publons.com/researcher/4834847/andronikos-skiadopoulos/)

- Eartquake Spectra/GRADEVINAR/ASCE Journal of Structural Engineering

SKILLS

Languages
- Greek (Native)
- English (Fluent, Michigan proficiency certificate, TOEFL Score: 102/120)
- German (Conventional, Goethe-Zertifikat B1)
- French (Elementary proficiency, A1-A2)

Computer Skills
- MATLAB, Python, Fortran
- AutoCAD, OpenSees, Abaqus, SAP2000, SOFiSTiK AG, Autodesk Fusion 360, Seismostruct, Plaxis

Teaching Statement

Experience

Since 2018, when I commenced my doctoral studies, I have served as a teaching assistant and as a lecturer for the graduate course 'Advanced Steel Design' (CIVIL-435) at EPFL. As a teaching assistant, my responsibilities included guiding the students with the weekly assignments. Given my experience with the course material, I had the privilege of delivering several guest lectures dealing with advanced topics in structural steel seismic and wind design, seismic hysteretic behavior of structural steel components, and seismic behavior of conventional and innovative steel lateral load resisting systems. This past year I was officially appointed as a course lecturer. In this role, I redesigned parts of the course to adapt to my teaching philosophy, while I oversaw course materials, take-home exercises, and the final examination and grading. As a lecturer, I received positive and constructive feedback from the students. In addition to my role as a lecturer, I have been heavily involved in the supervision of both semester-long projects (eight in total) as well as more involved Masters theses (five in total). These projects feature a variaty of topics that span across seismic design and the fundamental understanding of structural stability and mechanics using hands on educational tools that enhance the learning experience of the students. Finally, I have been actively participating in outreach activities of EPFL's educational center including the design of a more focused material to inspire high-school and gymnasium students to select Civil Engineering as part of their future career perspective. The above experiences have considerably enriched my supervising and teaching experience. Moreover, I appreciate how teamwork could contribute to new research ideas that could potentially lead to publications.

Philosophy

My roles as a teaching assistant and lecturer have afforded me the opportunity to thoroughly examine, apply, and contemplate teaching techniques that I intend to employ as a future professor. These strategies enable me to effectively convey essential concepts to my students and foster a classroom environment where every student can access equal learning opportunities. I have come to recognize that "learning-by-doing" and actively involving students in a classroom significantly enhances their learning experience and the acquisition of essential problem-solving skills. To foster an interactive teaching environment, I employ recent technological developments. Some of these methods involve the utilization of clickers, which not only fosters student engagement but also provides me with valuable insights into the extent of students' comprehension of the course material. Furthermore, I played a key role in the development of an innovative online platform, which hosts comprehensive structural performance databases, interactive models, and fragility curves for various structural components (https://resslab-hub.epfl.ch/), and I integrated this platform into my teaching approach. My vision is to extend this initiative to a broader range of interactive tools on structural mechanics and design. Additionally, I provide students with the chance to review my class presentations using the online lecture recording system. I consider this to be particularly beneficial for students facing learning challenges, as it enables them to engage with the course content at their preferred speed. A pivotal element of my teaching philosophy revolves around fostering interactive relationships among students and between students and the instructor. To facilitate this, I encourage small group collaborations for both weekly assignments and semester projects. I provide personalized feedback on assignments and maintain weekly meetings with students to track their overall progress. This approach has successfully cultivated an engaging learning atmosphere and strengthened the bond between students and the instructor, resulting in students' growing interest in conducting research within our research group. As a professor, I aspire to ignite in my students the same passion for learning that has kept me in academia.

Courses

Considering my multidisciplinary background, as part of the Purdue University faculty, I am very comfortable on teaching a wide range of courses that are currently offered at both the undergraduate and graduate levels. These include *Behavior Of Metal Structures, Advanced Structural Steel Design, Structural Stability, Structural Dynamics, Earthquake Engineering*, and *Advanced Structural Mechanics*. These courses cover subjects that I am particularly passionate about as they are directly related to my research interests. Looking ahead, I am interested in developing a course related to performance-based earthquake engineering (PBEE). In light of the increase in computational power, the advancements in structural modeling, and the need to design resilient structures against multi-hazards, this topic is becoming increasingly important for the structural engineering profession. This course will introduce students to the basics of seismic hazard analysis, regional standards and guidelines related to PBEE, methods for the seismic assessment of new and existing buildings, retrofitting techniques of existing buildings, and finally the quantification of earthquake-induced losses. This course would be a valuable addition to the curriculum at Purdue University, in the fields of seismic design, structural dynamics, and nonlinear analysis.

RESEARCH STATEMENT

Past and Active Research

The overarching goal of my research vision pertains to the development of infrastructure systems resilient to natural hazards along with the development of new concepts that enable deconstruction and reuse of reclaimed members after their first use. The above rely on a solid foundation I have built over the past few years as part of my current research studies that fuse advanced computational methods, multi-scale experimentation and performance-based natural hazards engineering.

Since 2018, my primary research focus has been on the development of new concepts with emphasis on the instability-free performance of welded connections under seismic loading. This has been investigated on several fronts. From a computational standpoint, I developed a mechanics-based model that accurately predicts the mechanical behavior of shear-dominant joints. This model has been validated by comprehensive physical experiments fused with high-fidelity nonlinear continuum finite element simulations that rely on rigorous concepts of fracture mechanics. Consequently, I recently developed a new beam-to-column connection typology for steel moment frames that defies the current design paradigm. I have leveraged concepts of performance-based earthquake engineering to demonstrate that steel moment frames featuring such connections exhibit superior seismic performance by minimizing structural repairs in the aftermath of earthquakes. In parallel with my computational work, I have gained considerable experience with experimentation across different scales. These involve experiments both at the material as well as structural scale.

Just recently, as an outcome of my PhD thesis research contributions, I was honored to receive the 2022 Raymond C. Reese Research Prize from the American Society of Civil Engineers. Besides, I highly regard the contributions of my work to the engineering practice, as part of my work has been effectively adopted in the European and Canadian seismic design standards. Moreover, I was able to file a joint patent with EPFL's technology transfer office and the world's largest steel-making company. Currently, I research the development of new micro-mechanics-based models for simulating ductile fracture initiation and propagation with a wide range of applications including seismic-resistant steel structures as well as distance-heating welded concrete steel piping networks. My background in reliability analysis and performance-based engineering allows me to assess both the functionality and safety of complex systems over their service life.

Direction of Future Research

In the coming years, I plan to contribute to new methodological developments for the reliable assessment of infrastructure systems, as well as the development of design, and retrofitting solutions towards a resilient and sustainable built environment to natural hazards, such as earthquakes. Current challenges in infrastructure design for enhanced life-cycle performance require the development of advanced methods for prognosticating the performance of new and existing materials as well as systems under complex loading and operating conditions. Thus, I envision my research work on simulation-based engineering science and multi-scale experimentation to advance knowledge on how key damaging mechanisms compromise a system's ability to carry loads and potentially conceive alternative approaches that facilitate enhanced performance and potential for reusability.

Development of models for assessing aging infrastructure

A major concern associated with aging infrastructure is the increased vulnerability to severe damage (or collapse) when subjected to extreme loading, such as seismic, blast, and wind. Assessing existing structures under extreme loads necessitates the development of accurate models that simulate ultimate limit states, which are mostly characterized by the spread of plasticity, geometric instabilities, and/or fracture. Methods to simulate all aspects of fracture are still evolving and they are mostly validated at the material scale. I plan to advance knowledge on predicting fracture due to ultra-low-cycle fatigue of metals with direct applications on infrastructure systems under extreme loading by acknowledging rate- and temperature-dependent phenomena that are neglected in available models. Particularly, I am interested in developing new models for simulating fracture from the initiation phase to the onset of brittle cleavage fracture with particular emphasis on simulating ductile crack propagation, where there is a lack of well-established models. To link the developed methods with the performance assessment of existing structures, I intend to establish relationships between the material properties identified through non-destructive testing and the fracture parameters of our models using data-driven techniques.

Initially, the focus will be on structural steel with direct implications on the robust design of large-scale civil engineering infrastructure, such as steel buildings, bridges, and wind-critical infrastructure that are subject to fatigue due to extreme loading conditions. More broadly, I am interested in leveraging some of these methods to other engineering materials for a wider range of applications, including concrete structures, composite steel-concrete structural systems, and structures utilizing high-strength steel. The development of the fracture modeling methodology will encompass computational, analytical, and experimental approaches. While my work within this research area will be more fundamental, I also plan to conduct experiments at the material scale with customized strain-based loading protocols to validate the models I envision developing. The tests entail loading schemes to achieve multiaxial stress states that will manifest material characteristics in the nonlinear regime and will enable reliable calibrations of the envisioned models.

Development of concepts for deconstruction and reuse

The construction sector is widely recognized as a major contributor to global resource consumption, accounting for approximately 35% of the world's total energy consumption, according to the International Energy Agency. Hence, an increasing need exists among policymakers and stakeholders to embrace responsibility for the recycling of structural components at the end of their life-cycle. For this reason, I plan to develop new methods for allowing the deconstruction and reuse of reclaimed structural members after their first use. Particularly, I aim to develop innovative connection details that facilitate disassembly and reuse in beam-to-column and beam-to-slab connections for both steel and composite steel-concrete structures. Concerning beam-to-column connections, I will exploit the beneficial aspects of panel zone shear yielding to minimize structural damage in beam-to-column connections and potentially limit geometric tolerances when plasticity occurs. A challenge that yet pertains to composite steel-concrete structures regards the separation of the decking slab from the steel beams. Although research exists on demountable beam-to-slab connections, available studies mostly conducted static push-out tests to evaluate their performance. However, push-out tests are not representative of the realistic force and deformation patterns. For this purpose, I plan to use and potentially expand the Bowen Laboratory of Purdue University to characterize experimentally the performance of the developed connection details in the subassembly and the system level.

Finally, I plan to combine some of the proposed construction details with concepts on performance-based engineering to quantify how these could potentially impact the functional recovery of a building in the aftermath of natural hazards. I foresee the above contributions to be a stepping stone to a sustainable built environment. While my initial focus will be on steel and composite steel-concrete structures, I intend to expand the scope of this research to structures made of other construction materials. I anticipate that my research will be fundamental, while certain aspects of it will provide valuable insights to inform our engineering design and assessment standards.

Composite steel-concrete systems subjected to extreme loading and climate hazards

Over the past several years, we have witnessed rapid population growth and urbanization. Consequently, a disproportionate number of people migrate to major cities, thereby creating a greater need for taller buildings. Additionally, to ensure a sustainable built environment, it is crucial to incorporate the notion of resilient cities into structural design for seismic and climate hazards. Composite steel-concrete columns are an excellent choice for high-rise buildings because they efficiently utilize concrete to withstand compressive axial loads while delaying local instabilities in the restrained steel tube. Moreover, composite steel-concrete beams offer significantly greater stiffness and strength in comparison to bare beams, which is crucial for the wind and seismic design of high-rise buildings. One critical concern related to composite steel-concrete columns is the adverse impact of the differential axial shortening they cause with respect to the concrete core, and the assessment of the factors influencing this phenomenon.

In high-rise buildings, load path re-distributions could potentially endanger the overall safety of a structure. For this reason, I plan on conducting system-level experiments by leveraging the hybrid simulation experimental technique, while incorporating the seismic hazard and the exposure of the construction materials to high humidity and heat cycles in a time-dependent approach that considers shrinkage and creep phenomena. I plan to develop a new constitutive law formulation that will capture accurately these time effects along with plasticity. In this way, I can systematically quantify the contributions of important mechanisms that provide lateral load resistance, such as the framing action and floor continuity, which are usually disregarded in idealized subassembly tests with overly simplified boundary conditions. Furthermore, in keeping with the growing trend of accelerated construction over the last few years, my objective is to explore modular construction solutions for high-rise buildings, an area where research is currently limited.

Proposed Panel Zone Model for Seismic Design of Steel Moment-Resisting Frames

Andronikos Skiadopoulos, S.M.ASCE[1]; Ahmed Elkady, Ph.D., M.ASCE[2]; and Dimitrios G. Lignos, M.ASCE[3]

Abstract: This paper proposes a new mechanics-based model for the seismic design of beam-to-column panel zone joints in steel moment-resisting frames. The model is based on realistic shear stress distributions retrieved from continuum finite element (CFE) analyses of representative panel zone geometries. Comparisons with a comprehensive experimental data set suggest that the proposed model predicts the panel zone stiffness and shear strength with a noteworthy accuracy, even in panel zones featuring columns with thick flanges (thicker than 40 mm), as well as in cases with high beam-to-column aspect ratios (larger than 1.5). In that respect, the proposed model addresses the limitations of all other available models in the literature. If doubler plates are deemed necessary in the panel zone design, the CFE simulations do not depict any doubler-to-column web shear stress incompatibility, provided the current detailing practice is respected. Hence, the total thickness of the column web and doubler plates should be directly used in the proposed panel zone model. The panel zone shear strength reduction due to the axial load effects should be based on the peak axial compressive load, including the transient component due to dynamic overturning effects in exterior joints. It is found that the commonly used von Mises criterion suffices to adequately predict the shear strength reduction in the panel zone. **DOI: 10.1061/(ASCE)ST.1943-541X.0002935.** © *2021 American Society of Civil Engineers.*

Author keywords: Steel moment-resisting frames; Panel zone shear resistance; Beam-to-column connections; Panel zone model; Balanced design; Doubler plate ineffectiveness.

Introduction

In capacity-designed steel moment-resisting frame (MRF) systems, a balanced beam-to-column connection design is promoted. In principle, the panel zone joint may experience limited inelastic behavior. A challenge in mobilizing the panel zone in the seismic energy dissipation is the increased potential for premature connection fracture when improperly detailed (Chi et al. 1997; El-Tawil et al. 1999; Lu et al. 2000; Mao et al. 2001; Ricles et al. 2000, 2004).

Experimental research (Kim and Lee 2017; Lee et al. 2005; Shin and Engelhardt 2013) indicates that a properly detailed fully restrained beam-to-column joint designed with controlled panel zone yielding may lead to improved seismic performance compared to what is perceived as a *strong* panel zone design (where the panel zone remains elastic). In particular, data from assembled inelastic panel zone databases (Al-Shawwa and Lignos 2013; El Jisr et al. 2019; Skiadopoulos and Lignos, forthcoming) suggest that at story drift demands corresponding to 4% rad, modern fully restrained beam-to-column connections (AISC 2016a) do not experience

premature weld fractures when their panel zone joints attain shear distortions up to $10\gamma_y$ (where γ_y is the panel zone yield shear distortion angle). Others (Chi and Uang 2002; Ricles et al. 2004) found that when panel zones exhibit inelastic behavior within a steel MRF beam-to-column connection, the column twist demands due to beam plastic hinge formation become fairly minimal. This issue is prevalent in steel MRF designs featuring deep columns, which are prone to twisting (Elkady and Lignos 2018a, b; Ozkula et al. 2017). To reliably mobilize the inelastic behavior of a panel zone, its shear stiffness and strength should be accurately predicted during the steel MRF seismic design phase.

Models to simulate the inelastic panel zone behavior in terms of shear strength, V_{pz}, and shear distortion angle, γ, are available in the literature (Fielding and Huang 1971; Kato et al. 1988; Kim and Engelhardt 2002; Krawinkler 1978; Lee et al. 2005; Wang 1988). Referring to Fig. 1 and Eq. (1), these models comprise a shear-dominated elastic stiffness, K_e, up to the yield shear strength, V_y [Eq. (2)]. This is deduced by assuming a uniform shear stress distribution in the column web. An inelastic hardening branch with postyield stiffness, K_p, defines the panel zone's postyield behavior up to a shear strength, V_p [Eq. (3)], at $4\gamma_y$. This strength accounts for the contribution of the surrounding elements (continuity plates and column flanges). Finally, a third branch, where the shear strength is assumed to stabilize, is typically accounted for with a post-γ_p slope that is expressed as a percentage of the elastic stiffness, as discussed subsequently:

$$K_e = \frac{V_y}{\gamma_y} = 0.95 d_c \cdot t_{pz} \cdot G \tag{1}$$

$$V_y = \frac{f_y}{\sqrt{3}} \cdot 0.95 d_c \cdot t_{pz} \tag{2}$$

$$V_p = V_y(1 + 3K_p/K_e) \tag{3}$$

in which, the panel zone thickness $t_{pz} = t_{cw} + t_{dp}$ when doubler plate(s) are present; t_{cw} = thickness of column web; t_{dp} = total

---

[1]Doctoral Assistant, Dept. of Architecture, Civil and Environmental Engineering, École Polytechnique Fédérale de Lausanne, Station 18, Lausanne 1015, Switzerland. Email: andronikos.skiadopoulos@epfl.ch

[2]Lecturer, Dept. of Civil, Maritime and Environmental Engineering, Univ. of Southampton, Southampton SO16 7QF, UK; formerly, Postdoctoral Research Scientist, Dept. of Architecture, Civil and Environmental Engineering, École Polytechnique Fédérale de Lausanne, Lausanne 1015, Switzerland. Email: a.elkady@soton.ac.uk

[3]Associate Professor, Dept. of Architecture, Civil and Environmental Engineering, École Polytechnique Fédérale de Lausanne, Station 18, Lausanne 1015, Switzerland (corresponding author). ORCID: https://orcid.org/0000-0003-0682-4660. Email: dimitrios.lignos@epfl.ch
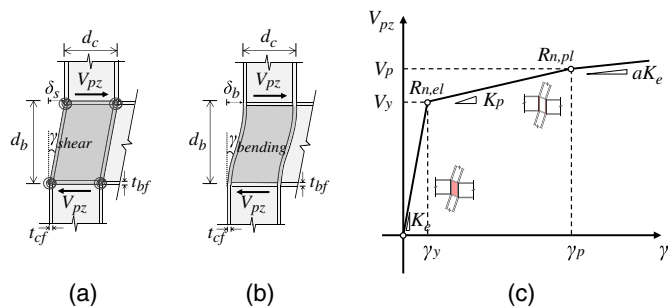
Fig. 1. Panel zone kinematics and mathematical model assumptions: (a) panel zone shear deformation; (b) panel zone bending deformation; and (c) typical trilinear panel zone model.

thickness of doubler plate(s); d_c = column depth; f_y = steel material yield stress; and G = steel material modulus of rigidity. The bending deformation of the panel zone [Fig. 1(b)] is neglected in this case.

Krawinkler (1978) proposed the trilinear model (hereinafter referred to as the Krawinkler model) shown in Fig. 1(c), which has been adopted in current design provisions with minor modifications throughout the years (AISC 2016c; CEN 2005). Once the panel zone yields uniformly at γ_y, the Krawinkler model assumes that the column web is not capable of withstanding any additional shear. Depending on the column cross-sectional profile, its flanges and continuity plates (if installed) participate in resisting the postyield panel zone shear demand. Referring to Fig. 1(c), the postyield stiffness, K_p, of the Krawinkler model was derived using the principle of virtual work for the panel zone kinking locations based on small-scale subassembly experiments (flange thickness between 10 and 24 mm). Referring to Fig. 1(c), the aforementioned model is valid up to $\gamma_p = 4\gamma_y$. Alternative γ_p values can be found in the literature. For instance, Wang (1988) proposed a value of $3.5\gamma_y$, whereas Kim et al. (2015) related this value mathematically to a joint's geometric and material properties. The post-γ_p stiffness is usually taken as 3% of K_e (Gupta and Krawinkler 2000; PEER/ATC 2010; Slutter 1981), an acknowledgment that the shear resistance is only attributed to material strain hardening. Krawinkler (1978) suggested that for joints involving stocky columns (flanges thicker than 30–40 mm), further experiments should be conducted to verify the predicted shear strength of his model.

Considering the assumptions and limitations of this model (Brandonisio et al. 2012; El-Tawil et al. 1999; Jin and El-Tawil 2005; Kim and Engelhardt 2002; Krawinkler 1978; Lee et al. 2005; Qi et al. 2018; Soliman et al. 2018), several researchers have attempted to propose more robust $V_{pz} - \gamma$ relations. In some of these studies (Castro et al. 2005; Chung et al. 2010; Han et al. 2007; Kim et al. 2015; Lee et al. 2005), the resultant V_y was more or less similar to that of the Krawinkler model [i.e., Eq. (2)] excluding distinct differences in the assumed effective shear area. The postyield stiffness, K_p, was refined empirically based on available experimental data. Tsai and Popov (1988) showed that the average shear stress in the panel zone is 20% lower than the peak shear stress developed in the panel zone web center, suggesting that the uniform shear distribution for calculating V_y is unjustifiable (Charney et al. 2005; Chung et al. 2010; Kim and Engelhardt 2002; Lin et al. 2000). Kim and Engelhardt (2002) and Lin et al. (2000) formulated the preceding findings empirically based on limited experimental data featuring column flange thicknesses less than 35 mm. Other studies leveraged the finite-element method to examine panel zone inelastic behavior (Hjelmstad and Haikal 2006; Krishnan and Hall 2006; Léger et al. 1991; Li and Goto 1998; Mulas 2004), without reaching a consensus on an improved panel zone model to be used in the seismic design of steel MRFs.

From a design standpoint, panel zone joints may moderately participate in energy dissipation during an earthquake according to the North American provisions (AISC 2016b; CSA 2019). The code-based design shear strength (either the panel zone shear yield strength, $R_{n,el}$, or postyield strength, $R_{n,pl}$) is computed based on the Krawinkler model (i.e., V_y and V_p, respectively). In Japan (AIJ 2012), the panel zone shear strength is computed as per $R_{n,el}$ AISC (2016c), with the difference that $1/\sqrt{3}$ is considered instead of the 0.6 factor. However, the panel zone shear demand imposed by beams is reduced by 25% to implicitly contemplate the neglected column shear force contribution and the disregarded panel zone postyield strength. In Europe, CEN (2005) considers the contribution of a column web in a similar manner with $R_{n,el}$. If continuity plates are present, an additional term is included to compute the panel zone shear strength. This term is based on the plastic moment resistance of the column flanges at kinking locations [Fig. 1(a)].

Fig. 2 depicts the analytically derived elastic stiffness, K_e, of various panel zone geometries with/without doubler plates versus the measured one, $K_{e,m}$, from collected full-scale experiments (Skiadopoulos and Lignos, forthcoming). In the case of test data without doubler plates, Fig. 2(a) suggests that common panel zone models (CEN 2005; Kim and Engelhardt 2002; AISC 2016c) overestimate K_e by up to 30%. This is attributed to the uniform yielding assumption at γ_y along with the depreciation of the panel
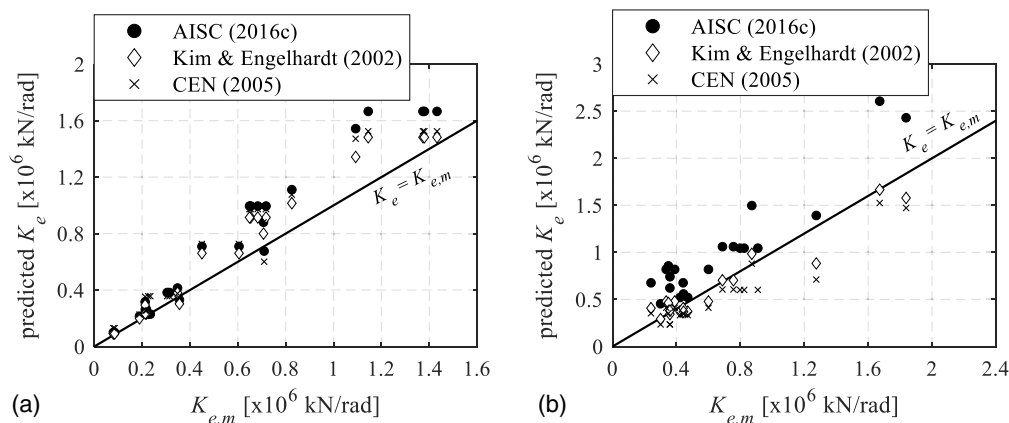

Fig. 2. Comparison of analytically derived, K_e, and measured, $K_{e,m}$, panel zone elastic stiffness: (a) test data without doubler plates; and (b) test data with doubler plates.

zone bending deformation mode [Fig. 1(b)] depending on the panel zone aspect ratio and column flange thickness.

Compelling issues with conflicting observations are also found in cases where doubler plates are utilized to reach a desirable panel zone shear strength. Depending on the weld details, the doubler plate efficiency (ratio of shear stresses in the doubler plate to those in the column web) does not exceed 50% (Kim and Engelhardt 2002); hence, half of their thickness, at most, participates in connection stiffness and strength. For this reason, the panel zone model by CEN (2005) accounts for only one doubler plate even when two plates are required by design. Referring to Fig. 2(b), the data suggest that K_e, based on CEN (2005), is underpredicted by nearly 20%. Lee et al. (2005) found that doubler plates welded to column webs by fillets, according to the AISC (2016b) provisions, allow for excellent stress compatibility between the plates and the column web. These conclusions are in line with earlier work on fillet-welded doubler plates (Bertero et al. 1973) and on complete joint penetration (CJP) welded plates (Ghobarah et al. 1992). More recently, Shirsat and Engelhardt (2012) showed that the stress compatibility between column web and doubler plate is lower for deep columns utilizing thick doubler plates (plate thicknesses $t_{dp} \geq 26$ mm). Referring to Fig. 2(b), the AISC panel zone model that accounts for both doubler plates (if applicable) generally overestimates K_e.

Fig. 3(a) depicts the deviation of the analytically predicted post-yield stiffness, K_p (as per AISC 2016c; Lee et al. 2005), from the measured one, $K_{p,m}$, with respect to the column flange thickness, t_{cf}. For t_{cf} larger than 40 mm, K_p, at a targeted shear distortion angle of $4\gamma_y$, is overpredicted by up to 40%, as per the AISC (2016c) model. Referring to Fig. 3(b), the same observations hold true for V_p according to the AISC (2016c) panel zone model. Note that for the cyclic test data, the extraction of the panel zone measured parameters of interest is based on the average values of the positive and negative first cycle envelopes, as shown in Fig. 3(c). The panel zone measured strength at γ_y and $4\gamma_y$ is, then, determined, and as such, $K_{p,m}$ is defined based on these two reference points. The model by Lee et al. (2005) consistently underestimates K_p [Fig. 3(a)] since it was benchmarked with limited data from assemblies comprising columns with flange thicknesses less than 30 mm. The Kim et al. (2015) model assumes that the post-yield panel zone response is controlled by the plastic column flange bending capacity under normal stresses. However, this assumption, which is the same as in the CEN (2005) panel zone model, is non-conservative for steel columns featuring thick flanges (i.e., $t_{cf} > 50$ mm) [Fig. 3(b)]. These constitute a considerable amount (up to 40%) of the total shear force.

To capture the interaction of axial load and shear within the panel zone joint, a reduction factor $r = \sqrt{1 - n^2}$ (where $n = P/P_y$, and P and P_y are the applied axial compressive load and axial yield strength of a steel column, respectively) has been proposed (Chung et al. 2006; Krawinkler 1978). This is based on the von Mises criterion (von Mises 1913). This is also consistent with the Japanese provisions (AIJ 2012). In the US, a panel zone shear strength reduction is used according to a fit to the $r - n$ curve, when the panel zone is designed based on $R_{n,el}$ (AISC 2016c). Otherwise, if design is based on $R_{n,pl}$, a reduction factor is applied to improbably high axial load demands ($n > 0.75$). This tends to overestimate the panel zone shear strength by nearly 15% for $n = 0.5$. In Europe, regardless of the axial demand-to-capacity ratio of the column, the shear resistance is accounted for through a constant reduction factor of 0.9 (Ciutina and Dubina 2003).

To address the aforementioned challenges, this paper proposes a mechanics-based panel zone model that could be used for the seismic design of steel MRF systems. This model is informed by continuum finite-element (CFE) analyses validated based on
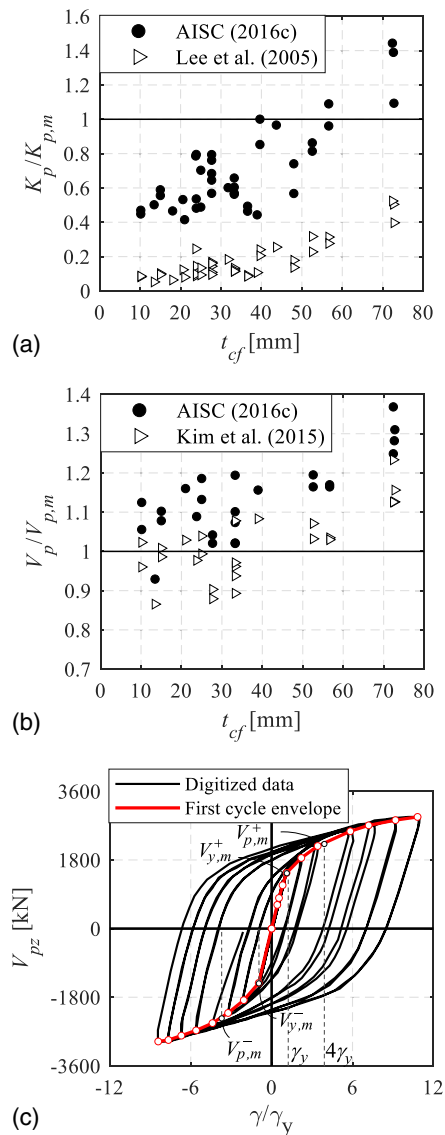

Fig. 3. Comparison of inelastic panel zone test data without doubler plates: (a) $K_p/K_{p,m}$ versus t_{cf}; (b) $V_p/V_{p,m}$ versus t_{cf}; and (c) first cycle envelopes for panel zone measured shear stiffness and strength deduction. (Data from Kim et al. 2015.)

available experimental data. According to the proposed model, panel zone joints are categorized according to the shear stress evolution in the column web and flanges. Moreover, improved panel zone shear strength equations that account for realistic stress distributions within web panels and column flanges at three levels of shear distortion (γ_y, $4\gamma_y$, and $6\gamma_y$) are proposed. Doubler plate stress compatibility with the column web is also examined for panel zone configurations comprising CJP and fillet weld details according to current construction practice. The axial load effect on the panel zone shear strength and stiffness is also examined for both interior and end columns within steel MRFs in an effort to generalize the proposed model.

Mechanics of Panel Zone Behavior through CFE Analysis

A CFE model is developed to examine the stress profile within a panel zone joint at various levels of inelastic shear distortion.
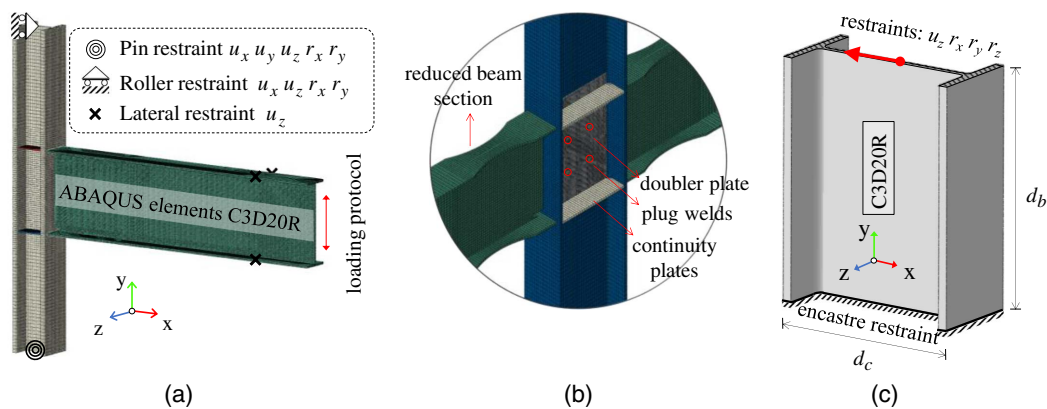
Fig. 4. Detailed and reduced-order CFE models: (a) detailed CFE model; (b) doubler plate detailing; and (c) reduced-order CFE model.

The commercial finite-element analysis software Abaqus (version 6.14-1) (SIMULIA 2014) is used for this purpose. This section describes the CFE modeling approach and its validation along with the main panel zone parameters of interest. The CFE model validation is demonstrated with two full-scale beam-to-column connection tests. The first test [Specimen UCB-PN3, FEMA (1997)] features an exterior subassembly with a stocky column (W14 × 257) and a 900-mm-deep beam (W36 × 150). The second test [Specimen SPEC-6, Ricles et al. (2004)] features an interior subassembly with deep members (W30 × 108 beams and a W24 × 131 column). All members were fabricated from Grade 50 steel (nominal yield stress $f_y = 345$ MPa).

Description and Validation of CFE Modeling Approach

The CFE model, which is shown in Fig. 4(a), is composed of 20-node quadratic brick elements (C3D20R) with reduced integration and a maximum dimension of 20 mm. These elements do not typically experience hourglassing or shear locking effects. To determine the optimum element type and mesh size, a mesh sensitivity analysis is conducted with four element types (i.e., C3D20, C3D20R, C3D8, C3D8R). Moreover, local imperfections in the beams are incorporated according to the first critical buckling eigenmode. Web imperfections are deemed critical and are tuned to an amplitude of $d_b/250$, which is consistent with prior related studies (Elkady and Lignos 2018b). Residual stresses according to Young (1971) are incorporated into the deep members. For the W14 × 257 column, the residual stress distribution by Sousa and Lignos (2017) is adopted. The CFE model captures the steel material nonlinearity with a multiaxial combined isotropic/kinematic hardening law (Lemaitre and Chaboche 1990) within the J2 plasticity constitutive model (von Mises 1913). The input model parameters are based on prior work by de Castro e Sousa et al. (2020). Referring to Fig. 4(b), the CJP welds along the perimeter of the doubler plate are explicitly modeled. Four plug welds are simulated with 15-mm fasteners that constrain all six degrees of freedom. The continuity plates are tied in the column flanges and the doubler plate. Referring to Fig. 5, the agreement between the measured and simulated results both at the global (load-story drift ratio response) and local level (panel zone shear force–shear distortion response) is noteworthy regardless of the inelastic shear distortion. As for the UCB-PN3 specimen, the agreement of the simulated and measured data with regard to the global behavior is noteworthy [Fig. 5(a)]. In Fig. 5(b), the simulated panel zone response agrees well with the test data up to an inelastic shear distortion of 0.5% rad (i.e., second to last loading cycle). After reviewing the experimental report (Popov et al. 1996), it is found

that the reason for the observed discrepancy between the measured and simulated panel zone response is the occurrence of beam weld fracture in the second to last loading cycle. This was not simulated in the CFE model. Following the occurrence of weld fracture, the shear demand in the panel zone diminished, thereby decreasing the associated inelastic shear distortion. This is also confirmed from the UCB-PN1 specimen, from the same test program, that involved a nominally identical subassembly with UCB-PN3. However, premature fracture occurred at a much later loading cycle.

In an effort to expedite computation, a reduced-order panel zone CFE model is developed, as shown in Fig. 4(c). This model does not include continuity plates. Instead, a rigid body constraint is applied at the column's top and bottom edges (i.e., at the locations of the beam flanges) to prevent stress concentrations during the imposed loading. According to the AISC (2016c) specifications, continuity plates are deemed necessary when the column cannot withstand the beam flange concentrated forces. Unlike slender column profiles, in stocky ones, the column itself is able to sustain the concentrated beam forces, so continuity plates may be disregarded (AISC 2016b, Section E3.6f). In addition, the panel zone strength and stiffness parameters would not be influenced by the presence of continuity plates. Accordingly, assuming fixed end boundaries is justifiable in both cases. Out-of-plane displacements and rotations as well as in-plane rotations are restrained at the panel zone edges. Hence the panel zone joint behaves as a beam in contraflexure. Referring to Figs. 5(b and d), the simulated responses based on the detailed and reduced-order models are nearly identical for the examined subassemblies. Therefore, the reduced-order panel zone CFE model is adopted henceforth.

Deduced Panel Zone Performance Parameters

The simulation matrix comprises eight panel zone geometries. These are designed to have the same V_y with specimen UCB-PN3, i.e., the column web thickness and depth are kept constant. The varied geometric parameters are the panel zone aspect ratio, d_b/d_c, the column flange width, b_{cf}, and the column flange thickness, t_{cf}. The first two parameters are chosen to examine the effect of the bending deformation mode on K_e, whereas t_{cf} is chosen to examine the influence of the column flange thickness on the panel zone shear strength. The panel zone models are subjected to monotonic inelastic shear distortions up to $6\gamma_y$.

Fig. 6 shows the primary panel zone performance parameters of interest. The elastic panel zone shear stiffness, K_e, is deduced from the elastic branch slope of the $V_{pz} - \gamma$ behavior. The yield strength, V_y, is deduced based on the yield initiation according to the von Mises criterion (von Mises 1913) in the panel zone center.
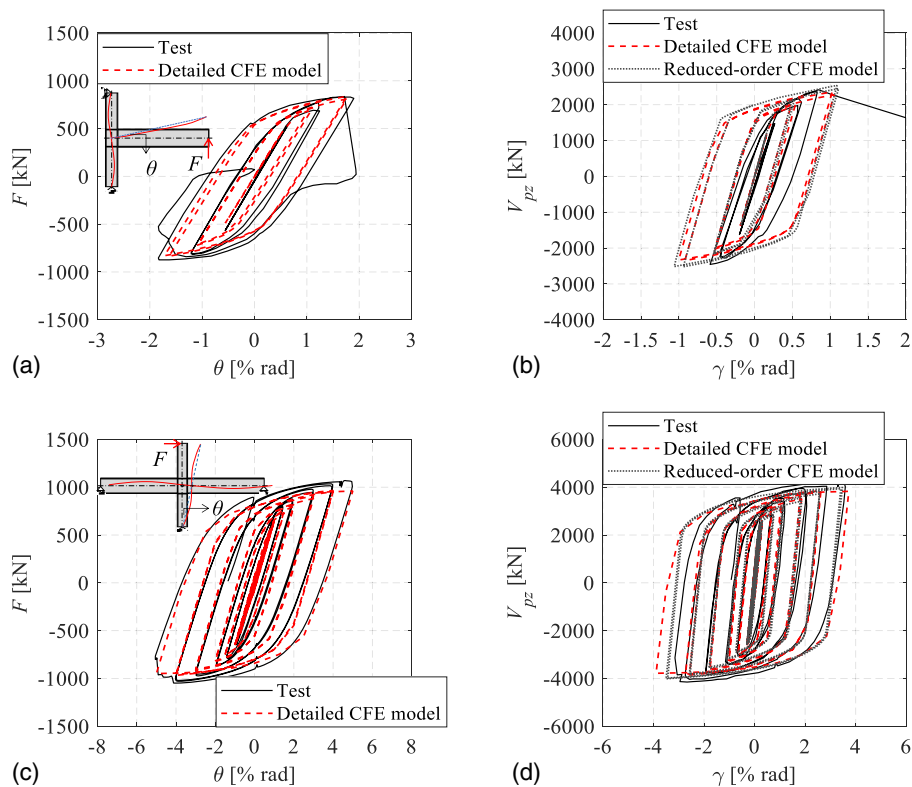
Fig. 5. Comparison of CFE model prediction and test data: (a) load–story drift ratio (data from FEMA 1997); (b) load–panel zone shear distortion (data from FEMA 1997); (c) load–story drift ratio (data from Ricles et al. 2004); and (d) load–panel zone shear distortion (data from Ricles et al. 2004).
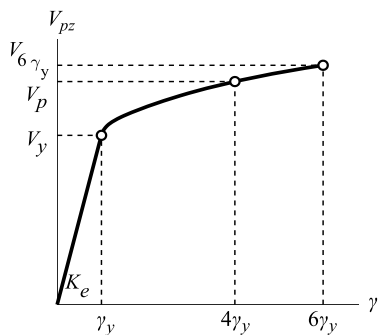

Fig. 6. Deduced panel zone performance parameters.

Finally, the postyield panel zone shear strength is deduced at two representative shear distortion levels, $4\gamma_y$ (V_p) and $6\gamma_y$ ($V_{6\gamma_y}$). The latter is considered, since there may be appreciable reserve shear strength attributed to the column flange contribution along with strain hardening due to column web shear yielding.

Discussion

Fig. 7 shows a comparison of representative CFE simulations for various panel zone aspect ratios, d_b/d_c, and the predicted behavior according to the Krawinkler model. As expected, the figure suggests that the deviation of the predicted elastic stiffness, K_e [Eq. (1)], the yield strength, V_y [Eq. (2)], and the postyield strength, V_p [Eq. (3)], from the CFE results may be appreciable depending on the panel zone aspect ratio and the column flange thickness. In particular, for slender panel zones (i.e., $d_b/d_c = 1.5$ and

$t_{cf} = 24$ mm) the measured elastic stiffness is about 30% lower than the predicted one since the Krawinkler model neglects the bending contribution [Fig. 1(b)]. However, for stocky and shallow panel zones with an aspect ratio of one and thick flanges ($t_{cf} \cong 50$ mm), where the shear deformation mode is dominant, the Krawinkler model predicts K_e reasonably well, though the panel zone stiffness is still underpredicted by 10%–15% owing to the assumed effective shear area (Charney et al. 2005). The same observations hold true for V_y. The Krawinkler model overestimates V_p by more than 20% for stocky and shallow panel zones. For the cross-sectional range that the same model was calibrated for, the postyield shear strength is only overestimated by up to 10%.

The aforementioned deviations can be justified by examining the stress distributions within the panel zone. Fig. 8 shows the shear stress distributions for two characteristic panel zone geometries, normalized by the yield shear stress, τ_y ($\tau_y = f_y/\sqrt{3}$), at a shear distortion angle equal to γ_y, $4\gamma_y$, and $6\gamma_y$. The shear stress distributions are extracted from the column cross section corresponding to the beam centerline. Superimposed in the same figure are planes representing the average shear stress in the column web. Referring to Fig. 8(a), the common assumption of a uniform shear distribution in the column web is not rational for slender panel zones, particularly at shear distortions near yielding, whereas the column flange contribution to shear yielding is indeed negligible.

Referring to Fig. 8(b), stocky and shallow panel zones experience almost uniform shear stresses in their web regardless of the shear angle distortion. The contribution of the column flanges to the attained shear stresses (maximum of $4\%\tau_y$) may seem insignificant for shear distortion levels of γ_y. However, since the flange area of stocky cross sections outweighs that of their web, the resultant force is significant (15%–40% of the total panel zone shear force, depending on the shear distortion level).
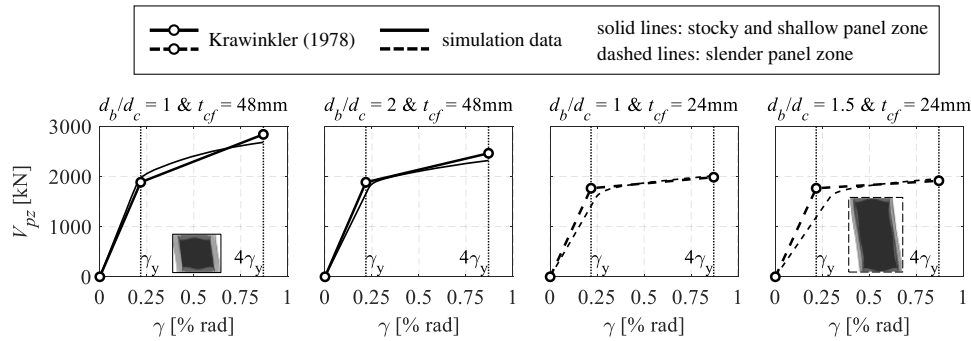
Fig. 7. Representative CFE analysis results with varying web panel zone aspect ratio and column flange thickness.
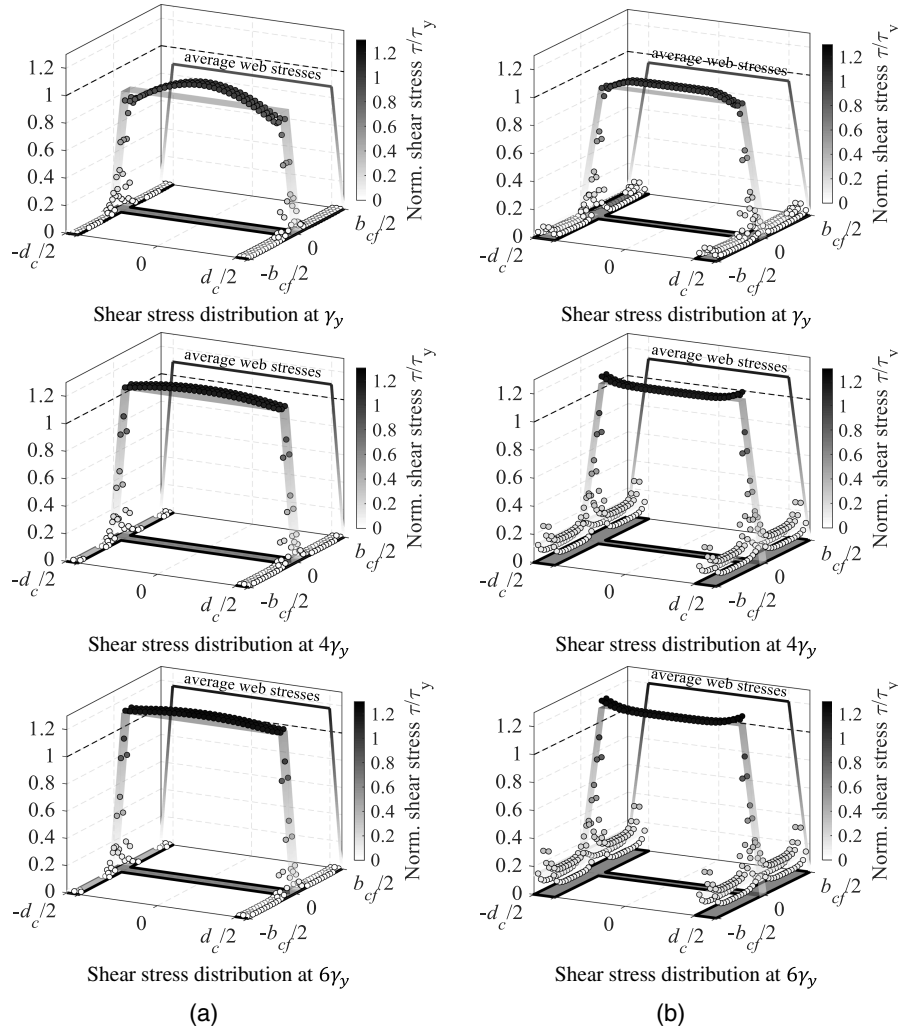

Fig. 8. Shear stress distributions at γ_y, $4\gamma_y$, and $6\gamma_y$ for slender and stocky and shallow panel zones: (a) slender panel zone (i.e., $d_b/d_c = 1.5$ and $t_{cf} = 25$ mm); and (b) stocky and shallow panel zone (i.e., $d_b/d_c = 1.0$ and $t_{cf} = 50$ mm).

Proposed Panel Zone Model

Panel Zone Elastic Stiffness

The proposed panel zone elastic stiffness, K_e [Eq. (4)], is derived based on both shear and bending deformation modes, as shown in Fig. 1. The shear mode is accounted for based on Eq. (5). The bending mode is deduced based on the elastic stiffness (in terms of $V_{pz} - \gamma$ relation) of a beam in contraflexure, according to Eq. (6):

$$K_e = \frac{V_{pz}}{\gamma} = \frac{K_s \cdot K_b}{K_s + K_b} \tag{4}$$

$$K_s = A_v \cdot G = t_{pz} \cdot (d_c - t_{cf}) \cdot G \tag{5}$$

$$K_b = \frac{12 \cdot E \cdot I}{d_b^3} \cdot d_b \tag{6}$$

The proposed model assumes a panel zone shear strength equilibrium instead of shear deformation compatibility. Therefore,
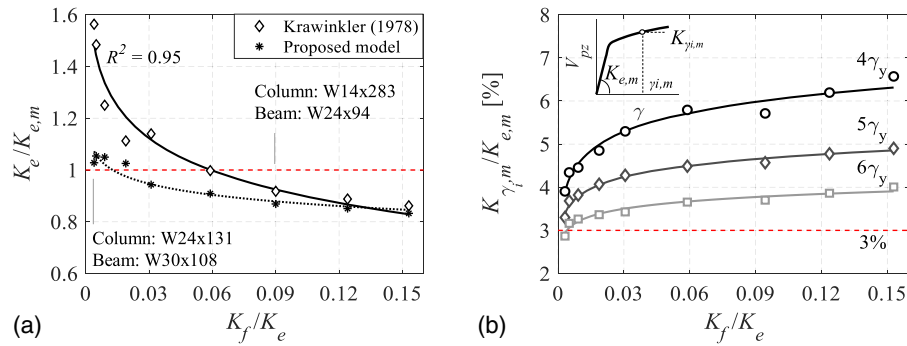
Fig. 9. (a) Deviation of predicted K_e from measured $K_{e,m}$ with respect to K_f/K_e; and (b) normalized panel zone stiffness at representative shear distortion levels with respect to K_f/K_e.

the proposed panel zone stiffness is computed based on Eq. (4) by considering the two deformation modes in series (i.e., $\gamma = \gamma_{shear} + \gamma_{bending}$) (Fig. 1). In Eqs. (4)–(6), I is the second moment of area of the column cross section (including the doubler plate thickness, if any) with respect to the column's strong axis, and A_v is the effective shear area according to Charney et al. (2005). Although other panel zone models (AISC 2016c; Fielding and Huang 1971; Kato et al. 1988; Lui and Wai-Fah 1986; Mulas 2004) assume an effective depth, $d_{eff} = d_c$, the panel zone shear stiffness (and strength) tends to be overestimated by about 10% for stocky column cross sections ($t_{cf} > 40$ mm) based on the foregoing assumption. Note here that the second moment of area, I, refers to that of the full column cross section. Other researchers who attempted to address the bending deformation mode issue (Kim et al. 2015) accounted for the column flange deformation mode independently of the column web.

Panel Zone Shear Strength

To predict a realistic yield and postyield panel zone shear strength, the shear stress distributions in the panel zone from Fig. 8 are employed. The panel zone shear force, V_{pz}, at a distortion, γ, may be approximated by Eq. (7), where V_f is the shear force resisted by a single column flange, and V_w is the shear force resisted by the column web. In turn, V_f may be assumed to be proportional to the ratio of the column flange stiffness, K_f, to the panel zone's elastic stiffness, K_e, according to Eq. (8). The column flange stiffness may be computed using Eq. (9) by considering both shear and bending deformation modes, as depicted by Eqs. (10) and (11), respectively:

$$V_{pz} = 2V_f + V_w \tag{7}$$

$$V_f = (K_f/K_e) \cdot V_{pz} \tag{8}$$

Eq. (10) assumes a uniform shear stress distribution in the column flanges, while Eq. (11) assumes contraflexure deformation with respect to the weak axis of the column flanges:

$$K_f = \frac{K_{sf} \cdot K_{bf}}{K_{sf} + K_{bf}} \tag{9}$$

$$K_{sf} = 2 \cdot (t_{cf} \cdot b_{cf} \cdot G) \tag{10}$$

$$K_{bf} = 2 \cdot \left[\frac{12E(b_{cf} \cdot t_{cf}^3/12)}{d_b^3} \cdot d_b \right] \tag{11}$$

In the preceding equations, the K_f/K_e ratio provides an estimate of the panel zone shear force resisted by the column flanges. In particular, Fig. 9(a) shows how K_f/K_e influences the deduced K_e for the examined panel zone geometries discussed earlier. In the vertical axis, these parameters are either predicted by the proposed or the Krawinkler model. The predicted stiffness, K_e, is normalized by the $K_{e,m}$ deduced from the CFE results. The dashed line at an abscissa value of 1.0 represents the ideal agreement between the virtual tests and the analytical model predictions.

Referring to Fig. 9(a), the proposed panel zone stiffness from Eq. (4) shows improved accuracy over the Krawinkler model, particularly for slender panel zone geometries ($K_f/K_e < 0.02$). For stocky and shallow panel zone geometries ($K_f/K_e > 0.07$), the effective area limitation as per Charney et al. (2005) leads to at least the same accuracy as the Krawinkler model since the bending deformation mode is negligible.

Fig. 9(b) shows the normalized postyield panel zone stiffness, K_{γ_i}, at various shear distortions (i.e., $4\gamma_y$, $5\gamma_y$, and $6\gamma_y$) with respect to K_f/K_e. The K_{γ_i} is deduced from the tangential slope of the $V_{pz} - \gamma$ relation. Note that beyond $4\gamma_y$, the tangent stiffness is used to provide a consistent comparison with the constant $0.03K_e$ post-$4\gamma_y$ that has been historically assumed in the literature (Gupta and Krawinkler 2000; Slutter 1981). This figure suggests that at $4\gamma_y$, the postyield panel zone stiffness reaches $0.07K_e$, whereas at $6\gamma_y$ it attains $0.04K_e$. The K_{γ_i}/K_e, at $4\gamma_y$, of stocky and shallow panel zones ($K_f/K_e > 0.07$) doubles compared to slender ones. Consequently, the empirical post-$4\gamma_y$ stiffness of $0.03K_e$ (Gupta and Krawinkler 2000; PEER/ATC 2010; Slutter 1981) is irrational for most panel zone geometries. Instead, the panel zone shear strength at a shear distortion angle of $6\gamma_y$ should be used with V_p to define the corresponding slope. This may also be more effective for optimal balanced design of beam-to-column joints in capacity-designed steel MRFs. Large panel zone shear distortions may raise concerns regarding localized deformations, consequential implications for system level response, and increased potential for weld fractures (Chi et al. 1997; El-Tawil et al. 1999; Lu et al. 2000; Mao et al. 2001; Ricles et al. 2000, 2004). However, experimental data from recently compiled databases with over 100 post-Northridge bare steel and composite-steel beam-to-column connections (El Jisr et al. 2019; Skiadopoulos and Lignos, forthcoming) that exhibited inelastic behavior in their web panels did not experience premature fracture, even at inelastic shear distortions up to $10\gamma_y$, as discussed earlier.

The panel zone shear strength can generally be computed using Eq. (12) by summing up the surface integral of the shear stresses along the panel zone's web and flange areas. A realistic shear stress distribution should be deduced at a given shear distortion level for
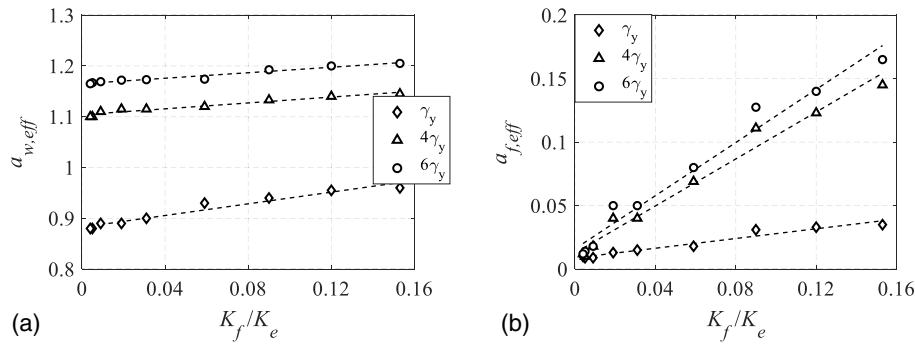
Fig. 10. Normalized average shear stress at γ_y, $4\gamma_y$, and $6\gamma_y$ for (a) web; and (b) flange.

this purpose. Given the discrete finite-element mesh, the surface integral in Eq. (12) can be replaced by the double summation of the shear stresses as given by Eq. (13):

$$V_{pz} = \int_A \tau dA = \int_{A_w} \tau dA_w + 2 \int_{A_f} \tau dA_f \qquad (12)$$

The parameters a_w and a_f, introduced in Eq. (13), represent the shear stress of each element in the column web and each flange, respectively, normalized by the shear stress at yielding, τ_y. In these equations, the yield stress of the web and flanges is assumed to be the same. Since the column flanges and web element size was kept constant in the CFE model, Eq. (13) can be rewritten as in Eq. (14):

$$V_{pz} = \frac{f_y}{\sqrt{3}} \cdot \sum_{-d_c/2}^{d_c/2} \sum_{-t_{cw}/2}^{t_{cw}/2} a_w(x,y)\delta_x\delta_y$$
$$+ \frac{f_y}{\sqrt{3}} \cdot 2 \sum_{-b_{cf}/2}^{b_{cf}/2} \sum_{-t_{cf}/2}^{t_{cf}/2} a_f(x,y)\delta_x\delta_y \qquad (13)$$

$$V_{pz} = \frac{f_y}{\sqrt{3}} \cdot \frac{d_c \cdot t_{cw}}{N_w} \cdot \sum_{-d_c/2}^{d_c/2} \sum_{-t_{cw}/2}^{t_{cw}/2} a_w(x,y)$$
$$+ \frac{f_y}{\sqrt{3}} \cdot 2 \frac{(b_{cf} - t_{cw}) \cdot t_{cf}}{N_f} \cdot \sum_{-b_{cf}/2}^{b_{cf}/2} \sum_{-t_{cf}/2}^{t_{cf}/2} a_f(x,y) \qquad (14)$$

where N_w and N_f are the number of finite elements of the web and each flange, respectively. Finally, as per Eq. (15), the panel zone shear strength can be expressed in terms of a_{eff} [Eq. (16)], which is the average shear stress within the column flanges or web (i.e., sum of all stresses divided by the number of elements in a given component), normalized by τ_y:

$$V_{pz} = a_{w,eff} \cdot \frac{f_y}{\sqrt{3}} \cdot (d_c - t_{cf}) \cdot t_{cw} + a_{f,eff} \cdot \frac{f_y}{\sqrt{3}} \cdot (b_{cf} - t_{cw}) \cdot 2t_{cf}$$
$$(15)$$

$$a_{w,eff} = \frac{\sum_{-d_c/2}^{d_c/2} \sum_{-t_{cw}/2}^{t_{cw}/2} \tau_w \delta x \delta y}{t_{cw} \cdot (d_c - t_{cf}) \cdot \tau_y} \quad \text{and}$$
$$a_{f,eff} = \frac{\sum_{-b_{cf}/2}^{b_{cf}/2} \sum_{-t_{cf}/2}^{t_{cf}/2} \tau_f \delta x \delta y}{t_{cf} \cdot b_{cf} \cdot \tau_y} \qquad (16)$$

Fig. 10 illustrates the normalized average shear stresses of the column web and flanges from Eq. (16), as a function of K_f/K_e, at

shear distortions of γ_y, $4\gamma_y$, and $6\gamma_y$. The linear regression curves for these relationships are superimposed in this figure, and their statistical values (mean, standard deviation, and coefficient of determination, R^2) are summarized in Table 1 for reference. Fig. 10(a) suggests that, in general, and even for high shear distortions ($\gamma = 6\gamma_y$), the influence of K_f/K_e on the column web stress contribution is not significant, as suggested by the mild slope of the fitted trend lines. Quantitatively, this is expressed by the miniscule standard deviation values shown in Table 1 at $4\gamma_y$ and $6\gamma_y$. Accordingly, the average stress of the web at these distortions may be approximated by a single value regardless of the panel zone geometry. Referring to Fig. 10(b), when $K_f/K_e > 0.07$ (stocky panel zones), the average stress of the column flange is significant for shear distortions larger than γ_y. In contrast, for slender panel zones ($K_f/K_e < 0.02$), the column flange average stress is negligible; hence, the column flange contribution to the panel zone shear strength is not important.

A set of panel zone shear strength equations at γ_y (i.e., V_y), $4\gamma_y$ (i.e., V_p), and $6\gamma_y$ (denoted by $V_{6\gamma_y}$) are proposed in support of the contemporary seismic design of steel MRFs. According to Eq. (17), the proposed V_y is as follows:

$$V_y = \frac{[0.58(K_f/K_e) + 0.88] \cdot \frac{f_y}{\sqrt{3}} \cdot (d_c - t_{cf}) \cdot t_{pz}}{1 - K_f/K_e}$$
$$= \frac{f_y}{\sqrt{3}} \cdot a_y \cdot (d_c - t_{cf}) \cdot t_{pz} \qquad (17)$$

where $a_y = 0.9$ and 1.0 for slender and stocky panel zones, respectively. Note that for stocky panel zones, Eq. (17) matches the V_y of the Krawinkler model.

The proposed panel zone shear strength for V_p and $V_{6\gamma_y}$ is given by Eq. (18) along with recommended values for $a_{w,eff}$ and $a_{f,eff}$ in Table 2 directly extracted from representative shear stress profiles of panel zone geometries. Interpolation may be used for the

Table 1. Statistical parameters for linear regression curves of $a_{eff} - K_f/K_e$ relationships

Location	Distortion level	Mean	Standard deviation	R^2
Web	γ_y	0.91	0.032	0.95
	$4\gamma_y$	1.1	0.016	0.94
	$6\gamma_y$	1.2	0.015	0.96
Flange	γ_y	0.019	0.011	0.95
	$4\gamma_y$	0.063	0.051	0.98
	$6\gamma_y$	0.073	0.058	0.97

Table 2. Normalized average shear stress values and expressions in web and flanges based on proposed model

Equation		General case	Simplified case	
			Slender panel zone	Stocky panel zone
Web ($a_{w,eff}$)	$4\gamma_y$ (V_p)	1.1		
	$6\gamma_y(V_{6\gamma_y})$	1.15		
Flange ($a_{f,eff}$)	$4\gamma_y$ (V_p)	$0.93(K_f/K_e) + 0.015$	0.02	0.1
	$6\gamma_y(V_{6\gamma_y})$	$1.05(K_f/K_e) + 0.02$	0.03	0.1

corresponding a_{eff} values when the panel zone geometry is neither slender nor stocky (i.e., $K_f/K_e = 0.02$–0.07):

$$V_{pz} = \frac{f_y}{\sqrt{3}} \cdot [a_{w,eff} \cdot (d_c - t_{cf}) \cdot t_{pz} + a_{f,eff} \cdot (b_{cf} - t_{pz}) \cdot 2t_{cf}]$$

(18)

Proposed Panel Zone Model Validation

Fig. 11 shows a comparison of the panel zone's hysteretic response from characteristic full-scale tests (Ricles et al. 2004; Shin 2017) and the predicted envelope curve based on the proposed model. For reference, the AISC (2016c) model is superimposed in the same figure. The additional third branch slope of $0.03K_e$ is also considered beyond V_p (Gupta and Krawinkler 2000; PEER/ATC 2010; Slutter 1981). The comparisons highlight the superior accuracy of the proposed model in predicting the panel zone's shear strength and stiffness over the AISC model, which consistently overestimates the same quantities by nearly 30%. Moreover, the assumed $0.03K_e$ stiffness in the third branch is not justifiable for slender panel zones, as discussed earlier [Fig. 11(a)].

An assembled inelastic panel zone database (Skiadopoulos and Lignos, forthcoming) comprising specimens without doubler plates in the panel zone is also used to further validate the accuracy of the proposed panel zone stiffness and Eq. (18) for both V_p and $V_{6\gamma_y}$. Referring to Fig. 12(a), the proposed panel zone stiffness matches the experimental data relatively well. The maximum error is up to 15% and for only two cases. Referring to Fig. 12(b), while the AISC (2016c) panel zone model does not depict the influence of column flange thickness, t_{cf}, on V_p, the proposed model is sufficient regardless of the panel zone geometry. Referring to Fig. 12(c),

same trends hold true for $V_{6\gamma_y}$. Notably, for cross sections with $t_{cf} > 40$ mm, the proposed model is remarkably better than the current state of the seismic design practice.

Effect of Doubler Plates

The impact of utilizing doubler plates and their influence on the proposed model sufficiency are examined by means of supplemental CFE simulations featuring shallow and stocky (W14 × 398) as well as deep (W24 × 131) column cross sections with a one-sided thick doubler plate ($t_{dp} > 40$ mm). Table 3 summarizes the virtual test matrix. It is composed of panel zones in which the doubler plates are either welded with CJP or fillets to the respective column. The respective details are shown schematically in Figs. 13(a and b). Note that the examined welded configurations are consistent with the current practice (AISC 2016b; AWS 2016). The shallow and stocky column (W14 × 398) does not necessitate the presence of continuity plates according to the AISC (2016b) provisions. The doubler plate thickness is determined by the fillet radii of the column cross section to avoid welding in its k-area (Lee et al. 2005). Since for both cross sections the fillet radius, r, used for detailing equals 33 mm, this leads to a doubler plate thickness of $t_{dp} = 35$ mm (1.375 in.). The corresponding fillet welds have a leg thickness of $t_w = 48$ mm by assuming that the filler metal classification strength, $F_{EXX} = 1.2F_{ycw}$ (F_{ycw} = yield stress of column web base material). The calculated fillet weld material thickness satisfies the AISC (2016b) provisions. The doubler plate yield stress is assumed to be $F_{ydp} = 1.1F_{ycm}$. Neither a plug welding nor a horizontal welding on the top and bottom of doubler plates is necessary for the examined cases according to AISC (2016b). Either way, the preceding weld details would have increased the shear stress compatibility between the doubler plate and the column web. The column region is modeled with the procedures discussed earlier. The doubler plate, which extends by $0.5d_b$ from the beam flanges, is modeled with quadratic brick elements with reduced integration (C3D20R). These are used to better capture the stress distribution through the thickness of the doubler plate. Hard contact, which allows for separation but not penetration, is used between the doubler plate and the column web. In turn, the doubler plate is tied with the welding material, which was modeled explicitly as shown in Fig. 13.

Three loading histories are used—a monotonic, a ramped cyclic symmetric (AISC 2016b), and a collapse-consistent loading protocol (Suzuki and Lignos 2020)—to account for potential
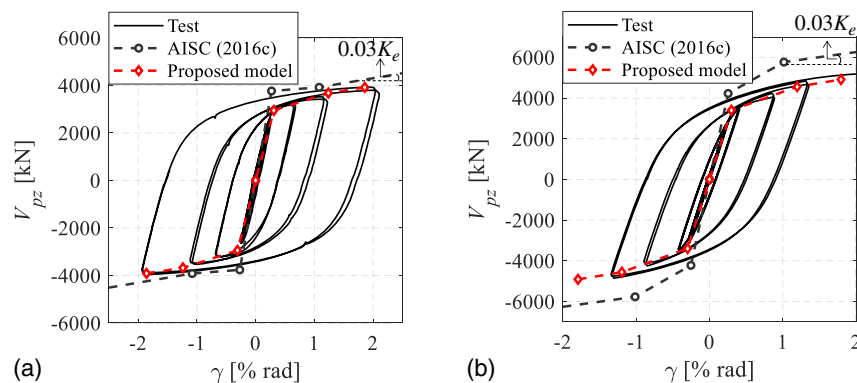

Fig. 11. Comparison of measured and predicted panel zone hysteretic responses: (a) slender panel zone, $K_f/K_e = 0.003$ (beam: W30 × 108, column: W24 × 131) (data from Ricles et al. 2004); and (b) stocky panel zone, $K_f/K_e = 0.07$ (beam: W36 × 150, column: W14 × 398) (data from Shin 2017).
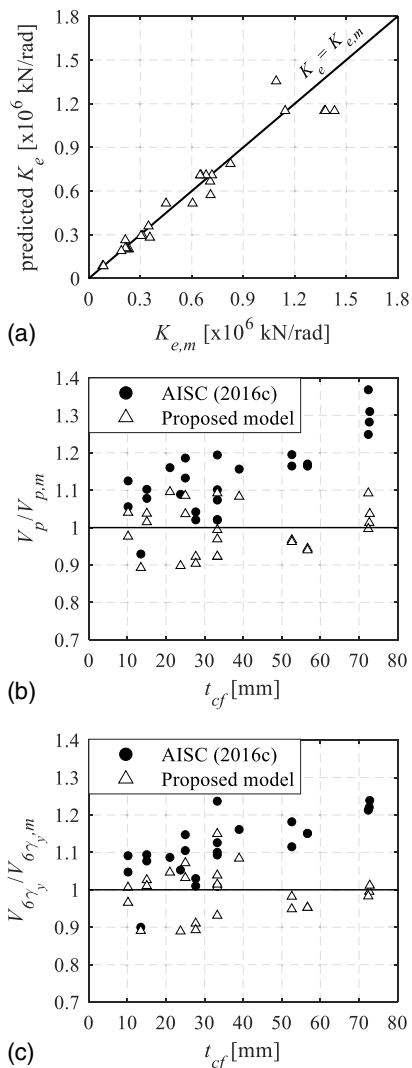
Fig. 12. Comparison of proposed panel zone stiffness and shear strength at $4\gamma_y$ and $6\gamma_y$ versus measured ones from inelastic panel zone test data without doubler plates: (a) $K_e/K_{e,m}$; (b) $V_p/V_{p,m}$; and (c) $V_{6\gamma_y}/V_{6\gamma_{y,m}}$.

Table 3. Virtual test matrix for examination of doubler plate effectiveness

Column	Beam	Doubler plate thickness (mm)	Welding type	Loading protocol
W14 × 398	W36 × 150	35	CJP Fillet	Cyclic symmetric Monotonic Cyclic symmetric Collapse-consistent
W24 × 131	W30 × 108		CJP Fillet	Cyclic symmetric Monotonic Cyclic symmetric Collapse-consistent

accumulation of doubler plate shear stress incompatibility throughout the loading history. The shear stress incompatibility between the doubler plate and the column web is quantified based on the relative difference between the average shear stresses in the column web, $\bar{\tau}_{cw}$, and doubler plates, $\bar{\tau}_{dp}$, i.e., $(\bar{\tau}_{cw} - \bar{\tau}_{dp})/\bar{\tau}_{dp}$.
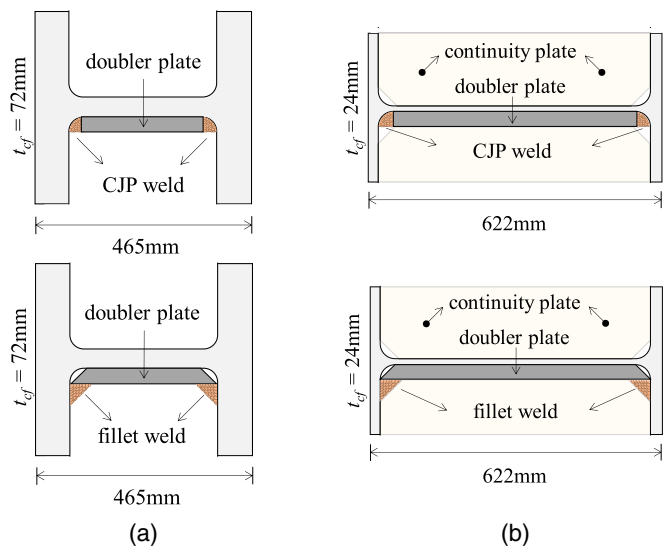
Fig. 13. CFE model CJP and fillet weld details: (a) column: W14 × 398; and (b) column: W24 × 131.

Figs. 14(a and b) show the preceding metric with respect to the accumulated panel zone shear distortion, $\Sigma\gamma$, for deep (W24 × 131) as well as shallow and stocky (W14 × 398) columns, respectively. Prior to panel zone yielding (i.e., γ_y), the stresses in the column web are higher than those in the doubler plate by 10%–30%, depending on the cross section and the weld specification. However, once both the doubler plate and the column web yield, the relative difference in their shear stress demand will be no more than −10%. This is attributed to the fact that the yield stress of the doubler plate is deliberately assumed to be 10% higher than that of the column web. This indicates no evident stress incompatibility between the doubler plate and the column web.

Referring to Figs. 14(a and b), a CJP weld provides higher shear stress compatibility (more than 90%) compared to fillet-welded doubler plates (70%–80% at shear distortions lower than γ_y). It is also observed that the relative difference is initially higher for stocky and shallow columns compared to deep ones. However, after panel zone yielding, this difference diminishes. This is more apparent in Fig. 14(c) under the collapse-consistent loading protocol, regardless of the examined column cross section. In brief, Fig. 14 suggests that the doubler plate ineffectiveness is not an issue for beam-to-column connections detailed according to AISC (2016b) and AWS (2016). For thick fillet-welded doubler plates, if the requirement for very thick fillet welds (so that the stresses exerted by the column are properly attained by the doubler plate) is met, the doubler plate(s) and the column web attain fairly similar shear stresses. Therefore, the total panel zone thickness, including the double plate(s) (i.e., $t_{pz} = t_{cw} + t_{dp}$), may be directly employed in Eqs. (4), (17), and (18). Fig. 15 illustrates indicative comparisons between the proposed model and data from full-scale beam-to-column joints with doubler plates retrieved from the analyzed inelastic panel zone cases.

The authors are of the opinion that the doubler plate-to-column web shear-stress incompatibility, which was mostly highlighted in prior studies on pre-Northridge beam-to-column connections (Slutter 1981), is attributed to the uncertainty of the welding material and the weld specifications that were used at that time. Differences in material properties between doubler plates (e.g., use of A36 plates) and the corresponding column (e.g., A992 or A572 Gr. 50) could have attributed to some of the reported differences.
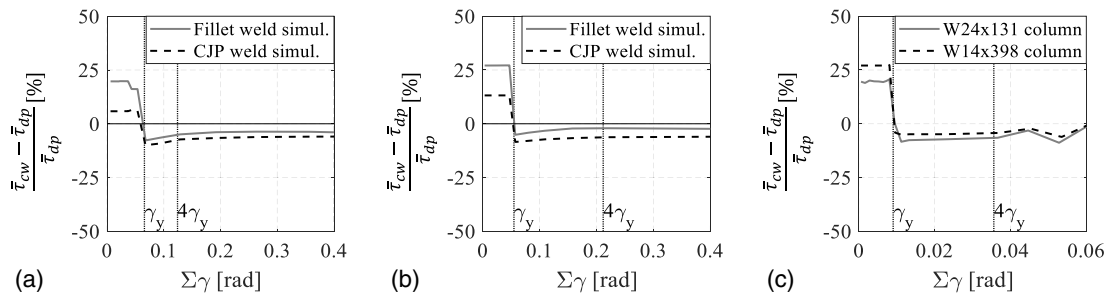
Fig. 14. Relative difference in average shear stresses between doubler plate and column web versus accumulated panel zone shear distortion: (a) column: W24 × 131—symmetric cyclic protocol; (b) column: W14 × 398—symmetric cyclic protocol; and (c) collapse-consistent protocol.
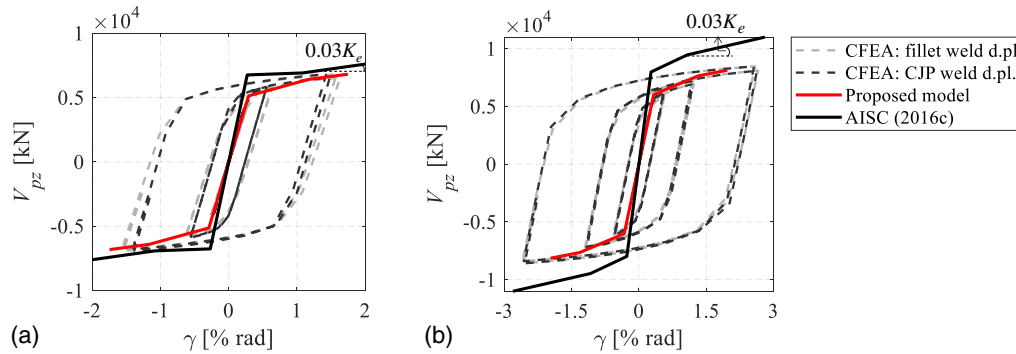

Fig. 15. Comparison of measured and predicted response of panel zones with fillet- and CJP-welded doubler plates: (a) W24 × 141 column; and (b) W14 × 398 column.

Effect of Axial Load

This section examines how the axial load should be considered within the proposed model to design/model inelastic panel zones in end (exterior) and interior steel MRF beam-to-column connections. In the former, columns experience axial load variations due to the transient axial load component. Doubler plates are omitted in these simulations since this effect was separately examined in the previous section. Table 4 summarizes the virtual test matrix that was examined in this case. In brief, a gravity load ratio, P_g/P_y, of 15%, 30%, and 50% is considered for interior columns, whereas $P_g/P_y = 15$% is assumed for end columns. The first two values are deemed reasonable based on nonlinear response history analyses of representative four- and eight-story steel MRF designs (Elkady and Lignos 2014, 2015) according to current design specifications.

Table 4. Virtual test matrix for examination of axial load effect

Column	Beam	No. of stories	Joint location	P_g/P_y (%)
W14 × 398	W36 × 150	—	Interior	15
				30
				50
		4	End	15
		8		
W24 × 131	W30 × 108	—	Interior	15
				30
				50
		4	End	15

The last gravity load ratio may be representative in existing high-rise steel MRF buildings designed prior to the 1994 Northridge earthquake (Bech et al. 2015). The axial load demand variation in end columns is depicted based on representative loading histories developed for experimental testing of steel MRF columns (Suzuki and Lignos 2020). In particular, the imposed axial load demand, P/P_y, varies from −10% (tension) to 40% (compression) for the eight-story and from 5% to 25% for the four-story MRF, as retrieved from Suzuki and Lignos (2020). This is coupled with the imposed same shear distortion demand as the interior columns.

According to the AISC (2016c) specifications, no reduction in the panel zone shear strength will be introduced if it is designed to attain inelastic deformations (i.e., $n < 0.75$). If the panel zone was designed to remain elastic [based on $R_{n,el}$ from AISC (2016c) specifications], then a reduction based on the von Mises criterion (von Mises 1913) would be employed. In prior work by Kim et al. (2015), it was assumed that the axial load was only sustained by the column flanges. However, this does not hold true because the present study suggests that the column web contribution in sustaining the axial load demand may be as high as 40%. As such, in the proposed model, n accounts for the full column cross section with regard to the axial yield strength calculation. The relative difference between the panel zone shear resistance with/without the applied axial load throughout the loading history is computed as $(V_{pz}^{n=0} - V_{pz}^{n>0})/V_{pz}^{n=0}$ to evaluate the influence of the axial load.

Interior Columns

Fig. 16 shows the relative difference in interest versus the accumulated panel zone shear distortion, $\sum \gamma$, for the examined
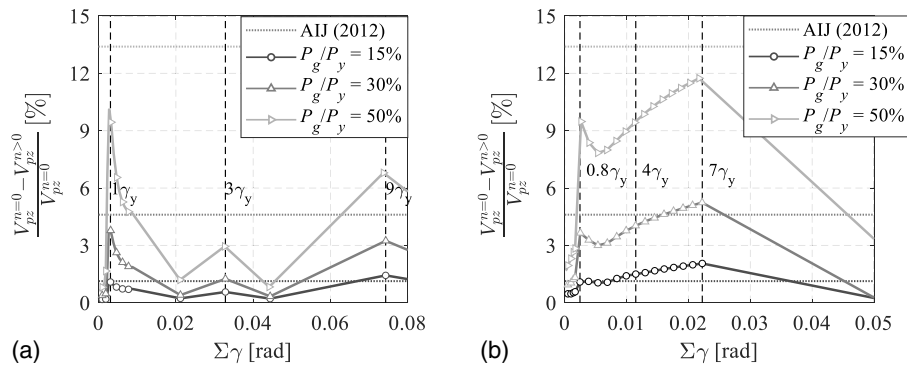
Fig. 16. Panel zone relative difference between panel zone shear strength with/without applied axial load versus accumulated panel zone shear distortion for interior columns: (a) W24 × 131 column; and (b) W14 × 398 column.

interior columns. In the same figure, a line is superimposed representing the relative difference according to AIJ (2012). The two plots of this figure are not schematically comparable since the panel zone shear distortion history differs in both cases. Moreover, owing to the imposed cyclic loading history, the relative difference reaches zero when the panel zone shear strength reaches zero as well. It is observed that the von Mises criterion, which is adopted by AIJ (2012) and AISC (2016c) for elastic panel zone design, corresponds well to the results regardless of the $\sum \gamma$ level. However, for inelastic panel zone design that no reduction in strength would be applied according to AISC (2016c), the panel zone shear resistance is overestimated by more than 10% for $P_g/P_y >30\%$, depending on the cross section. However, the aforementioned gravity load ratio range is uncommon in contemporary steel MRF designs (Elkady and Lignos 2014, 2015; Suzuki and Lignos 2020).

End Columns

Fig. 17 depicts the reduction in shear strength for both interior and end column panel zones for an eight-story MRF. It is observed that applying the von Mises criterion only for the applied gravity load leads to marginally unconservative results (approximately 10%). Therefore, the panel zone shear strength reduction should be applied for the absolute peak load ratio P/P_y including the transient axial load component. For a four-story MRF, the panel zone shear strength reduction is negligible (less than 4%) owing to the decreased axial load variation in end columns.
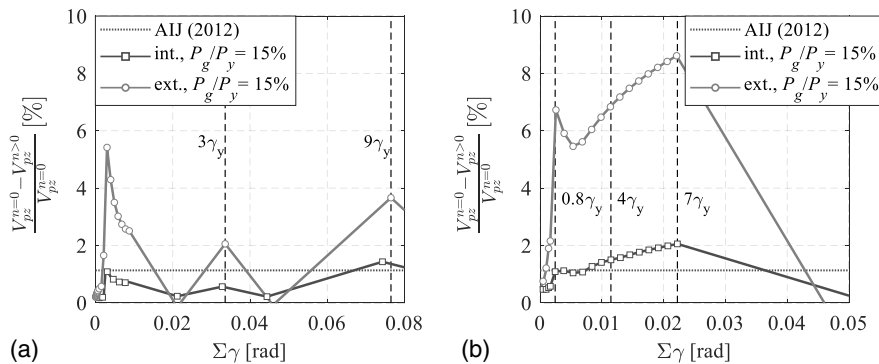
Limitations of Present Study

The proposed panel zone model neglects the influence of the composite action on the panel zone behavior. This is an important aspect to consider (Castro et al. 2005; El Jisr et al. 2019; Elkady and Lignos 2014; Kim and Engelhardt 2002). On the other hand, practical methods to decouple slabs from steel columns/panel zones are available (Chaudhari et al. 2019; Tremblay et al. 1997). While the effect of cyclic hardening on the panel zone shear strength was disregarded, during design-basis earthquakes, capacity-designed steel MRFs are likely to experience modest lateral drift demands (i.e., 2%); therefore, the panel zone is likely to experience shear distortions of nearly $4\gamma_y$, depending on the panel zone-to-beam relative strength ratio. Cyclic hardening is fairly minor for this range of shear distortions; thus, the proposed model should predict fairly well the panel zone shear strength. Moreover, at seismic intensities associated with low-probability seismic events (i.e., 2% in 50 years), the steel MRF behavior is expected to be asymmetric owing to ratcheting (Lignos et al. 2011, 2013). Shake table collapse experiments (Lignos et al. 2013; Suita et al. 2008) suggest that panel zone inelastic behavior is fairly similar to that depicted by the examined collapse-consistent loading protocol. Moreover, the use of A36 doubler plates with A992 Grade 50 steel columns was not investigated. While this practice appeared to be a default choice in pre-Northridge steel MRF designs, the use of A572 Grade 50 doubler plates with A992 Grade 50 steel columns appears to be the current practice in modern seismic-resistant steel MRFs. Finally, the proposed model should be further validated for beam-to-column connections comprising hollow structural columns.

Fig. 17. Panel zone relative reduction due to axial force versus accumulated panel zone shear distortion for both interior and exterior columns (eight-story steel MRF): (a) W24 × 131 column; and (b) W14 × 398 column.

Summary and Conclusions

This paper presents a new panel zone model for the seismic design and analysis of beam-to-column panel zone joints in capacity-designed MRFs. The proposed model, which is developed on the basis of structural mechanics, reflects the realistic stress distributions within a panel zone joint geometry. These distributions are extracted from CFE models, which are thoroughly validated to available experimental data from pre- and post-Northridge interior and exterior subassemblies. Improved equations are proposed for predicting the panel zone stiffness and shear strength at discrete levels of panel zone shear distortion pertinent to the balanced design of steel MRF beam-to-column joints according to current seismic provisions.

The CFE simulation results underscore that the commonly used assumption of uniform shear yielding is only valid in panel zone geometries featuring stocky and shallow column cross sections regardless of the inelastic shear distortion level.

The elastic stiffness, K_e [Eq. (4)], of the proposed panel zone model considers both shear and bending deformations based on shear strength equilibrium within the panel zone. Hence, its performance in predicting the elastic stiffness of slender panel zones (beam-to-column depth ratios $d_b/d_c \geq 1.5$) is superior compared to available models in the literature as well as the ones available in current seismic provisions.

The proposed equation [Eq. (17)] for the panel zone shear strength at yield, V_y (i.e., shear distortion of γ_y), matches that of the Krawinkler (1978) model for panel zones that are shear deformation-dominant (i.e., stocky cases) but performs much better in cases where the bending contribution is significant.

Comparisons with available full-scale test data suggest that the proposed model predicts the panel zone shear strength, V_p, [Eq. (18); Table 2], at a shear distortion of $4\gamma_y$ with a noteworthy accuracy even when panel zones feature columns with relatively thick flanges (i.e., $t_{cf} \geq 40$ mm). The current model in the AISC (2016c) seismic specifications overpredicts V_p by 20%–50% depending on the panel zone geometry. In that respect, the proposed model addresses a well-known limitation of available models in the literature.

The CFE simulations reveal that the commonly assumed value of $0.03K_e$ for the stiffness beyond $4\gamma_y$ shear distortions is not justifiable in most panel zone geometries. This is due to the increased column flange contribution to the panel zone strength at large inelastic shear distortions ($\gamma > 4\gamma_y$). For this reason, an expression is proposed to predict the panel zone shear strength, $V_{6\gamma_y}$ [Eq. (18); Table 2], at a shear distortion of $6\gamma_y$.

Based on the examined cases, it is also found that the doubler plate to column web shear stress incompatibility does not appear to be an issue for beam-to-column connections, which are detailed according to current seismic provisions and detailing criteria (AISC 2016b; AWS 2016). Consequently, neither fillet nor CJP welded doubler plates should be treated differently either by reducing their strength or by intentionally accounting for one of the two doubler plates (i.e., CEN 2005). The authors are of the opinion that the doubler plate ineffectiveness reported in the literature is mostly due to weld specifications and construction practices prior to the 1994 Northridge earthquake.

Supplemental CFE simulations suggest that the von Mises criterion (von Mises 1913) may still be used to reduce the predicted panel zone shear strength for both interior and end columns in steel MRFs regardless of the employed lateral loading history. The shear strength reduction should always be based on the peak axial compressive load imposed on the corresponding column, including the transient axial component due to dynamic overturning effects.

Dedication

This paper is dedicated to the memory of Professor Helmut Krawinkler, former professor at Stanford University, who was among the first to identify the importance of the panel zone on the seismic behavior of steel MRFs in the early 1970s. This study builds upon his outstanding contribution and would not have been possible without it.

Data Availability Statement

Some or all data, models, or code generated or used during the study are available in a repository (doi: https://www.doi.org/10.5281/zenodo.3689756) or online in accordance with funder data retention policies. Some or all data, models, or code that support the findings of this study are available from the corresponding author upon reasonable request. The proposed model has been implemented in TCL procedures that can be used for system level simulations with the OpenSees simulation platform. These procedures are made publicly available through GitHub (https://github.com/RESSLab-Team/Panel_Zone_Model_OpenSees).

Acknowledgments

References

AIJ (Architectural Institute of Japan). 2012. *Recommendations for design of connections in steel structures*. [In Japanese.] Tokyo: Architectural Institute of Japan.

AISC. 2016a. *Prequalified connections for special and intermediate steel moment frames for seismic applications*. ANSI/AISC 358-16. Chicago: AISC.

AISC. 2016b. *Seismic provisions for structural steel buildings*. ANSI/AISC 341-16. Chicago: AISC.

AISC. 2016c. *Specification for structural steel buildings*. ANSI/AISC 360-16. Chicago: AISC.

Al-Shawwa, N., and D. G. Lignos. 2013. "Web-based interactive tools for performance-based earthquake engineering." Accessed November 29, 2019. http://resslabtools.epfl.ch/.

AWS (American Welding Society). 2016. *Structural welding code-seismic supplement*. AWS D1.8/D1.8M:2016. Miami: AWS.

Bech, D., B. Tremayne, and J. Houston. 2015. "Proposed changes to steel column evaluation criteria for existing buildings." In *Proc., 2nd ATC-SEI Conf. Improving the Seismic Performance of Existing Buildings and Other Structures*, 255–272. San Francisco: Earthquake Engineering Research Institute. https://doi.org/10.1061/9780784479728.022.

Bertero, V., H. Krawinkler, and E. P. Popov. 1973. *Further studies on seismic behavior of steel beam-column subassemblages*. Berkeley, CA: Earthquake Engineering Research Center, Univ. of California, Berkeley.

Brandonisio, G., A. De Luca, and E. Mele. 2012. "Shear strength of panel zone in beam-to-column connections." *J. Constr. Steel Res.* 71 (Apr): 129–142. https://doi.org/10.1016/j.jcsr.2011.11.004.

Castro, J. M., A. Y. Elghazouli, and B. A. Izzuddin. 2005. "Modelling of the panel zone in steel and composite moment frames." *Eng. Struct.* 27 (1): 129–144. https://doi.org/10.1016/j.engstruct.2004.09.008.

CEN (European Committee for Standardization). 2005. *Design of steel structures—Part 1-8: Design of joints*. EN 1993-1-8: Eurocode 3. Brussels, Belgium: CEN.

Charney, F. A., H. Iyer, and P. W. Spears. 2005. "Computation of major axis shear deformations in wide flange steel girders and columns." *J. Constr. Steel Res.* 61 (11): 1525–1558. https://doi.org/10.1016/j.jcsr.2005.04.002.

Chaudhari, T., G. MacRae, D. Bull, C. Clifton, and S. Hicks. 2019. "Experimental behaviour of steel beam-column subassemblies with different slab configurations." *J. Constr. Steel Res.* 162 (Nov): 105699. https://doi.org/10.1016/j.jcsr.2019.105699.

Chi, B., and C.-M. Uang. 2002. "Cyclic response and design recommendations of reduced beam section moment connections with deep columns." *J. Struct. Eng.* 128 (4): 464–473. https://doi.org/10.1061/(ASCE)0733-9445(2002)128:4(464).

Chi, W. M., G. G. Deirlein, and A. Ingraffea. 1997. *Finite element fracture mechanics investigation of welded beam-column connections*. Ithaca, NY: SAC Joint Venture, Cornell Univ.

Chung, K., S. Kishiki, Y. Matsumoto, and S. Yamada. 2006. "Experimental study on the hysteresis behavior of panel subjected to multi-axial cyclic loadings." [In Japanese.] *J. Struct. Constr. Eng.* 71 (602): 203–210. https://doi.org/10.3130/aijs.71.203_2.

Chung, K., S. Yamada, and I. Yang. 2010. "Simplified uni-axial hysteretic damage model for panel zone of structural steel under earthquake loads." *Int. J. Steel Struct.* 10 (3): 267–281. https://doi.org/10.1007/BF03215836.

Ciutina, A. L., and D. Dubina. 2003. "Influence of column web stiffening on the seismic behaviour of beam-to- column joints." In *Proc. Conf. on Behaviour of Steel Structures in Seismic Areas*, 269–275. Rotterdam, Netherlands: A.A. Balkema.

CSA (Canadian Standard Association). 2019. *Design of steel structures*. CAN/CSA S16-19. Rexdale, Canada: CSA.

de Castro e Sousa, A., Y. Suzuki, and D. Lignos. 2020. "Consistency in solving the inverse problem of the Voce-Chaboche constitutive model for plastic straining." *J. Eng. Mech.* 146 (9): 04020097. https://doi.org/10.1061/(ASCE)EM.1943-7889.0001839.

El Jisr, H., A. Elkady, and D. G. Lignos. 2019. "Composite steel beam database for seismic design and performance assessment of composite-steel moment-resisting frame systems." *Bull. Earthquake Eng.* 17 (6): 3015–3039. https://doi.org/10.1007/s10518-019-00564-w.

Elkady, A., and D. G. Lignos. 2014. "Modeling of the composite action in fully restrained beam-to-column connections: Implications in the seismic design and collapse capacity of steel special moment frames." *Earthquake Eng. Struct. Dyn.* 43 (13): 1935–1954. https://doi.org/10.1002/eqe.2430.

Elkady, A., and D. G. Lignos. 2015. "Effect of gravity framing on the overstrength and collapse capacity of steel frame buildings with perimeter special moment frames." *Earthquake Eng. Struct. Dyn.* 44 (8): 1289–1307. https://doi.org/10.1002/eqe.2519.

Elkady, A., and D. G. Lignos. 2018a. "Full-scale testing of deep wide-flange steel columns under multiaxis cyclic loading: Loading sequence, boundary effects, and lateral stability bracing force demands." *J. Struct. Eng.* 144 (2): 04017189. https://doi.org/10.1061/(ASCE)ST.1943-541X.0001937.

Elkady, A., and D. G. Lignos. 2018b. "Improved seismic design and nonlinear modeling recommendations for wide-flange steel columns." *J. Struct. Eng.* 144 (9): 04018162. https://doi.org/10.1061/(ASCE)ST.1943-541X.0002166.

El-Tawil, S., E. Vidarsson, T. Mikesell, and S. K. Kunnath. 1999. "Inelastic behavior and design of steel panel zones." *J. Struct. Eng.* 125 (2): 183–193. https://doi.org/10.1061/(ASCE)0733-9445(1999)125:2(183).

FEMA. 1997. *Connection test summaries*. Washington, DC: FEMA.

Fielding, D. J., and J. S. Huang. 1971. "Shear in steel beam-to-column connections." *Weld. Res. Suppl.* 50 (7): 313–326.

Ghobarah, A., R. M. Korol, and A. Osman. 1992. "Cyclic behavior of extended end-plate joints." *J. Struct. Eng.* 118 (5): 1333–1353. https://doi.org/10.1061/(ASCE)0733-9445(1992)118:5(1333).

Gupta, A., and H. Krawinkler. 2000. "Dynamic P-delta effects for flexible inelastic steel structures." *J. Struct. Eng.* 126 (1): 145–154. https://doi.org/10.1061/(ASCE)0733-9445(2000)126:1(145).

Han, S. W., G. U. Kwon, and K. H. Moon. 2007. "Cyclic behaviour of post-Northridge WUF-B connections." *J. Constr. Steel Res.* 63 (3): 365–374. https://doi.org/10.1016/j.jcsr.2006.05.003.

Hjelmstad, K. D., and G. Haikal. 2006. "Analysis of steel moment frames with deformable panel zones." *Steel Struct.* 6 (2): 129–140.

Jin, J., and S. El-Tawil. 2005. "Evaluation of FEMA-350 seismic provisions for steel panel zones." *J. Struct. Eng.* 131 (2): 250–258. https://doi.org/10.1061/(ASCE)0733-9445(2005)131:2(250).

Kato, B., W. F. Chen, and M. Nakao. 1988. "Effects of joint-panel shear deformation on frames." *J. Constr. Steel Res.* 10: 269–320. https://doi.org/10.1016/0143-974X(88)90033-8.

Kim, D.-W., C. Blaney, and C.-M. Uang. 2015. "Panel zone deformation capacity as affected by weld fracture at column kinking location." *Eng. J.* 53 (1): 27–46.

Kim, K. D., and M. D. Engelhardt. 2002. "Monotonic and cyclic loading models for panel zones in steel moment frames." *J. Constr. Steel Res.* 58 (5–8): 605–635. https://doi.org/10.1016/S0143-974X(01)00079-7.

Kim, S.-Y., and C.-H. Lee. 2017. "Seismic retrofit of welded steel moment connections with highly composite floor slabs." *J. Constr. Steel Res.* 139 (Dec): 62–68. https://doi.org/10.1016/j.jcsr.2017.09.010.

Krawinkler, H. 1978. "Shear in beam-column joints in seismic design of steel frames." *Eng. J.* 15 (3): 82–91.

Krishnan, S., and J. F. Hall. 2006. "Modeling steel frame buildings in three dimensions. I: Panel zone and plastic hinge beam elements." *J. Eng. Mech.* 132 (4): 345–358. https://doi.org/10.1061/(ASCE)0733-9399(2006)132:4(345).

Lee, D., S. C. Cotton, J. F. Hajjar, R. J. Dexter, and Y. Ye. 2005. "Cyclic behavior of steel moment-resisting connections reinforced by alternative column stiffener details. II: Panel zone behavior and doubler plate detailing." *Eng. J.* 42 (4): 215–238.

Léger, P., P. Paultre, and R. Nuggihalli. 1991. "Elastic analysis of frames considering panel zones deformations." *Comput. Struct.* 39 (6): 689–697. https://doi.org/10.1016/0045-7949(91)90212-5.

Lemaitre, J., and J. L. Chaboche. 1990. *Mechanics of solid materials*. Cambridge, UK: Cambridge University Press.

Li, X.-S., and Y. Goto. 1998. "A three-dimensional nonlinear seismic analysis of frames considering panel zone deformations." *J. Struct. Mech. Earthquake Eng.* 1998 (605): 1–13. https://doi.org/10.2208/jscej.1998.605_1.

Lignos, D. G., T. Hikino, Y. Matsuoka, and M. Nakashima. 2013. "Collapse assessment of steel moment frames based on E-Defense full-scale shake table collapse tests." *J. Struct. Eng.* 139 (1): 120–132. https://doi.org/10.1061/(ASCE)ST.1943-541X.0000608.

Lignos, D. G., H. Krawinkler, and A. S. Whittaker. 2011. "Prediction and validation of sidesway collapse of two scale models of a 4-story steel moment frame." *Earthquake Eng. Struct. Dyn.* 40 (7): 807–825. https://doi.org/10.1002/eqe.1061.

Lin, K. C., K. C. Tsai, S. L. Kong, and S. H. Hsieh. 2000. "Effects of panel zone deformations on cyclic performance of welded moment connections." In *Proc., 12th WCEE*. Auckland, New Zealand: New Zealand National Society for Earthquake Engineering.

Lu, L. W., J. M. Ricles, C. Mao, and J. W. Fisher. 2000. "Critical issues in achieving ductile behaviour of welded moment connections." *J. Constr. Steel Res.* 55 (1–3): 325–341. https://doi.org/10.1016/S0143-974X(99)00092-9.

Lui, E. M., and C. Wai-Fah. 1986. "Frame analysis with panel zone deformation." *Int. J. Solids Struct.* 22 (12): 1599–1627. https://doi.org/10.1016/0020-7683(86)90065-X.

Mao, C., J. Ricles, L. W. Lu, and J. Fisher. 2001. "Effect of local details on ductility of welded moment connections." *J. Struct. Eng.* 127 (9): 1036–1044. https://doi.org/10.1061/(ASCE)0733-9445(2001)127:9(1036).

Mulas, M. G. 2004. "A structural model for panel zones in non linear seismic analysis of steel moment-resisting frames." *Eng. Struct.* 26 (3): 363–380. https://doi.org/10.1016/j.engstruct.2003.10.009.

Ozkula, G., J. Harris, and C.-M. Uang. 2017. "Observations from cyclic tests on deep, wide-flange beam-columns." *Eng. J.* 54 (1): 45–60.

PEER/ATC (Pacific Earthquake Engineering Research Center/Applied Technology Council). 2010. *Modeling and acceptance criteria for seismic design and analysis of tall buildings*. Redwood City, CA: ATC.

Popov, E. P., M. Blondet, L. Stepanov, and B. Stojadinović. 1996. *Full-scale beam-column connection tests—Experimental investigations of beam-column subassemblages.* Rep. No. SAC-96/01. Redwood City, CA: Applied Technology Council.

Qi, L., J. Paquette, M. Eatherton, R. Leon, T. Bogdan, N. Popa, and E. Nunez. 2018. "Analysis of fracture behavior of large steel beam-column connections." In *Proc., 12th Int. Conf. on Advances in Steel-Concrete Composite Structures ASCCS 2018*. Valencia, Spain: Universitat Politècnica València. https://doi.org/10.4995/ASCCS2018.2018.7122.

Ricles, J. M., C. Mao, L.-W. Lu, and J. W. Fisher. 2000. *Development and evaluation of improved details for ductile welded unreinforced flange connections.* Bethlehem, PA: SAC Joint Venture, Lehigh Univ.

Ricles, J. M., X. Zhang, L.-W. Lu, and J. W. Fisher. 2004. *Development of seismic guidlines for deep-column steel moment connections.* ATLSS Rep. Bethlehem, PA: Lehigh Univ.

Shin, S. 2017. "Experimental and analytical investigation of panel zone behavior in steel moment frames." Ph.D. thesis, Dept. of Civil, Architectural and Environmental Engineering, Univ. of Texas at Austin.

Shin, S., and M. D. Engelhardt. 2013. "Experimental study on panel zone behavior in steel moment resisting frames." In *Proc., 7th Int. Symp. on Steel Structures*. Jeju, Korea: Korean Society of Steel Construction.

Shirsat, P. S., and M. D. Engelhardt. 2012. "Preliminary analysis of doubler plate attachment details for steel moment frames." In *Proc., 15th WCEE*. Lisboa, Portugal: Sociedade Portuguesa de Engenharia Sismica.

SIMULIA. 2014. *ABAQUS user's manual version 6.14.* Providence, RI: SIMULIA.

Skiadopoulos, A., and D. G. Lignos. Forthcoming. "Development of inelastic panel zone database." *J. Struct. Eng.* https://doi.org/10.1061/(ASCE)ST.1943-541X.0002957.

Slutter, R. G. 1981. *Tests of panel zone behavior in beam-column connections*. Bethlehem, PA: Lehigh Univ.

Soliman, A. A., O. A. Ibrahim, and A. M. Ibrahim. 2018. "Effect of panel zone strength ratio on reduced beam section steel moment frame connections." *Alexandria Eng. J.* 57 (4): 3523–3533. https://doi.org/10.1016/j.aej.2018.07.017.

Sousa, A. A., and D. G. Lignos. 2017. *Residual stress measurements of European hot-rolled I-shaped steel profiles.* Technical Rep. No. 231302. Lausanne, Switzerland: École Polytechnique Fédérale de Lausanne.

Suita, K., S. Yamada, M. Tada, K. Kasai, Y. Matsuoka, and Y. Shimada. 2008. "Collapse experiment on 4-story steel moment frame: Part 2 detail of collapse behavior." In Vol. 1217 of *Proc., 14th World Conf. Earthquake Engineering*. Beijing: International Association for Earthquake Engineering.

Suzuki, Y., and D. G. Lignos. 2020. "Development of collapse-consistent loading protocols for experimental testing of steel columns." *Earthquake Eng. Struct. Dyn.* 49 (2): 114–131. https://doi.org/10.1002/eqe.3225.

Tremblay, R., N. Tchebotarev, and A. Filiatrault. 1997. "Seismic performance of RBS connections for steel moment resisting frames: Influence of loading rate and floor slab." In *Proc., STESSA 97*. Salerno, Italy: Edizioni.

Tsai, K. C., and E. P. Popov. 1988. *Steel beam-column joints in seismic moment resisting frames.* EERC Rep. No. 88-19. Berkeley, CA: Univ. of California, Berkeley.

von Mises, R. 1913. "Mechanik der festen körper im plastisch-deformablen zustand." *Nachr. Ges. Wiss. Göttingen Math.-Phys. Kl.* 1 (1): 582–592.

Wang, S. J. 1988. "Seismic response of steel building frames with inelastic joint deformation." Ph.D. thesis, Dept. of Civil Engineering, Lehigh Univ.

Young, B. W. 1971. "Residual stresses in hot-rolled members." In *Proc., Int Colloquium on Column Strength, Int. Association for Bridge and Structural Engineering*, 25–38. Zurich, Switzerland: International Association for Bridge and Structural Engineering.

Proposed Backing Bar Detail in Welded Beam-to-Column Connections for Seismic Applications

Andronikos Skiadopoulos, S.M.ASCE[1]; and Dimitrios G. Lignos, M.ASCE[2]

Abstract: The use of prequalified welded unreinforced flange-welded web (WUF-W) beam-to-column connections in capacity-designed steel moment-resisting frames necessitates the removal of the weld backing bar at the bottom beam flange-to-column flange groove welded portion. Weld root back gouging and fillet weld reinforcement is also necessary to minimize the fracture potential at this location. This paper revisits the current detailing of WUF-W connections in order to propose simplifications in their fabrication process by intentionally keeping a customized beveled backing bar in place without impairing the connection's ductility under seismic loading. The analysis relies on traditional fracture mechanics applied in three-dimensional continuum finite element models. The modeling approach is validated with welded unreinforced flange-bolted web (WUF-B) pre-Northridge connection tests. The results suggest that field-welded connections with the proposed beveled backing bar reach lateral drift demands of at least 4%–6% rads even when flange groove welds feature a low-toughness E70T-4 weld electrode, which was typical in pre-Northridge WUF-B connections. Fillet weld reinforced backing bars provide inferior connection ductility compared to the proposed beveled backing bar. The simulation results from a series of prequalified WUF-W connections that respect the current seismic design and fabrication requirements, indicate that when the beveled backing bar configuration is intentionally left in place after completing the complete joint penetration groove welds, WUF-W connections can sustain lateral drift demands of at least 6% rads prior to fracture regardless of the panel zone strength, the steel beam depth, and the flange thickness of the respective beam and column. Limitations as well as suggestions for future work are also discussed. **DOI: [10.1061/(ASCE)ST.1943-541X.0003374](https://doi.org/10.1061/(ASCE)ST.1943-541X.0003374).** © 2022 American Society of Civil Engineers.

Author keywords: Steel moment-resisting frames; Welded beam-to-column connections; Fracture; Continuum finite element modeling; Beveled backing bars; Inelastic panel zone; Prequalified connections.

Introduction

Comprehensive evaluations in field-welded steel moment-resisting frame (MRF) buildings prior to 2000 (FEMA 2000b) and corroborating experimental studies after the 1994 Northridge earthquake (FEMA 2000a) highlighted a number of issues with regard to the, admittedly, poor seismic performance of field-welded unreinforced flange-bolted web (WUF-B) beam-to-column connections (FEMA 2000a, b). This connection is shown in Fig. 1(a). Particular emphasis was placed on the bottom beam flange-to-column flange groove welded portion, which is shown schematically in Fig. 1(b).

In typical pre-Northridge WUF-B connections, the backing bars of rectangular shape were often left in place after completing the beam-to-column complete joint penetration (CJP) groove welds (FEMA 2000a). These welds were usually realized with self-shielded flux-cored arc welding (FCAW-SS) with a low-toughness weld electrode E70T-4. Referring to Fig. 1(c), the backing bar imposed a notch condition within the column and/or the beam flanges.

Moreover, an additional crack-like flaw, a_0, often penetrated through the CJP weld root. The depth of this flaw was not uniform along the beam flange width, as shown schematically in Fig. 1(c). It maximized in the beam web centerline, where the welding process was interrupted. The presence of backing bars restricted weld inspections for potential flaws that were deemed critical in low-toughness groove welds at the time. Kaufmann and Fisher (1996) found that a_0 varied between 3 and 10 mm. The backing bar-to-column flange notch condition [noted as location "L1" hereinafter as per Fig. 1(b)], together with the high strain demands in the outer beam bottom flange fiber and the increased triaxial stresses due to the column web restraint, often triggered crack initiation and fracture at the same location (Mahin 1998; Miller 1998; Yang and Popov 1995). Fig. 2 highlights a WUF-B connection where the particular fracture pattern initiated from the bottom backing bar at L1 and penetrated through the CJP weld material.

Referring to Fig. 1(b), discontinuities adjacent to the beam flange-to-column flange CJP weld of pre-Northridge WUF-B connections often turned into crack-like flaws during the shrinkage of the weld material that was restrained by the surrounding base metal. These flaws, which are usually situated in the heat-affected zone (HAZ), may be located either at the outer and/or the inner flange fiber (denoted as location "L2" hereinafter). Depending on the accuracy of the nondestructive inspection method, the depth of these crack-like flaws usually ranges from 0.1 to 0.5 mm (ASTM 2015, 2017, 2018). The increased fracture potential due to the presence of the presented crack-like flaws together with the inferior base and weld material toughness requirements of pre-Northridge connections often lead to fracture that initiated at L2 and propagated through the CJP weld or the base metal of the beam flange. However, advancements in welding procedures (AWS 2010) and

---

[1]Doctoral Assistant, Resilient Steel Structured Laboratory, School of Architecture, Civil and Environmental Engineering, École Polytechnique Fédérale de Lausanne, Station 18, Lausanne 1015, Switzerland. Email: andronikos.skiadopoulos@epfl.ch

[2]Associate Professor, Resilient Steel Structured Laboratory, School of Architecture, Civil and Environmental Engineering, École Polytechnique Fédérale de Lausanne, Station 18, Lausanne 1015, Switzerland (corresponding author). ORCID: https://orcid.org/0000-0003-0682-4660. Email: dimitrios.lignos@epfl.ch
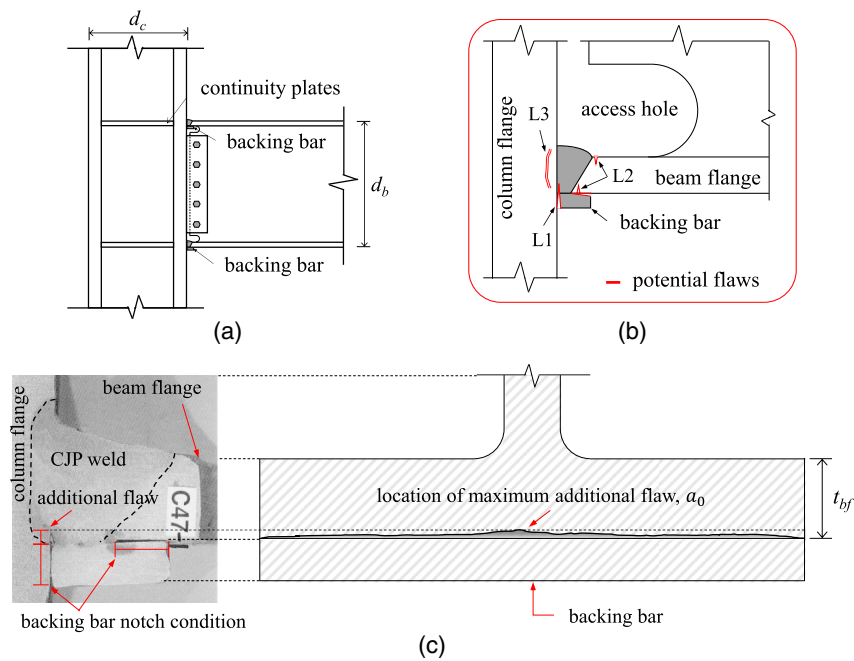
Fig. 1. Welded unreinforced flange-bolted web (WUF-B) pre-Northridge connection: (a) typical configuration; (b) potential locations for crack initiation; and (c) typical bottom beam flange-to-column flange connection detail and schematic of additional flaw profile along the beam flange width (data from Paret 2000, © ASCE).
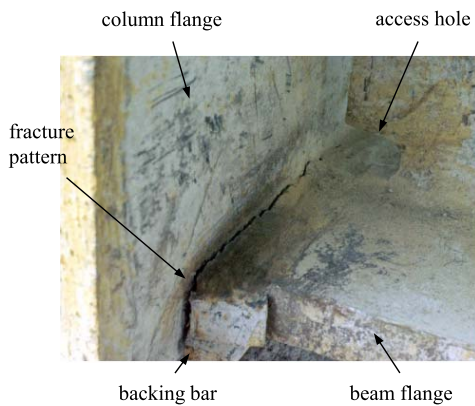

Fig. 2. Fracture pattern observed during the 1994 Northridge earthquake in a welded unreinforced flange, bolted-web connection. (Image courtesy of Professor Michael Engelhardt, University of Texas at Austin.)

electrode specifications for demand-critical welds (AISC 2016b) in prequalified beam-to-column connections reduce considerably the fracture potential at L2.

Krawinkler (1995) found that the inferior through-thickness steel material properties often lead to fracture due to lamellar tearing in pre-Northridge connections (denoted as location "L3" hereinafter) when steel columns featured relatively thick flanges ($t_{cf} > 38$ mm). This reflects current practice requirements for nondestructive testing evaluation (AISC 2016b). The inferior through-thickness steel material properties result from the hot rolling process that transforms the metal inclusions to thin and long discontinuities parallel to the base metal longitudinal direction (Miller 2017). These can separate at a certain amplitude of imposed strain demands, thereby compromising the overall ductility of the connection. However, structural steel materials with through-thickness strength and toughness properties, which are equivalent to those in the longitudinal one, are currently

available (Kanno 2016; Miki et al. 2002). For instance, in Europe, the through-thickness Z-direction demand, Z_{Ed}, determines the Z-direction material resistance, Z_{Rd}, to be utilized (CEN 2004). In the United States, the use of A913 Gr. 50 or 65 steel is an interesting alternative (Bouchard and Axmann 2000). Therefore, divot fracture at L3 is unlikely to occur in today's connections provided that the presented material requirements are respected.

Finally, the weld access hole geometry of the WUF-B connection often triggered crack initiation near the toe of the weld access hole. While there is no apparent initial sharp crack-like flaw in this area, microvoid nucleation, growth, and coalescence (Kanvinde 2017) often lead to fracture initiation and propagation due to the concentration of high plastic strain demands and triaxial stresses. However, this crack type is stable, and it is not considered to compromise the overall connection ductility under cyclic loading (Suzuki and Lignos 2021).

The aforementioned considerations have been articulated in current standards (AISC 2016a; AWS 2010) and other concerted efforts (Landolfo et al. 2018) to enhance the seismic ductility of prequalified field-welded beam-to-column connections. Referring to Fig. 3, an improved weld access hole geometry is utilized based on rigorous finite element analysis studies (El-Tawil et al. 2000; Ricles et al. 2002a). This geometry minimizes the strain localization at the toe of the bottom beam flange weld access hole. Detailed surveys from prior testing in prequalified field-welded connections suggest that fracture initiation at this location is unlikely to occur at lateral drift demands prior to 6% rads (Skiadopoulos and Lignos 2021). Moreover, the use of welded-web attachments in prequalified welded unreinforced flange-welded web (WUF-W) beam-to-column connections (see Fig. 3), which is the primary focus of this paper, is imperative in an effort to reduce the, arguably large, seismic shear transfer and its prying effects into the beam flanges (Richard 2003).

In today's WUF-W connections, the bottom beam flange backing bar should be removed after the completion of the CJP welds.
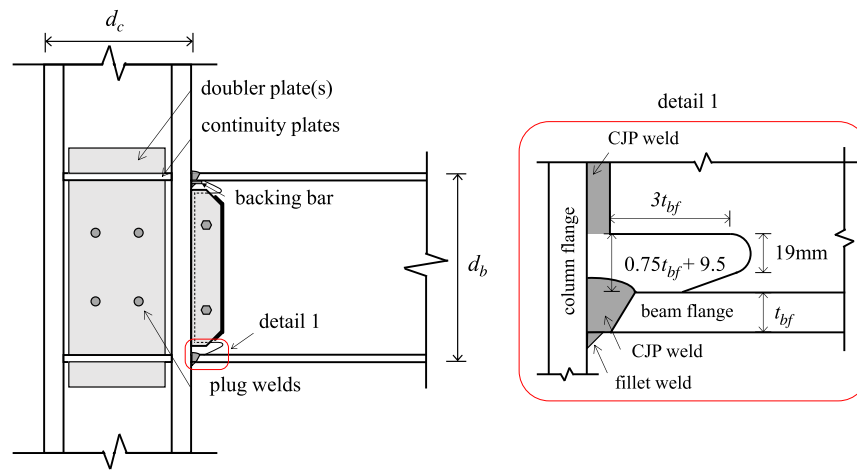
Fig. 3. Typical welded unreinforced flange-welded web (WUF-W) prequalified connection detailing.

Weld root back gouging and fillet weld reinforcement (see Fig. 3) is necessary. Albeit this connection detailing minimizes the fracture potential (Chi et al. 2000), its fabrication is time consuming, thereby leading to increased fabrication costs (FEMA 2000a; Miller 2017; Popov et al. 1998). With today's toughness requirements for demand-critical CJP welds, which are commonly used in prequalified beam-to-column connections (AISC 2016b), possible built-in flaws do not necessarily lead to brittle fracture (Shaw et al. 2015). A thorough review of available experimental data in post-Northridge connections (Skiadopoulos and Lignos 2021) suggests that fracture at L2 is unlikely to occur prior to 5%–6% lateral drift demands. Therefore, cost-effective simplifications during the fabrication of WUF-W connections for seismic applications may be possible. For the same reason, similar simplifications have been proposed for welded base plate connections (Myers et al. 2009) as well as welded column splices (Shaw et al. 2015; Stillmaker et al. 2016).

In prior work (Chi et al. 2000; Wang et al. 2010; Yang et al. 2019), alternative backing bar configurations were explored in an effort to reduce the fracture potential at the bottom beam flanges of WUF-B connections. The general consensus from these studies was that modified backing bar details may somewhat reduce the fracture potential relative to that from the use of conventional backing bar geometries. However, the presented studies shared a number of limiting features. Particularly, these included (1) a single beam-to-column geometry; and (2) the use of two-dimensional (2-D) finite element models that generally underpredicted the fracture potential at the bottom beam flange by about 40% (Chi et al. 2000). Particularly, 2-D finite element models do not properly depict the increased restraint at the center of the beam-flange-to-column flange joint, increasing the triaxiality and generally leading to nearly two times higher fracture potential in this location than that of the beam flange tip (Chi et al. 2000).

Motivated by the above, this paper revisits, through simulation-assisted engineering, the commonly used practice in field-welded beam-to-column connections for seismic applications, aiming to propose potential fabrication detailing simplifications with emphasis on weld backing bar details. The proposed methodology, which features traditional fracture mechanics informed by 3-D continuum finite element (CFE) analyses, is validated by available pre-Northridge WUF-B connection full-scale experiments. A customized backing bar detail is then proposed that, although it is not removed after the completion of the CJP groove welds, decreases appreciably the fracture potential in both pre-Northridge and post-Northridge field-welded connections. In order to substantiate the

findings, several parameters are interrogated, including the panel zone design distortions, the beam depth, as well as the thickness of the beam and column flanges. Limitations as well as directions for future work are discussed.

Methodology

While the focus of this paper is to advance the seismic performance of post-Northridge WUF-W connections, knowledge and data acquired from prior work on pre-Northridge WUF-B connections are also of interest. The emphasis is on how to minimize the fracture potential at location L1. The current weld toughness requirements and weld practice (AISC 2016b; AWS 2016) for demand-critical welds, the nondestructive testing evaluation (AWS 2010) along with the updated weld access hole geometries (AISC 2016a), and the current base metal technology (Kanno 2016; Miki et al. 2002) ensure a minimum fracture potential at L2 and L3 and at the toe of the access hole as discussed earlier. The type of fracture at L1 dictates the pertinent fracture mechanics method to be employed, which is informed by CFE analyses. These comprise beam-to-column subassembly global models that do not include a backing bar and sharp crack-like built-in flaws in the locations of high fracture potential. These are explicitly considered in carefully developed and validated submodels, which are informed by the global connection models. The subsequent sections discuss the primary features of the employed methodology.

Employed Fracture Mechanics Methods, Primary Assumptions, and Sensitivity Analyses

The apparent sharp crack-like flaw (referred to as crack hereinafter) at L1 prohibits the applicability of micromechanics-based models (Jia and Kuwamura 2014; Kanvinde 2017). Instead, traditional fracture mechanics methods (Irwin 1961; Rice 1968; Wells 1961) should be employed. Location L1 is likely to experience relatively high stress and strain demands, regardless of the relative strength of the beam with respect to the column panel zone. For panel zone joints exhibiting highly inelastic shear distortions (e.g., $\gamma > 10$ to $12\gamma_y$, where γ_y is the panel zone shear distortion angle at yield), kinking in the panel zone edges may occur (Krawinkler 1978). The plastic zone is not bounded within the validity region of linear elastic fracture mechanics; thus, elastic-plastic fracture mechanics methods reflect a more realistic computation of the fracture potential at L1

© ASCE

04022102-3

J. Struct. Eng.

(Kanvinde et al. 2008; Stillmaker et al. 2016). The same holds true for beam-to-column connections featuring a strong panel zone design.

In elastic-plastic fracture mechanics, there are two well-established fracture metrics; the crack tip opening displacement (*CTOD*), which was originally proposed by Wells (1961), and the J-integral (Rice 1968). Fracture initiation occurs once the computed *CTOD* or J-integral demand exceeds the respective material toughness (*CTOD_C* and J_C, respectively). Referring to Fig. 4(a), the J-integral (also called the nonlinear energy release rate of a body) is defined by the change of the potential energy, Π, due to the extension, *da*, of a crack. The potential energy of a body is defined as the difference between the strain energy of the deformation and the potential energy of the tractions. Therefore, it can be proven that the J-integral is given by Eq. (1) for the two-dimensional x–y space

$$J = \int_\Gamma \left(w \, dy - T_i \frac{\partial u_i}{\partial x} \, ds \right) \tag{1}$$

where w = strain energy density; T_i = components of the boundary tractions vector; u_i = components of the displacement vector; and ds = increment along a contour Γ.

Referring to Fig. 4(a), arbitrarily selected contours Γ_1 and Γ_2 do not influence the J-integral computation. The J-integral is applicable to hyperelastic materials (i.e., deformation theory of plasticity), while it is not valid in materials experiencing irreversible plastic deformations (i.e., incremental theory of plasticity). However, the commercial finite element analysis software ABAQUS (version 6.14-1) (ABAQUS 2014) idealizes a steel material undergoing plastic deformations with an equivalent hyperelastic material; hence, the simulation results are deemed reasonable for monotonic loading regardless of the employed constitutive material law. These considerations hold

true for both two- and three-dimensional problems that include J-integral computations (Bakker 1984; Brocks and Scheider 2001).

Several pre-Northridge WUF-B connections experienced fracture at L1 prior to the first ground motion reversal (FEMA 1997); hence, the preceding small loading cycles did not practically influence the connection behavior. Moreover, shake table testing of steel MRFs with emphasis on collapse (Lignos et al. 2011, 2013) as well as tests that quantified the influence of loading history on the hysteretic behavior of steel connections (Yu et al. 2000), and their members (Suzuki and Lignos 2021) suggest that the use of monotonic loading is indicative when ground shaking in the forward directivity region of a fault rupture is characterized by a large pulse early in the ground motion history. However, it is recognized that this is not generalizable in cases where the seismic hazard is characterized by other types of ground motion.

While the stress-strain field in the crack vicinity may not be accurately represented by CFE analyses, the advantage of using the J-integral is that the integration along a path, which does not include that region, provides legitimate results (Brocks and Scheider 2001). Referring to Fig. 4(b), at L1, the J-integral is accurately computed by a contour that is far away from the crack vicinity (i.e., CO-6 instead of CO-1). Mesh and contour sensitivity analyses are, thus, imperative. Unlike the J-integral, the *CTOD* necessitates a much finer mesh to accurately estimate the displacement field in the crack vicinity. Consequently, the J-integral metric is employed in the subsequent analyses.

The employed CFE software (ABAQUS) utilizes the virtual crack extension method (deLorenzi 1982; Parks 1977) for the J-integral computation; hence, the potential crack extension direction (i.e., q-vector) should be defined. According to Erdogan and Sih (1963), the crack propagates in the direction of the principal plane. Assuming that the stress flow is perpendicular to the potential crack
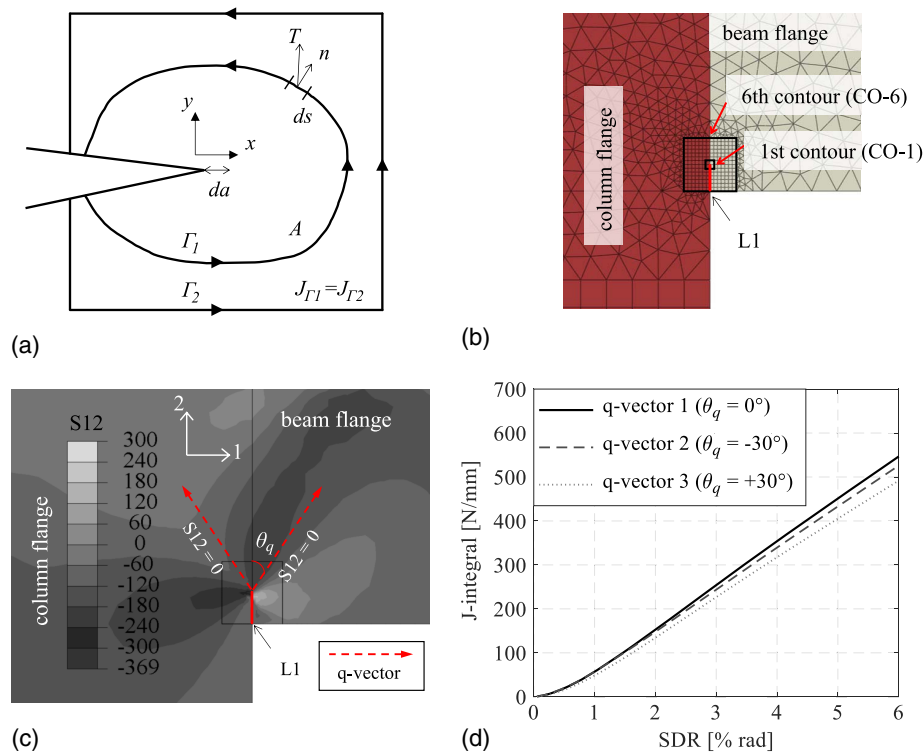

Fig. 4. J-integral computation specifics for a typical beam flange-to-column flange connection: (a) contours for J-integral computation; (b) continuum finite element model contours for the L1 crack; (c) shear stress field of the L1 crack and respective q-vector definitions; and (d) J-integral versus story drift ratio for different q-vector definitions.

at L1, the q-vector is parallel to the column's longitudinal direction; hence, it represents the mode I fracture mechanism. In reality, the shear stresses near the crack tip do not lead to principal planes that are parallel to the crack. Referring to Fig. 4(c) for a representative crack at L1, the principal plane deviates by about 30° (shown as θ_q) from the beam flange-to-column flange interface plane. As such, in principle, the q-vector should be defined based on these planes. Fig. 4(d) compares the J-integral evolution at L1 with respect to the story drift ratio (SDR) for the employed q-vector (i.e., $\theta_q = 0°$) and those corresponding to the principal plane angle (i.e., $\theta_q = \pm30°$). The insignificant difference between the J-integral computations of the examined cases suggests that $\theta_q = 0$ can be assumed in the CFE.

In welded connections, cracks may form at interfaces between different materials (e.g., in locations L1 and L2). This poses a challenge regarding the J-integral path independence at the interface (Brocks and Scheider 2001). Kolednik et al. (2005) and Simha et al. (2003) showed that if the bimaterial interface plane is parallel to the crack plane, the J-integral path independence is respected, assuming that the contours along which the J-integral is computed are perpendicular to the interface (Smelser and Curtin 1977). This condition is respected for the bimaterial interface between the beam and column flanges, as shown in Fig. 4(b).

Continuum Finite Element Modeling for Informing Fracture Mechanics Methods

To reduce the associated computational cost in the CFE analyses, the node-based submodeling technique of ABAQUS (version 6.14-1) (ABAQUS 2014) is employed. A global model of a beam-to-column connection is initially loaded monotonically. Once the analysis is conducted, nodal deformations of the global model at all degrees of freedom are applied as boundary conditions in the selected submodel nodes, which are common to the global model. The presence of cracks and weld backing bars influences the deformation field at the crack vicinity, while their far-field effect is minuscule. This implies that the crack at L1 and the backing bars can be neglected from the global model, whereas they can be explicitly considered in the submodel. Consequently, the submodel mesh is much finer than that of the global model.

In this section, the basic features of the two models are highlighted. Particularly, a representative global model is shown in Fig. 5, together with three submodel variants (noted as submodels 1, 2, and 3). The primary difference between the three submodels is associated with their boundary conditions. One of the three is selected based on a sensitivity analysis that is discussed later on in this section.

The global model utilizes twenty-node quadratic elements with reduced integration (C3D20R) with a characteristic element size of 15 mm. Local initial geometric imperfections are accounted for in the steel beams to properly trigger local buckling according to modeling recommendations by Elkady and Lignos (2018). The CFE model employs a combined isotropic/kinematic hardening law (Lemaitre and Chaboche 1990) with consistent input material model parameters for cyclic metal plasticity, as proposed by de Castro e Sousa et al. (2020) for A992 Gr. 50 steel (i.e., nominal yield stress, $f_y = 345$ MPa). Prior studies on the fracture potential of beam-to-column connections (Chi et al. 2000) have shown that the role of residual stresses is negligible; hence, they are disregarded in the context of the present study. The CFE modeling assumptions for the global CFE model have been thoroughly summarized and validated in prior studies by the authors (Skiadopoulos et al. 2021).
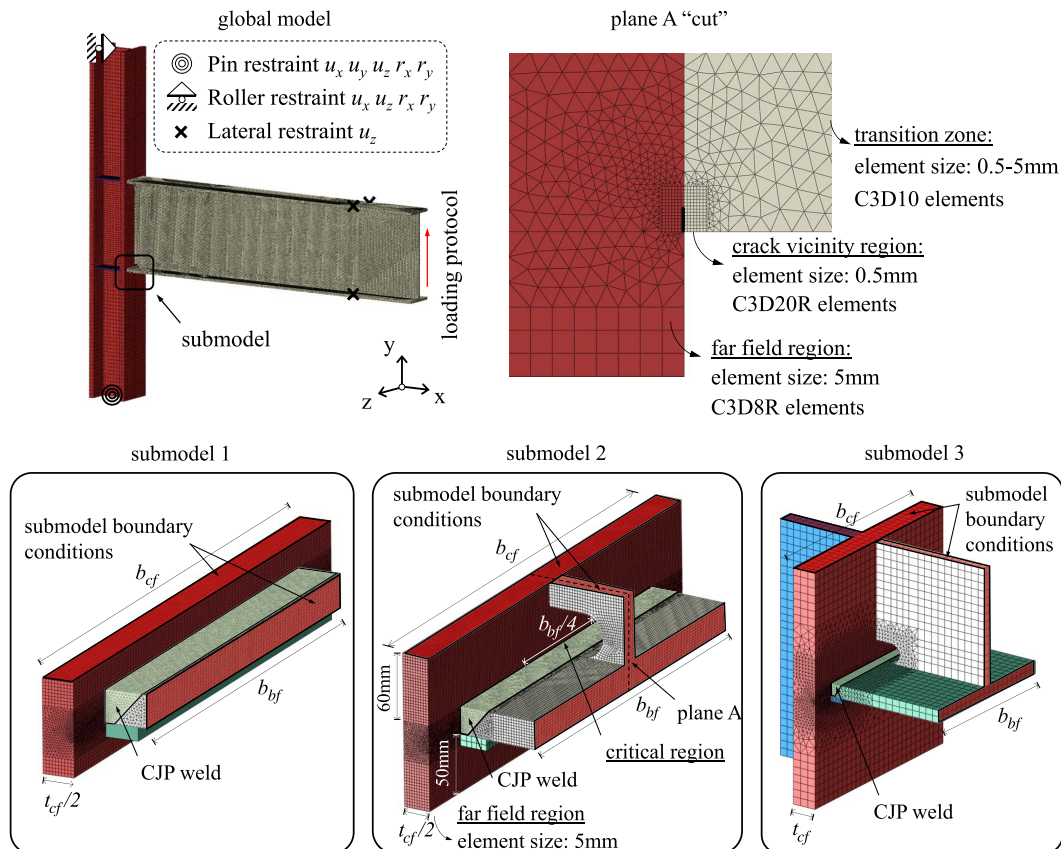

Fig. 5. Continuum finite element model of a beam-to-column connection; global model and submodel variants.
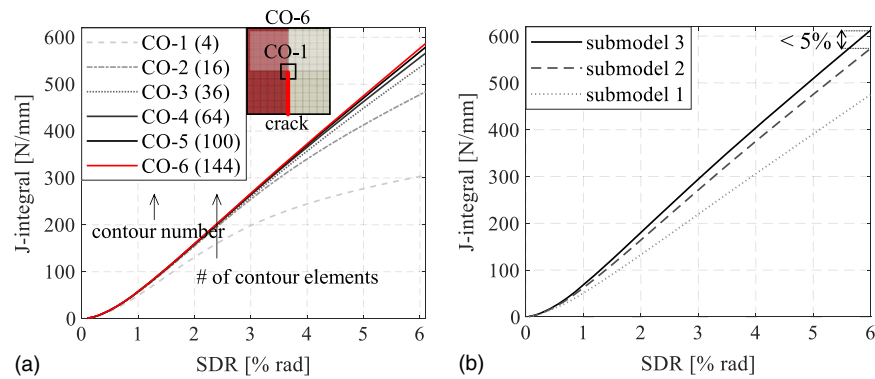
Fig. 6. Continuum finite element sensitivity analyses results: (a) contour number sensitivity analysis; and (b) submodel geometric sensitivity analysis.

The examined submodels constitute 20-node quadratic elements with reduced integration (C3D20R). The characteristic size for the J-integral contours near the crack vicinity in the critical region is 0.5 mm (see Fig. 5). The mesh is chosen to be finer over a width of $b_{cf}/4$ near the beam web centerline because the J-integral becomes maximum at this location. The far-field region employs eight-node quadratic elements with reduced integration (C3D8R) and a characteristic size of 5 mm. The submodels consider cracks of constant depth, a_0, throughout the beam flange width, which is a fairly conservative assumption [see Fig. 1(c)]. Two crack depths are assumed: 3 mm and 6 mm (Chi et al. 2000; Wang et al. 2010). The gradual transition from the very fine crack tip mesh to the coarser far-field mesh is achieved by 10-node tetrahedral elements (C3D10) as shown in the plane A "cut" of Fig. 5. The element sizes were determined by a sensitivity analysis in which the relative difference between simulation results was no more than 1%. These results are not presented herein due to brevity.

Fig. 6(a) depicts the variation of the J-integral with respect to SDR under monotonic loading for six different contours (CO-1 to CO-6) near the crack tip. The number of utilized elements for the computation of the J-integral at each contour is shown in parenthesis. For instance, the most approximate to the crack tip contour (i.e., CO-1) incorporates only four elements in the computations, whereas contour CO-6, which leads to more accurate J-integral calculations, incorporates 144 elements. For the selected element types and mesh size, the results converge according to the fifth contour. Hereinafter, the reported results are always extracted from the sixth contour.

Qualitatively, the global model underestimates the displacement field nearby the crack vicinity because it neglects the crack at L1. This may underestimate the J-integral computations of the submodel if its boundary conditions are chosen such that they are close to the crack vicinity. Consequently, a submodel geometric sensitivity analysis is conducted. Fig. 6(b) shows the variation of the J-integral with respect to SDR at the beam web centerline based on the three submodels. Submodel 1, which is considered to be the simplest one, underestimates the J-integral by about 30% for SDRs higher than 2% rads. On the other hand, submodel 2 provides nearly identical results to submodel 3, which is the most accurate one. As such, the geometry of submodel 2 is utilized for the analyses discussed hereinafter.

Overview and Scope of Fracture Analysis

In the upcoming sections, the fracture potential of welded connections is examined based on the methodology discussed earlier. The primary scope is to demonstrate that simpler fabrication detailing suffices to minimize the fracture potential of both pre-Northridge and post-Northridge beam-to-column connections. Of particular interest is to revisit if removal of the bottom backing bar is deemed necessary after the completion of the CJP groove welds between the bottom beam flange and the column flange. Referring to Fig. 7(a), a conventional backing bar is first considered. While this is not expected to lead to superior results, it is considered a reference case. A beveled backing bar [see Fig. 7(b)] is also examined. The premise in this case is to allow for the stress flow to pass through the backing bar due to its attachment to the column flange. The beveled angle, θ_b, can be optimized through CFE analyses. The angle of the normal stress flow is varied so as the fracture potential at L1 [see Fig. 1(b)] is minimized. All the examined beveled angles, θ_b, and crack depths are summarized in Table 1. The conventional backing bar geometries conform to AWS (2016).

The fracture analysis is mainly conducted on connection geometries featuring deep steel beams (i.e., W36x150) and web panel zones exhibiting inelastic shear distortions above $4\gamma_y$. The presented criteria are intentionally selected because they can significantly compromise the ductility of welded connections (Chi et al. 1997; El-Tawil et al. 1999; FEMA 2000a; Lu et al. 2000; Mao et al. 2001; Ricles et al. 2002a, 2004).

Assessment of Pre-Northridge WUF-B Connections

The chosen characteristic connection configuration to assess the differences between the two backing bar geometries in pre-Northridge WUF-B connections is the exterior subassembly UCB-PN3, which was tested by Yang and Popov (1995) at full scale as part of the SAC program (FEMA 1997). This specimen features a W36x150 deep beam and a W14x257 column. The beam-to-column web panel
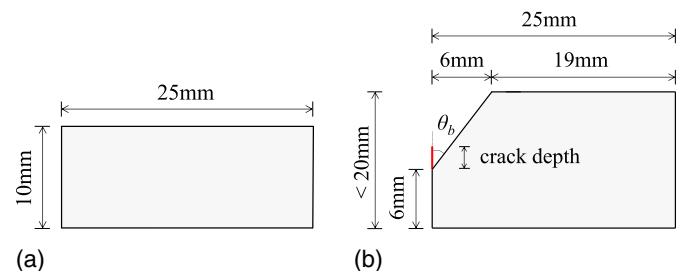

Fig. 7. Backing bar geometry: (a) conventional detail; and (b) beveled detail.

Table 1. CFE analyses beveled backing bar geometry characteristics

θ_b	Crack depth (mm)	θ_b	Crack depth (mm)	θ_b	Crack depth	θ_b	Crack depth
35°	0	25°	3	—	—	—	—
35°	0	30°	3	25°	6 mm	—	—
45°	0	35°	3	30°	6 mm	25°	9 mm
60°	0	45°	3	35°	6 mm	30°	9 mm
∞	0	60°	3	45°	6 mm	35°	9 mm

exhibited an inelastic shear distortion of $15\gamma_y$. The selected subassembly experienced fracture at the bottom beam flange CJP weld (at L1) prior to an SDR of 2% rads.

A 6 mm weld toe with a 45° angle CJP weld is assumed as per AWS (2010). The web and flange measured material properties for the beams and the column are considered as per FEMA (1997) and for the weld metal as per Kanvinde et al. (2008). Fig. 8 depicts the examined beam flange-to-column flange connections, together with the respective CFE submodels with $a_0 = 3$ mm. Three different connection details are examined. In Fig. 8(a), the model utilizes a conventional unreinforced backing bar. This has two potential crack tips; C1, which is adjacent to the backing bar and the column flange; and C2, which is adjacent to the backing bar and the beam flange. In Fig. 8(b), the WUF-B connection is analyzed without the presence of the backing bar. Finally, Fig. 8(c) illustrates the pre-Northridge WUF-B connection with a beveled backing bar left in place after the completion of the CJP groove weld. In this case, crack tips C1 and C2 are explicitly considered.

Fig. 9(a) shows the J-integral demand in the most critical location of the beam web centerline with respect to the SDR for all the analyzed cases. To put the results into perspective, the lower and upper bounds of the J-integral resistance (noted as J_{IC}) for the ASTM A572, Gr. 50 (i.e., $f_y = 345$ MPa, where f_y is the nominal

material yield stress) base metal of the column are superimposed in the same figure. These are computed according to Eq. (2)

$$J_{IC} = \lambda \cdot f_y \cdot CTOC_C \qquad (2)$$

where λ = dimensionless factor, which is related to the stress state and the material properties and may be empirically assumed equal to 1.2 (Chi et al. 2000); $CTOD_C$ = critical $CTOD$ and may be taken equal to 0.17 mm (Chi et al. 1997). The lower bound of J_{IC} is determined based on the nominal yield stress of the steel base material (i.e., $f_y = 345$ MPa), whereas the upper bound is based on its expected yield stress ($R_y f_y = 380$ MPa) as per AISC (2016b). The upper bound ($J_{IC} = 78$ N/mm) matches that of the Grade 480 E70T7 low-toughness filler metal, which was characteristic in pre-Northridge WUF-B connections (Kanvinde et al. 2008).

Referring to Fig. 9(a), when the crack depth is 6 mm, the fracture potential is 40% higher than that of a 3-mm one when the conventional backing bar is not removed after the completion of the groove weld. In the former, the stress concentration near the crack is higher than that in the latter. Note that the depicted J-integral is based on calculations on crack tip C1 [see Fig. 8(a)]. The J-integral demand at crack tip C2 is nearly zero because the backing bar is not attached to the column flange to let the stress flow pass through the backing bar.

The CFE submodel with conventional backing bars exhibits fracture well before an SDR of 2% rads. This is consistent with the experimental findings (FEMA 1997). However, it should be noted that bolt slipping was not considered in the CFE analysis. Bolt slipping would increase the beam flange strain demands and subsequently the fracture potential at the same location (FEMA 2000a; Han et al. 2007). The fracture potential of the conventional and the 'no backing bar' models are nearly identical. The reason is that the backing bar remains practically unstressed during loading because it is solely attached to the beam flange. This agrees with prior work by Chi et al. (2000). Therefore, there is no benefit from removing the
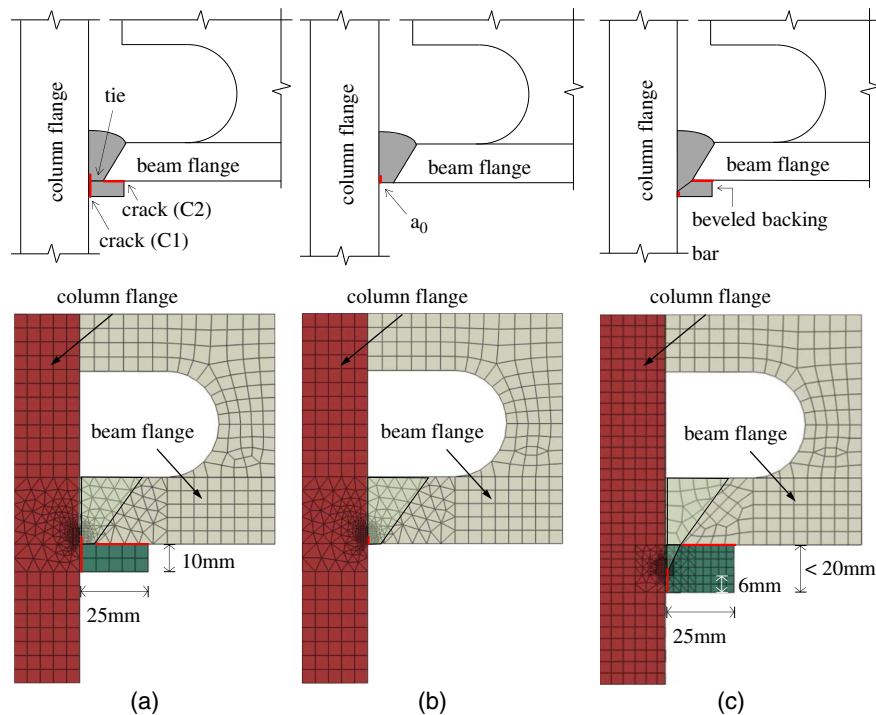

Fig. 8. Bottom beam flange-to-column flange weld detail along with their respective continuum finite element submodels: (a) conventional backing bar; (b) no backing bar; and (c) beveled backing bar-C1 crack tip.
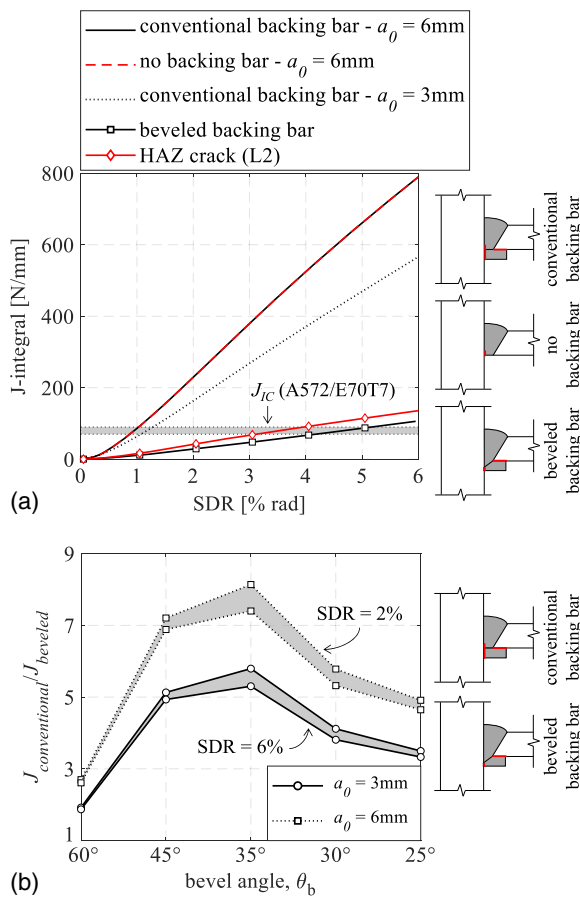
Fig. 9. J-integral comparisons for a typical pre-Northridge WUF-B connection and its variants: (a) J-integral versus story drift ratio; and (b) effect of bevel angle on J-integral.

backing bar if the edge crack is not reinforced with a fillet weld in this case.

Interestingly, Fig. 9(a) suggests that the same pre-Northridge WUF-B connection with a beveled backing bar detailing ($\theta_b = 35°$) is able to achieve an SDR of 4%–6% rads prior to fracture for the same low-toughness weld electrode (i.e., E70T7). Noteworthy stating that the fracture potential at L1 is lower than that at L2 for an assumed crack depth a_0 equal to 0.5 mm in the HAZ. This was assumed to extend 3 mm away from the weld toe (Ibrahim et al. 2019; Myers et al. 2009).

Fig. 9(b) compares the normalized J-integral demand with respect to the assumed bevel angle, θ_b. Particularly, the J-integral demand from the model with the conventional backing bar is normalized with respect to that from the model with the beveled backing bar. From the same figure, the largest ($\theta_b = 60°$) and the smallest ($\theta_b = 25°$) bevel angle lead to the highest fracture potential. Qualitatively, in the former, the crack tip is situated near the beam flange, thereby causing high-stress concentrations. In the latter, the smallest bevel angle has the crack tip away from the critical beam flange; thus, the J-integral is nearly zero at C1. Interestingly, in this case, C2 becomes critical because the stress flow passes through that crack tip. From a deformation compatibility perspective, once the backing bar attachment to the column flange increases (i.e., smallest bevel angle), C2 becomes critical. The optimal bevel angle is the one that imposes the same J-integral demand at both C1 and C2 crack tips. For the analyzed connection, this corresponds to $\theta_b = 35°$. In this case, the fracture potential is reduced by five to eight times relative

to that with the conventional backing bar depending on the assumed crack depth, a_0, and the SDR of interest, which is a significant decrease.

Effect of Fillet Weld Reinforcement on J-Integral Demand

It is generally known that a fillet weld reinforcement can reduce the fracture potential of welded connections due to the closure of potential mode I cracks (Chi et al. 2000; Wang et al. 2010; Yang et al. 2019). Indeed, a closed crack has a decreased displacement field when contrasted with an open crack under the same loading conditions.

In this section, we investigate the possibility of reducing the fracture potential of crack tips at C1 and C2 with a fillet weld reinforcement either between the backing bar and the column flange [noted as fillet weld 1 in Fig. 10(a)] or between the backing bar and the beam flange [noted as fillet weld 2 in Fig. 10(b)], respectively. Referring to Fig. 10(c), fillet welds 1 and 2 are also applied simultaneously.

Fig. 10(d) illustrates the effect of the fillet weld 1 reinforcement on the J-integral demand of the conventional backing bar detail with $a_0 = 6$ mm (i.e., deepest crack-like flaw). In the same figure, the results are contrasted with those from the optimal beveled backing bar detail (i.e., $\theta_b = 35°$) discussed earlier. While a fillet weld reinforcement does reduce the fracture potential at C1, interestingly, the corresponding fracture potential is almost four times higher than that with the beveled backing bar configuration. Albeit the fillet weld 1 reinforcement closes the edge crack C1, this is deemed to be more critical than the open crack C2. Therefore, the rest of the fillet weld reinforcement combinations are not examined because they would increase the J-integral at C1 and decrease it at C2.

The effect of fillet weld reinforcement is also examined for the pre-Northridge connection with a beveled backing bar in Fig. 10(e). By welding the backing bar to the bottom beam flange (i.e., fillet weld 2), the stress flow in the backing bar increases, thereby compromising the J-integral at this location. The same findings hold true for fillet weld 1. The optimal beveled backing bar configuration (i.e., $\theta_b = 35°$) balances the fracture potential between C1 and C2. Consequently, tack welds and fillet weld reinforcement between the beveled backing bar and the beam or column flanges outside the weld joint should be prohibited to achieve the highest connection ductility.

Effect of Axial Load on J-Integral Demand

End columns in steel MRFs may experience tensile excursions due to dynamic overturning effects (Suzuki and Lignos 2020). The applied axial load within the panel zone decreases its strength due to the axial-to-shear load interaction. Therefore, the likelihood of fracture due to kinking at C1 location increases. Youssef et al. (1995) highlighted fractures mainly in end columns that had increased axial load demands due to transient loading. To investigate this aspect, a tensile axial load ratio $P/P_y = 10\%$ (where P is the applied axial load and P_y is the axial yield strength of the column based on measured material properties) is applied to the steel column of the same connection examined earlier. Fig. 11 shows the J-integral demand with respect to SDR when the two examined backing bars (see Fig. 7) are considered. The results are contrasted to the respective cases with no axial load demands. Overall, the analyses suggest that the tensile axial load does not practically affect the J-integral demands regardless of the examined backing bar detail. However, it
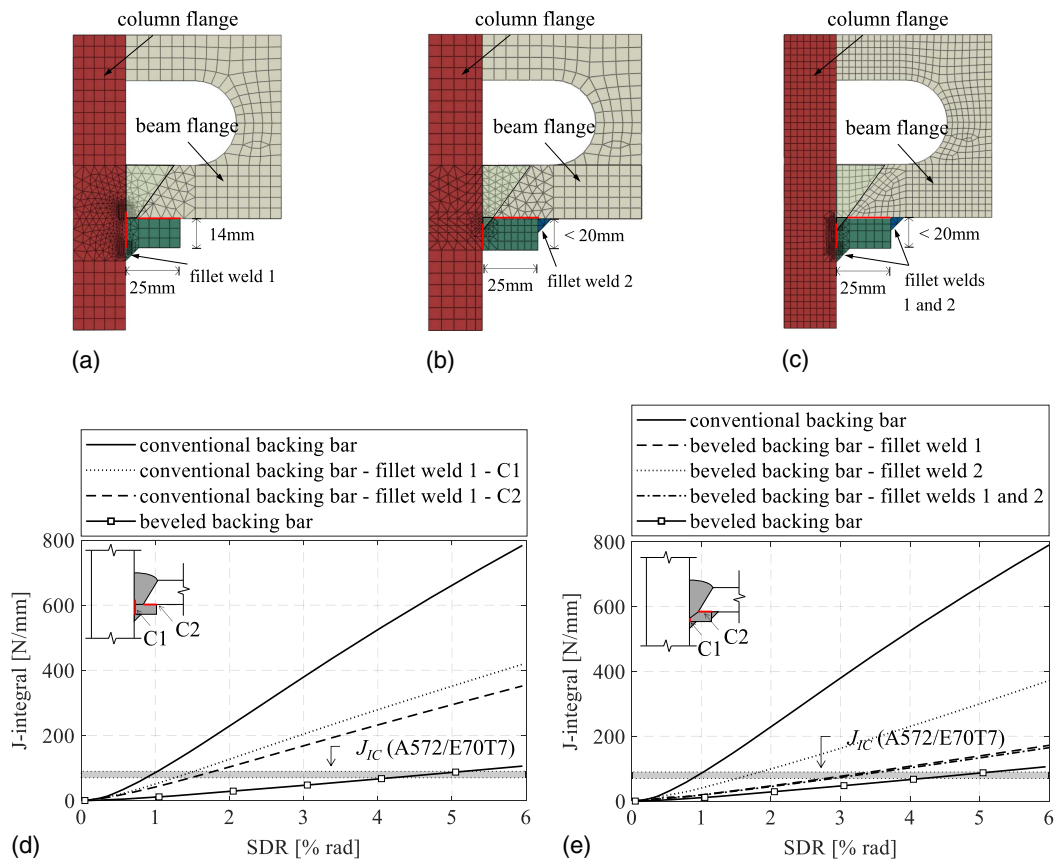
Fig. 10. Effect of fillet weld reinforcement on J-integral for pre-Northridge WUF-B connection detailing depending on the assumed continuum finite element submodel: (a) fillet weld 1 reinforced conventional backing bar; (b) fillet weld 2 reinforced beveled backing bar; (c) fillet weld 1 and 2 reinforced beveled backing bar; (d) fillet weld reinforced conventional backing bar effect on J-integral; and (e) fillet weld reinforced beveled backing bar effect on J-integral.
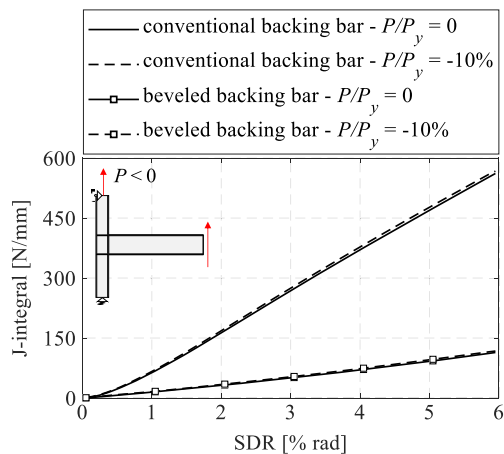

Fig. 11. Effect of column tensile axial force on J-integral for pre-Northridge WUF-B connections.

should be stated that this should be further verified when beam-to-column connections are under cyclic loading.

The general consensus from the CFE analyses presented in this section is that the proposed beveled backing bar configuration would have considerably delayed premature fractures in typical pre-Northridge WUF-B connections at location L1. Therefore, it is worth investigating the fracture potential of post-Northridge WUF-W connections when a beveled backing bar is intentionally

left in place after the completion of demand-critical CJP welds at the bottom flange of the steel beam with filler weld electrodes according to AISC (2016b).

Assessment of Post-Northridge WUF-W Connections

Prequalified WUF-W connections necessitate bottom beam flange backing bar removal, weld root back gouging, fillet weld reinforcement, and inspection of potential defects (AISC 2016a). These specifications practically provide zero fracture potential at the outer beam flange-to-column interface. Instead, fracture near the HAZ becomes critical. With the beveled backing bar configuration, potential defects in the weld root are positioned away from the beam flange, thus minimizing the fracture potential at the beam flange-to-column interface. The same holds true in cases where the bottom of the bevel may not be penetrated by the weld. However, referring to Fig. 9(a), the simulation results suggest that the beveled backing bar pushes the fracture-critical location to be near the HAZ, which is consistent with the current state of pre-qualified WUF-W connections.

A series of parametric analyses is conducted to examine the fracture potential of prequalified WUF-W connections when a beveled backing bar geometry is employed and, contrary to AISC (2016a), is not removed from the bottom flange of the steel beam. The analysis matrix, which is summarized in Table 2, includes the interior sub-assembly UT04 (denoted as Case 1), tested by Shin (2017), and the

**Table 2.** Post-Northridge subassembly CFE analysis matrix

Specimen ID	Beam cross section	Column cross section	Beam depth, d_b (mm)	Column depth, d_c (mm)	Beam flange thickness, t_{bf} (mm)	Column flange thickness, t_{cf} (mm)	R_u/R_n	Expected γ_{max}/γ_y
Case 1	W36X150	W14X398	911.9	464.8	23.9	72.4	0.50	22.0
Case 2	W36X150	W14X398	911.9	464.8	23.9	72.4	0.99	4.3
Case 3	W21X73	W24X176	538.5	640.1	18.8	34.0	0.53	23.8
Case 4	W30X116	W33X263	762.0	876.3	21.6	39.9	0.56	28.5
Case 5	W36X150	W36X256	911.9	950.0	23.9	43.9	0.54	28.5
Case 6	W36X256	W36X529	950.0	1,010.9	43.9	73.9	0.56	28.6

equivalent exterior one (denoted as Case 2). This subassembly features W36x150 beams and a W14x398 column. The rest of the analyzed cases (identified as Cases 3–6) conform to the current seismic design and fabrication standards (AISC 2016a, b, c; AWS 2010, 2016). In brief, the interior subassemblies comprise deep beams and columns (i.e., the panel zone aspect ratio is nearly equal to one). The beam and column depths range from 500 to 1,000 mm, while their flange thicknesses range from 19 to 44 mm (¾–1¾ in.) and from 34 to 74 mm (1⅜–2⅞ in.), respectively. The analyzed cases are within the design space of typical seismic designs of steel MRFs in North America (Elkady and Lignos 2014; NIST 2015). Nominally identical material properties are considered for the yield regions of the steel beams and columns in all cases.

The panel zone strength-to-resistance ratio, R_u/R_n, does not respect intentionally the requirements of AISC (2016c) to inhibit inelastic panel zone shear distortions. The panel zone strength, R_u, is computed according to the Skiadopoulos et al. (2021) design model, which is an improved representation of the AISC (2016c) panel zone model. The expected maximum panel zone inelastic shear distortions range from 20 to $25\gamma_y$.

In all examined cases, continuity plates with a thickness equal to that of the beam flange are deemed to be imperative. The CFE modeling approach is consistent with that presented earlier. The fracture potential of the examined cases is compared for three beveled backing bar geometries (bevel angles of 45°, 35°, and 30°).

Fig. 12 depicts the lateral strength, F, versus SDR and the panel zone shear distortion, γ, versus SDR relations for all the examined cases. Referring to Fig. 12(a), the examined subassemblies provide a wide range of lateral strength due to the selection of the beam and column cross sections. Fig. 12(b) suggests that the panel zone shear distortion is appreciable in most subassemblies at modest lateral drift demands (i.e., 2% rads) as well as at 4% rads.
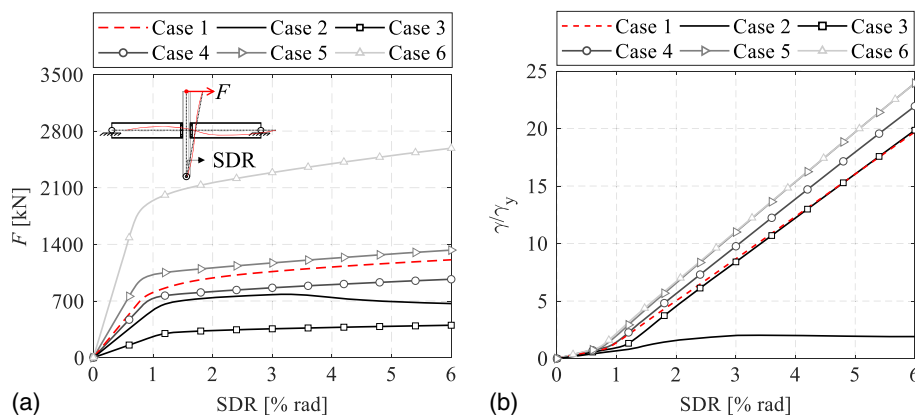
Effect of Panel Zone Design Distortions

Cases 1 (weak panel zone) and 2 (strong panel zone) are employed to assess the influence of panel zone design distortions on the connection performance. Because of the modified AISC (2016a) and AWS (2010) weld access hole in post-Northridge WUF-W connections (see Fig. 3), the stress flow near the backing bar is altered compared to that in their pre-Northridge WUF-B counterparts. Fig. 13(a) depicts the J-integral ratio between the conventional and the beveled backing bar with respect to the bevel angle for the models with $a_0 = 6$ mm. The results indicate that the fracture potential of WUF-W connections with beveled backing bars reduces by 7 to 5 times at lateral drift demands of 2% and 6% rads compared to the equivalent cases with conventional backing bars left in place after welding. Moreover, the optimal bevel angle is 45°, regardless of the panel zone strength.

Fig. 13(b) depicts the J-integral versus SDR relation for WUF-W connections with a conventional ($a_0 = 6$ mm) and the optimal beveled (i.e., $\theta_b = 45°$) backing bar configurations. Moreover, the J-integral demands are compared with the J-integral resistance of the E70T7-K2 weld electrode (Grade 480) that satisfies the minimum criteria for demand-critical welds (AISC 2016b) for prequalified beam-to-column connections. The median J_{IC} is equal to 208 N/mm, while the 5th and 95th percentiles are equal to 118 N/mm and 300 N/mm, respectively, based on prior pertinent work (Gomez et al. 2008; Kanvinde et al. 2008). Referring to Fig. 13(b), the conventional backing bar configuration leads to connection fractures prior to an SDR of 3–4% rads; hence, its removal is justifiable. Conversely, the same connection with the optimal beveled backing bar configuration exceeds an SDR of 6% rads even when compared with the 5th percentile of the weld electrode toughness.
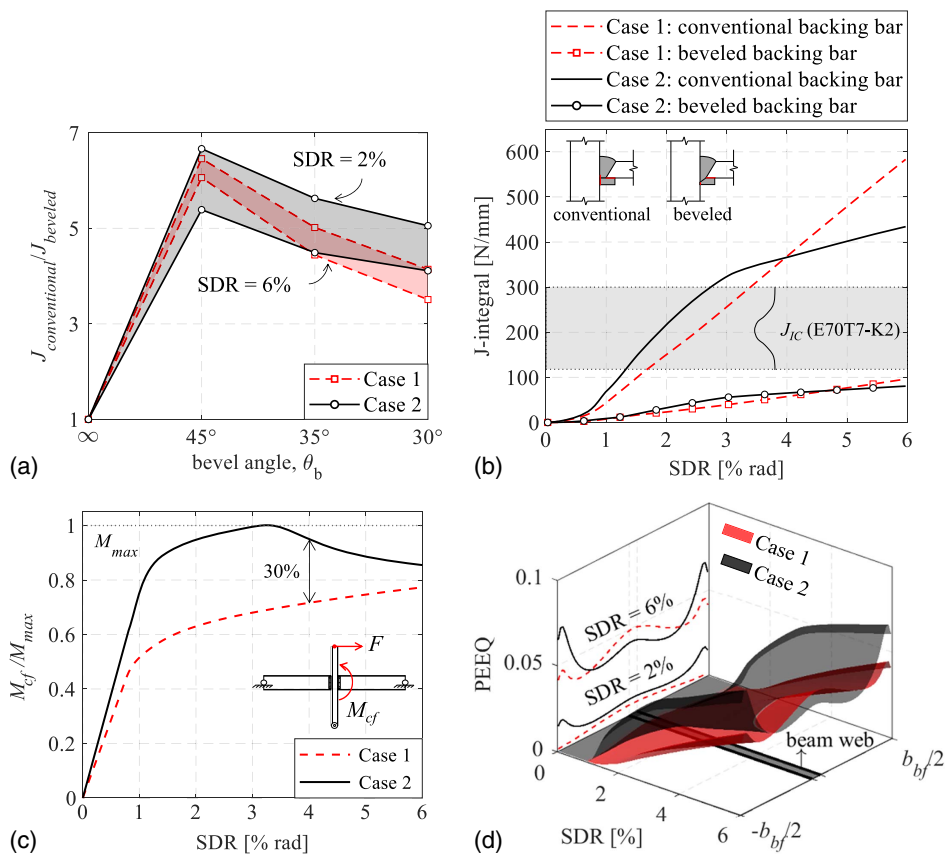

Fig. 12. Prequalified WUF-W connection: (a) applied force versus story drift ratio; and (b) normalized panel zone shear distortion versus story drift ratio.

Fig. 13. Prequalified WUF-W connections with weak and strong panel zones: (a) J-integral for conventional and beveled backing bars; (b) J-integral versus story drift ratio; (c) normalized moment at the column face versus story drift ratio; and (d) PEEQ distribution within the bottom beam flange versus story drift ratio.

Referring to Fig. 13(b), the fracture potential of WUF-W connections featuring a weak panel zone is 1.4 times higher than that of the strong one only when SDRs exceed 4% rads. Conversely, prior to 4% rads, WUF-W connections with a strong panel zone possess almost 30–50% higher fracture potential compared to those with a weak one. To explain this, Fig. 13(c) depicts the moment demand at the column face, M_{cf}, (normalized to the maximum attained moment, M_{max}) versus SDR. When the panel zone is designed to remain elastic (Case 2), the flexural demand at the column face of the WUF-W connection is at least 30% higher than that of its weak panel zone counterpart. Once local buckling occurs in the steel beam (i.e., SDR of about 3% rads), the flexural moment demand is capped in the strong panel zone case. Conversely, local buckling does not occur in cases where panel zones exhibit highly inelastic deformations (i.e., $\gamma > 20\gamma_y$) even at lateral drift demands higher than 6% rads.

Fig. 13(d) compares the cumulative equivalent plastic strain (PEEQ) of the outer beam flange fiber versus SDR for Cases 1 (weak panel zone) and 2 (strong panel zone). The distributions are extracted along the beam flange width from positions adjacent to the respective backing bar. Characteristic 2-D projections are illustrated in the same figure at an SDR of 2% and 6% rads. Prior to an SDR of 4% rads, in the weak panel zone case, M_{cf} is 30% smaller than that in its strong panel zone counterpart. As such, the PEEQ is higher in the latter than that in the former. After the onset of steel beam local buckling in the strong panel zone case, the PEEQ caps due to the high plastic concentration within the buckled region of the steel beam. Conversely, the weak panel zone attains relatively high inelastic deformations; hence, the PEEQ in the

critical web centerline region becomes 1.4 times higher than that of the strong panel zone case.

Beam Depth Effect

Referring to Table 2, Cases 3 to 5 feature beams with depths ranging from 500 to about 900 mm. The variation of the beam and column flange thickness and the panel zone design distortions is fairly minor in these models. Fig. 14(a) depicts the J-integral evolution with respect to SDR for the optimal beveled backing bar configuration (i.e., $\theta_b = 45°$). The shallower beam (i.e., $d_b = 540$ mm) possesses almost 1.3 times lower fracture potential compared to the deeper one (i.e., $d_b = 910$ mm). This is attributed to the increased strain demand in deep beams (El-Tawil et al. 1999). However, fracture is only expected at lateral drift demands exceeding 6% rads and by only assuming the 5th percentile of the E70T7-K2 weld electrode toughness, which is a fairly conservative assumption.

Beam Flange Thickness Effect

The beam flange thickness effect on the fracture potential of post-Northridge WUF-W connections is demonstrated by comparing Cases 1 and 6 (see Table 2). The former features a 24-mm beam flange thickness, while the latter features a 44-mm beam flange thickness. Fig. 14(b) depicts the J-integral evolution over SDR for the optimal beveled backing bar configuration. The beam with the thicker flange (i.e., beam flange thickness, $t_{bf} = 44$ mm) possesses a 20% higher fracture potential than that of the beam with a flange thickness, of 24 mm. In addition, fracture initiation only
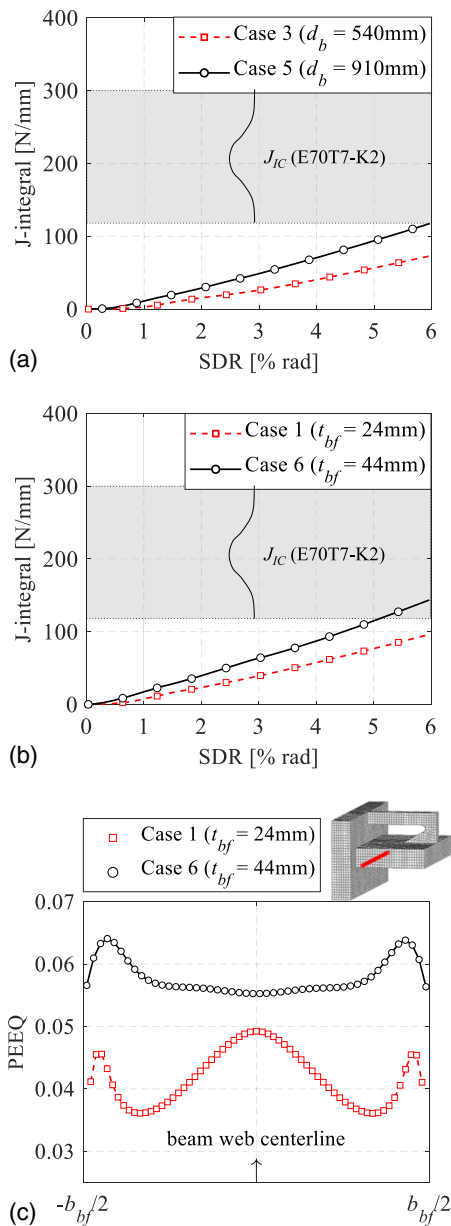
Fig. 14. Fracture assessment of prequalified WUF-W connections with a beveled backing bar: (a) effect of varying beam depth on J-integral; (b) effect of varying beam flange thickness on J-integral; and (c) PEEQ distribution along the beam flange width at 6% SDR for different beam flange thicknesses.

occurs at lateral drift demands larger than 5% rads regardless of the beam flange thickness.

The increased J-integral demand in the thicker beam flanges, which is highlighted in Fig. 14(b), may be explained by Fig. 14(c), which depicts the PEEQ along the beam flange width at an SDR of 6% rads. For the thicker beam flange, the plastic strains are increased in the web centerline location by almost 10%. This increase in the plastic strains is associated with a higher-pressure index (i.e., ratio of hydrostatic stress over the yield stress) in beams with thicker flanges (El-Tawil et al. 1998).

Column Flange Thickness Effect

Referring to Table 2, we can quantify the effect of the column flange thickness on the fracture potential of WUF-W connections

by comparing the results from Case 1 (column flange thickness, $t_{cf} = 72$ mm) and 5 ($t_{cf} = 44$ mm). Referring to Figs. 14(a and b), the fracture potential of the connection with thicker column flanges (i.e., Case 1) reduces by nearly 10% compared to that of the thinner column flange counterpart (i.e., Case 5) at SDRs ranging from 2% to 6% rads. Qualitatively, the kinking effect is more eminent in the thinner column flange element at inelastic panel zone distortions of $20–25\gamma_y$. This, subsequently, leads to the J-integral increase. However, this only occurs at relatively large lateral drift demands (i.e., larger than 5% rads).

Weld Toe Size Effect

The preceding analyses assumed a 6-mm weld toe size for the beam flange-to-column CJP weld. According to AWS (2010), a 10-mm weld toe size is also permissible; hence, this effect was also investigated. While the weld toe size does not affect the fracture potential of the connections with a beveled backing bar, the analyses suggest that a 45° and a 50° bevel angle are optimal for the 6-mm and 10-mm weld toe, respectively, assuming a built-in crack of $a_0 = 3$ mm. The results are not presented herein due to brevity.

Limitations

This paper focuses on the fracture potential of field-welded connections subjected to monotonic loading. Prequalified beam-to-column connections in capacity-designed steel MRFs experience inelastic cyclic drift demands, which cannot be assessed with the present methodology and employed fracture mechanics methods. On the other hand, in the present study, a uniform crack of two different depths (i.e., $a_0 = 3$ mm and $a_0 = 6$ mm) was assumed, which is deemed to be a conservative assumption [see Fig. 1(c)].

Fracture due to lamellar tearing in the column's through-thickness flange was disregarded by assuming that the toughness requirements in the Z-direction of the column flange are sufficient. This issue deserves more attention in connection geometries featuring thick column flange thicknesses (i.e., larger than 38 mm).

Another critical aspect relates to the role of the slab on the fracture potential of WUF-W connections. Prior investigations after the 1994 Northridge and 1995 Kobe earthquakes (FEMA 2000a; Mahin 1998; Nakashima et al. 2007) have demonstrated that when the slab is in fully composite or partially composite action with the floor beams, the neutral axis shifts toward the concrete slab, thereby increasing the inelastic strain demand at the beam's bottom flange welds when the slab is in compression (Nakashima et al. 2007; Ricles et al. 2002b). The increased strain demand may be prevented by isolating the slab from the steel column (Hobbs 2014; Tremblay et al. 1997).

Considering all the presented limitations, the findings of the present study should be substantiated by full-scale physical testing of WUF-W beam-to-column connections under reversed cyclic loading. Beveled backing bars with the optimal geometry (i.e., bevel angle of 45°) may be used and left in place after the completion of demand-critical CJP groove welds between the beam and column flanges to examine their effectiveness in reducing the fracture potential in WUF-W connections. Such investigations are currently underway by the authors.

Summary and Conclusions

This paper revisits concepts in prequalified field-welded connections aiming to identify fabrication simplifications by means of simulation-based engineering design. For this purpose, the paper explores the potential of keeping the bottom beam flange backing

bar in place after executing the CJP groove welds at this location. To reduce the associated fracture potential at this location, a customized beveled backing bar is proposed. The employed methodology for such an endeavor features traditional fracture mechanics informed by three-dimensional CFE analyses. The CFE approach is validated to available test data from typical welded unreinforced flange-bolted web (WUF-B) pre-Northridge connections. Several backing bar geometry details are examined with and without fillet weld reinforcements. These are compared with the proposed one. The connection performance is assessed by means of parametric studies on prequalified welded unreinforced flange-welded web (WUF-W) connections.

Based on the CFE simulations, WUF-B pre-Northridge connections can sustain a lateral drift demand of 4% to 6% rads prior to fracture when the customized beveled backing bar is employed, even when the low-toughness E70T7 filler metal is utilized for completing the beam flange-to-column flange CJP weld. The reason is that with the beveled backing bar the crack tip is situated away from the critical beam flange location. The peak lateral drift capacity prior to fracture in this case is improved by more than four times relative to that with a conventional backing bar.

The CFE results suggest that the optimal backing bar bevel angle, θ_b, for typical pre-Northridge WUF-B connections, is 35°. When θ_b decreases, the backing bar-to-beam flange crack tip C2 becomes critical; hence, the fracture potential at crack tips C1 and C2 are identical for the optimal bevel angle.

The fillet weld reinforcement in conventional backing bars closes the edge cracks and reduces the fracture potential of field-welded connections by up to two times. However, connections with the beveled backing bar still possess a fracture potential, which is one-fourth that of the fillet weld reinforced conventional backing bar.

The simulation studies reveal that the fracture potential of field-welded connections is practically not influenced by the tensile and/or compressive column axial load demands regardless of the employed backing bar geometry. This is attributed to the fact that the column axial load does not affect the beam moment demand, strongly influencing the connection ductility under lateral loading.

Contrary to WUF-B pre-Northridge connections, in prequalified WUF-W connections, the optimal beveled angle, θ_b, is found to be 45°. This is due to the modified weld access hole geometry that is adopted in WUF-W connections. The CFE results suggest that prequalified WUF-W connections with a beveled backing bar left in place after welding sustain lateral drift demands of at least 6% rads prior to fracture regardless of the panel zone strength, beam depth, as well as thickness of the beam and column flanges, given that the minimum criteria for demand-critical groove welds according to AISC (2016b) are respected.

Prequalified WUF-W connections featuring weak panel zones with $\gamma > 20\gamma_y$ possess nearly 1.5 times higher fracture potential compared to their strong panel zone counterparts at lateral drift demands above 4% rads. Interestingly, at SDRs less than 4% rads, the fracture potential of WUF-W connections with strong panel zones is nearly 1.5 higher than that of their weak panel zone counterparts. In the former, the moment at the column face is about 30% higher than that in the latter. However, in the strong panel zone case, the onset of local buckling in the beam caps the strain demands due to flexure at lateral drift demands of about 4% rads. On the other hand, at this drift range, panel zone kinking prevails in cases where the panel zone shear distortion is larger than $12\gamma_y$.

The fracture potential of WUF-W connections comprising shallow beams (e.g., $d_b \sim 550$ mm) is about 30% less compared to that in connections with deeper beams (e.g., $d_b \sim 900$ mm). Similarly, beams with thick flanges (e.g., $t_{bf} > 40$ mm) possess about 10%

higher fracture potential compared to beams with thinner flanges (e.g., $t_{bf} < 25$ mm) due to the higher-pressure index and the associated plastic strains in the former. On the other hand, steel columns with relatively thick flanges (e.g., $t_{cf} > 70$ mm) possess about 10% lower fracture potential compared to columns with thinner flanges (e.g., $t_{cf} < 45$ mm). This is attributed to the kinking effect, which is more eminent in the latter case.

Data Availability Statement

Some or all data, models, or code generated or used that support the findings of this study are available from the corresponding author upon reasonable request.

Acknowledgments

References

ABAQUS. 2014. *ABAQUS analysis user's manual version 6.14-1*. Providence, RI: Dassault Systems Simulia Corporation.

AISC (American Institute for Steel Construction). 2016a. *Prequalified connections for special and intermediate steel moment frames for seismic applications*. ANSI/AISC 358-16. Chicago: AISC.

AISC (American Institute for Steel Construction). 2016b. *Seismic provisions for structural steel buildings*. ANSI/AISC 341-16. Chicago: AISC.

AISC (American Institute for Steel Construction). 2016c. *Specification for structural steel buildings*. ANSI/AISC 360-16. Chicago: AISC.

ASTM. 2015. *Standard guide for magnetic particle testing*. ASTM E709-15. West Conshohocken, PA: ASTM International.

ASTM. 2017. *Standard specification for straight beam ultrasonic examination of rolled steel structural shapes*. ASTM A898/A898M-17. West Conshohocken, PA: ASTM International.

ASTM. 2018. *Standard practice for liquid penetrant examination for general industry*. ASTM E165/E165M-18. West Conshohocken, PA: ASTM International.

AWS (American Welding Society). 2010. *Structural welding code—Steel*. ANSI/AWS D1.1:2010. Miami: AWS.

AWS (American Welding Society). 2016. *Structural welding code-seismic supplement*. AWS D1.8/D1.8M:2016. Miami: AWS.

Bakker, A. 1984. *The three-dimensional J-Integral*. Rep. No. WTHD 167. Delft, Netherlands: Delft Univ. of Technology.

Bouchard, S., and G. Axmann. 2000. "ASTM A913 grades 50 and 65: Steels for seismic applications." In *Proc., 3rd Int. Conf. on Behavior of Steel Structures in Seismic Areas (STESSA)*, 11–17. Boca Raton, Florida: CRC Press.

Brocks, W., and I. Scheider. 2001. *Numerical aspects of the path-dependence of the J-integral in incremental plasticity: How to calculate reliable J-values in FE analysis*. Geesthacht, Germany: GKSS-Forschungszentrum.

CEN (European Committee for Standardization). 2004. *Eurocode 3: Design of steel structures—Part 10: Material toughness and through-thickness properties*. EN 1993-1-10. Brussels, Belgium: CEN.

Chi, W. M., G. G. Deirlein, and A. Ingraffea. 1997. *Finite element fracture mechanics investigation of welded beam-column connections*. Rep. No. SAC/BD-97/05. Sacramento, CA: SAC Joint Venture.

Chi, W.-M., G. G. Deierlein, and A. Ingraffea. 2000. "Fracture toughness demands in welded beam-column moment connections." *J. Struct. Eng.* 126 (1): 88–97. https://doi.org/10.1061/(ASCE)0733-9445(2000)126:1(88).

de Castro e Sousa, A., Y. Suzuki, and D. Lignos. 2020. "Consistency in solving the inverse problem of the Voce-Chaboche constitutive model for plastic straining." *J. Eng. Mech.* 146 (9): 04020097. https://doi.org/10.1061/(ASCE)EM.1943-7889.0001839.

deLorenzi, H. G. 1982. "On the energy release rate and the J-integral for 3-D crack configurations." *Int. J. Fract.* 19 (3): 183–193. https://doi.org/10.1007/BF00017129.

Elkady, A., and D. G. Lignos. 2014. "Modeling of the composite action in fully restrained beam-to-column connections: Implications in the seismic design and collapse capacity of steel special moment frames." *Earthquake Eng. Struct. Dyn.* 43 (13): 1935–1954. https://doi.org/10.1002/eqe.2430.

Elkady, A., and D. G. Lignos. 2018. "Improved seismic design and non-linear modeling recommendations for wide-flange steel columns." *J. Struct. Eng.* 144 (9): 04018162. https://doi.org/10.1061/(ASCE)ST.1943-541X.0002166.

El-Tawil, S., T. Mikesell, and S. K. Kunnath. 2000. "Effect of local details and yield ratio on behavior of FR steel connections." *J. Struct. Eng.* 126 (1): 79–87. https://doi.org/10.1061/(ASCE)0733-9445(2000)126:1(79).

El-Tawil, S., T. Mikesell, E. Vidarsson, and S. K. Kunnath. 1998. *Strength and ductility of FR welded-bolted connections*. Orlando, FL: Univ. of Central Florida.

El-Tawil, S., E. Vidarsson, T. Mikesell, and S. K. Kunnath. 1999. "Inelastic behavior and design of steel panel zones." *J. Struct. Eng.* 125 (2): 183–193. https://doi.org/10.1061/(ASCE)0733-9445(1999)125:2(183).

Erdogan, F., and G. C. Sih. 1963. "On the crack extension in plates under plane loading and transverse shear." *J. Basic Eng.* 85 (4): 519–525. https://doi.org/10.1115/1.3656897.

FEMA. 1997. *Connection test summaries*. FEMA-289. Washington, DC: FEMA.

FEMA. 2000a. *State of the art report on connection performance*. FEMA-355D. Washington, DC: FEMA.

FEMA. 2000b. *State of the art report on past performance of steel moment-frame buildings in earthquakes*. FEMA-355E. Washington, DC: FEMA.

Gomez, I. R., A. M. Kanvinde, Y. K. Kwan, and G. Y. Grondin. 2008. *Strength and ductility of welded joints subjected to out-of-plane bending*. Chicago: American Institute of Steel Construction.

Han, S. W., G. U. Kwon, and K. H. Moon. 2007. "Cyclic behaviour of post-Northridge WUF-B connections." *J. Constr. Steel Res.* 63 (3): 365–374. https://doi.org/10.1016/j.jcsr.2006.05.003.

Hobbs, M. 2014. "Effects of slab-column interaction in steel moment resisting frames with steel-concrete composite floor slabs." Master's thesis, Dept. of Civil and Natural Resources Engineering, Univ. of Canterbury.

Ibrahim, O. A., D. G. Lignos, and C. A. Rogers. 2019. "Recommendations for improved welding procedures for thick steel plates through thermo-mechanical analysis." *Int. J. Steel Struct.* 19 (1): 193–212. https://doi.org/10.1007/s13296-018-0110-2.

Irwin, G. R. 1961. "Plastic zone near a crack and fracture toughness." Vol. 4 of *Proc., Sagamore Research Conf.*, 63–78. Syracuse, NY: Syracuse Univ. Research Institute.

Jia, L.-J., and H. Kuwamura. 2014. "Ductile fracture simulation of structural steels under monotonic tension." *J. Struct. Eng.* 140 (5): 04013115. https://doi.org/10.1061/(ASCE)ST.1943-541X.0000944.

Kanno, R. 2016. "Advances in steel materials for innovative and elegant steel structures in japan–A review." *Struct. Eng. Int.* 26 (3): 242–253. https://doi.org/10.2749/101686616X14555428759361.

Kanvinde, A. M. 2017. "Predicting fracture in civil engineering steel structures: State of the art." *J. Struct. Eng.* 143 (3): 03116001. https://doi.org/10.1061/(ASCE)ST.1943-541X.0001704.

Kanvinde, A. M., B. V. Fell, I. R. Gomez, and M. Roberts. 2008. "Predicting fracture in structural fillet welds using traditional and micromechanical fracture models." *Eng. Struct.* 30 (11): 3325–3335. https://doi.org/10.1016/j.engstruct.2008.05.014.

Kaufmann, E. J., and J. W. Fisher. 1996. *Fracture analysis of failed moment frame weld joints produced in full-scale laboratory tests and buildings damaged in the Northridge earthquake*. Sacramento, CA: SAC Joint Venture.

Kolednik, O., J. Predan, G. X. Shan, N. K. Simha, and F. D. Fischer. 2005. "On the fracture behavior of inhomogeneous materials—A case study for elastically inhomogeneous biomaterials." *Int. J. Solids Struct. Micromech. Mater.* 42 (2): 605–620. https://doi.org/10.1016/j.ijsolstr.2004.06.064.

Krawinkler, H. 1978. "Shear in beam-column joints in seismic design of steel frames." *Eng. J.* 15 (3): 82–91.

Krawinkler, H. 1995. "Earthquake design and performance of steel structures." In *Proc., Pacific Conf. on Earthquake Engineering, PCEE 95*, VIC, Australia: Australian Earthquake Engineering Society.

Landolfo, R., et al. 2018. *EQUALJOINTS PLUS —Volume with information brochures for 4 seismically qualified joints*. Brussels, Belgium: European Convention for Constructional Steelwork.

Lemaitre, J., and J. L. Chaboche. 1990. *Mechanics of solid materials*. Cambridge, UK: Cambridge University Press.

Lignos, D. G., T. Hikino, Y. Matsuoka, and M. Nakashima. 2013. "Collapse assessment of steel moment frames based on E-Defense full-scale shake table collapse tests." *J. Struct. Eng.* 139 (1): 120–132. https://doi.org/10.1061/(ASCE)ST.1943-541X.0000608.

Lignos, D. G., H. Krawinkler, and A. S. Whittaker. 2011. "Prediction and validation of sidesway collapse of two scale models of a 4-story steel moment frame." *Earthquake Eng. Struct. Dyn.* 40 (7): 807–825. https://doi.org/10.1002/eqe.1061.

Lu, L. W., J. M. Ricles, C. Mao, and J. W. Fisher. 2000. "Critical issues in achieving ductile behaviour of welded moment connections." *J. Constr. Steel Res.* 55 (1–3): 325–341. https://doi.org/10.1016/S0143-974X(99)00092-9.

Mahin, S. A. 1998. "Lessons from damage to steel buildings during the Northridge earthquake." *Eng. Struct.* 20 (4–6): 261–270. https://doi.org/10.1016/S0141-0296(97)00032-1.

Mao, C., J. Ricles, L. W. Lu, and J. Fisher. 2001. "Effect of local details on ductility of welded moment connections." *J. Struct. Eng.* 127 (9): 1036–1044. https://doi.org/10.1061/(ASCE)0733-9445(2001)127:9(1036).

Miki, C., K. Homma, and T. Tominaga. 2002. "High strength and high performance steels and their use in bridge structures." *J. Constr. Steel Res.* 58 (1): 3–20. https://doi.org/10.1016/S0143-974X(01)00028-1.

Miller, D. K. 1998. "Lessons learned from the Northridge earthquake." *Eng. Struct.* 20 (4): 249–260. https://doi.org/10.1016/S0141-0296(97)00031-X.

Miller, D. K. 2017. *AISC steel design guide 21 welded connections—A primer for engineers*. 2nd ed. Chicago: American Institute of Steel Construction.

Myers, A. T., G. G. Deierlein, and A. M. Kanvinde. 2009. *Testing and probabilistic simulation of ductile fracture initiation in structural steel components and weldments*. Rep. No. 170. Stanford: Stanford Univ.

Nakashima, M., T. Matsumiya, K. Suita, and F. Zhou. 2007. "Full-scale test of composite frame under large cyclic loading." *J. Struct. Eng.* 133 (2): 297–304. https://doi.org/10.1061/(ASCE)0733-9445(2007)133:2(297).

NIST (National Institute of Standards and Technology). 2015. *Assessment of first generation performance-based seismic design methods for new steel buildings, Volume 1: Special Moment Frames. Technical Note (NIST TN) 1863-1*. Gaithersburg, MD: NIST.

Paret, T. F. 2000. "The W1 issue. I: Extent of weld fracturing during Northridge earthquake." *J. Struct. Eng.* 126 (1): 10–18. https://doi.org/10.1061/(ASCE)0733-9445(2000)126:1(10).

Parks, D. M. 1977. "The virtual crack extension method for nonlinear material behavior." *Comput. Methods Appl. Mech. Eng.* 12 (3): 353–364. https://doi.org/10.1016/0045-7825(77)90023-8.

Popov, E. P., T.-S. Yang, and S.-P. Chang. 1998. "Design of steel MRF connections before and after 1994 Northridge earthquake." *Eng. Struct.* 20 (12): 1030–1038. https://doi.org/10.1016/S0141-0296(97)00200-9.

Rice, R. H. 1968. "A path independent integral and the approximate analysis of strain concentration by notches and cracks." *J. Appl. Mech.* 35 (2): 379–386. https://doi.org/10.1115/1.3601206.

Richard, R. M. 2003. "Discussion of 'general issues influencing connection performance' by Charles W. Roeder." *J. Struct. Eng.* 129 (6): 838–840. https://doi.org/10.1061/(ASCE)0733-9445(2003)129:6(838.2).

Ricles, J. M., J. W. Fisher, L.-W. Lu, and E. J. Kaufmann. 2002a. "Development of improved welded moment connections for earthquake-resistant design." *J. Constr. Steel Res.* 58 (5–8): 565–604. https://doi.org/10.1016/S0143-974X(01)00095-5.

Ricles, J. M., C. Mao, L.-W. Lu, and J. W. Fisher. 2002b. "Inelastic cyclic testing of welded unreinforced moment connections." *J. Struct. Eng.* 128 (4): 429–440. https://doi.org/10.1061/(ASCE)0733-9445(2002)128:4(429).

Ricles, J. M., X. Zhang, L.-W. Lu, and J. W. Fisher. 2004. *Development of seismic guidelines for deep-column steel moment connections*. Rep. No. 04–13. Bethlehem, PA: Advanced Technology for Large Structural Systems, Lehigh Univ..

Shaw, S. M., K. Stillmaker, and A. M. Kanvinde. 2015. "Seismic response of partial-joint-penetration welded column splices in moment-resisting frames." *Eng. J.* 52 (2): 87–108.

Shin, S. 2017. "Experimental and analytical investigation of panel zone behavior in steel moment frames." Ph.D. thesis, Dept. of Civil, Architectural and Environmental Engineering, Univ. of Texas at Austin.

Simha, N. K., F. D. Fischer, O. Kolednik, and C. R. Chen. 2003. "Inhomogeneity effects on the crack driving force in elastic and elastic–plastic materials." *J. Mech. Phys. Solids* 51 (1): 209–240. https://doi.org/10.1016/S0022-5096(02)00025-X.

Skiadopoulos, A., A. Elkady, and D. G. Lignos. 2021. "Proposed panel zone model for seismic design of steel moment-resisting frames." *J. Struct. Eng.* 147 (4): 04021006. https://doi.org/10.1061/(ASCE)ST.1943-541X.0002935.

Skiadopoulos, A., and D. G. Lignos. 2021. "Development of inelastic panel zone database." *J. Struct. Eng.* 147 (4): 04721001. https://doi.org/10.1061/(ASCE)ST.1943-541X.0002957.

Smelser, R. E., and M. E. Curtin. 1977. "On the J-integral for Bi-material bodies." *Int. J. Fract.* 13 (3): 382–384. https://doi.org/10.1007/BF00040155.

Stillmaker, K., A. Kanvinde, and C. Galasso. 2016. "Fracture mechanics-based design of column splices with partial joint penetration welds." *J. Struct. Eng.* 142 (2): 04015115. https://doi.org/10.1061/(ASCE)ST.1943-541X.0001380.

Suzuki, Y., and D. G. Lignos. 2020. "Development of collapse-consistent loading protocols for experimental testing of steel columns." *Earthquake Eng. Struct. Dyn.* 49 (2): 114–131. https://doi.org/10.1002/eqe.3225.

Suzuki, Y., and D. G. Lignos. 2021. "Experimental evaluation of steel columns under seismic hazard-consistent collapse loading protocols." *J. Struct. Eng.* 147 (4): 04021020. https://doi.org/10.1061/(ASCE)ST.1943-541X.0002963.

Tremblay, R., N. Tchebotarev, and A. Filiatrault. 1997. "Seismic performance of RBS connections for steel moment resisting frames: Influence of loading rate and floor slab." In *Proc., STESSA '97*. Milano, Italy: Edizioni.

Wang, Y., H. Zhou, Y. Shi, and H. Chen. 2010. "Fracture behavior analyses of welded beam-to-column connections based on elastic and inelastic fracture mechanics." *Int. J. Steel Struct.* 10 (3): 253–265. https://doi.org/10.1007/BF03215835.

Wells, A. A. 1961. "Unstable crack propagation in metals: Cleavage and fast fracture." In Vol. 1 of *Proc., Crack Propagation Symp.*, Cranfield, England: College of Aeronautics.

Yang, T.-S., and E. P. Popov. 1995. *Behavior of pre-Northridge moment resisting steel connections*. Berkeley: Earthquake Engineering Research Center, Univ. of California.

Yang, Y., Y. Wang, F. Yang, and Q. An. 2019. "Influence of weld details on fracture behavior of connections using high-strength steel." *J. Constr. Steel Res.* 153 (Feb): 578–587. https://doi.org/10.1016/j.jcsr.2018.11.004.

Youssef, N. F. G., D. Bonowitz, and J. L. Gross. 1995. *A Survey of Steel Moment-Resisting Frame Buildings Affected by the 1994 Northridge Earthquake*. Gaithersburg, MD: National Institute of Standards and Technology.

Yu, Q. S., C. Gilton, and C.-M. Uang. 2000. *Cyclic response of RBS moment connections: Loading sequence and lateral bracing effects*. Rep. No. SAC/BD-00/22. Sacramento, CA: SAC Joint Venture.

Full-Scale Experiments of Cyclically Loaded Welded Moment Connections with Highly Dissipative Panel Zones and Simplified Weld Details

Andronikos Skiadopoulos, Aff.M.ASCE[1]; Dimitrios G. Lignos, M.ASCE[2]; Masaki Arita[3]; and Satoru Hiroshima[4]

Abstract: This paper presents the experimental results of two welded unreinforced flange-welded web (WUF-W) beam-to-column connections that defy the current design paradigm of prequalified welded connections. The proposed WUF-W connections feature customized beveled backing bars that are intentionally left in place after the completion of the beam flange-to-column face complete joint penetration welds. The connection design aims at a stable hysteretic response by exploiting the beneficial aspects of appreciable panel zone shear yielding (i.e., inelastic shear distortions of at least $15\gamma_y$, where γ_y is the panel zone shear distortion at yield), by considering a shear strength-to-demand ratio of 0.8. To prevent divot fracture in the column, minimum through-thickness toughness requirements were imposed for the steel column material. The experimental results suggest that the proposed WUF-W connections achieve a stable hysteretic response up until lateral drift demands of at least 7% rad, while a non-softening response was assured up to 9% rad. The beveled backing bars minimize the associated fracture potential near the beam web centerline, which is a primary concern in prequalified field welded moment connections when conventional weld backing bars are employed. The tests suggest that, under a symmetric cyclic loading protocol, local buckling near the steel beams is prevented up until a lateral drift demand of 6% rad, which is an important finding from structural repairability and stability standpoints. The ultimate failure modes of the welded connections, which are attributable to ductile crack initiation and propagation, are consistent regardless of the employed lateral loading histories, which involved standard symmetric cyclic and collapse-consistent loading protocols. The implications for the seismic design of steel moment resisting frames (MRFs) and the limitations of the present work are discussed. **DOI: 10.1061/JSENDH.STENG-12128.** © *2023 American Society of Civil Engineers.*

Author keywords: Steel moment resisting frames; Welded beam-to-column connections; Beveled backing bars; Inelastic panel zone; Pre-qualified connections; Ductile cracks; Instability-free performance.

Introduction

The dynamic stability of capacity-designed steel moment resisting frames (MRFs) relies on the anticipated seismic performance of their fully restrained beam-to-column connections. Depending on the targeted panel zone shear strength-to-demand ratio, the permissible level of panel zone inelastic shear distortions may be up to $4\gamma_y$ (where γ_y is the panel zone shear distortion at yield), according to today's seismic design provisions (e.g., AISC 2016b).

The current state-of-the-art in prequalified fully restrained welded beam-to-column connections, as described in AISC (2016a), has been influenced by research, which was mostly conducted after the 1994 Northridge earthquake (Mahin et al. 2002; Malley 1998). At that time, common deficiencies that compromised the cyclic behavior of welded unreinforced flange-bolted web (WUF-B) connections were: (1) non-optimized access hole geometry (Lu et al. 2000; Mao et al. 2001; Ricles et al. 2002a, 2003); (2) inadequate weld material toughness requirements (Chi et al. 2000); (3) inferior base material quality control and through-thickness properties (Krawinkler 1995; Tremblay et al. 1995); and (4) the presence of the weld backing bar in the bottom beam flange-to-column connection after the execution of the complete joint penetration (CJP) groove welds at this location. The notch at the bottom beam flange backing bar together with additional flaws that may be introduced from the interruption of the welding process at the beam web location led to high strain demands at the backing bar-to-column face weld root. These were enlarged particularly in connection geometries that featured deep beams and/or inelastic panel zone designs (Chi et al. 1997; El-Tawil 2000; El-Tawil et al. 1999; Whittaker et al. 1998). The role of the concrete slab on the observed behavior of welded connections was also stressed (Hajjar et al. 1998; Leon et al. 1998).

Follow-up experimental studies on WUF-B connections with improved material and connection details (Han et al. 2007; Stojadinović et al. 2000) demonstrated the need for welding a portion of the shear tab to the beam web, which led to the development of the

[1]Postdoctoral Resarcher, Civil Engineering Institute, School of Architecture, Civil and Environmental Engineering (ENAC), École Polytechnique Fédérale de Lausanne (EPFL), Station 18, Lausanne 1015, Switzerland. ORCID: https://orcid.org/0000-0002-3813-4325. Email: andronikos.skiadopoulos@epfl.ch

[2]Professor and Department Chair, Civil Engineering Institute, School of Architecture, Civil and Environmental Engineering (ENAC), École Polytechnique Fédérale de Lausanne (EPFL), Station 18, Lausanne 1015, Switzerland (corresponding author). ORCID: https://orcid.org/0000-0003-0682-4660. Email: dimitrios.lignos@epfl.ch

[3]Senior Researcher, Research & Development, Nippon Steel Corporation, Shintomi 20-1, Futtsu, Chiba 293-8511, Japan. ORCID: https://orcid.org/0000-0002-8799-089X. Email: arita.a58.masaki@jp.nipponsteel.com

[4]Senior Researcher, Research & Development, Nippon Steel Corporation, Shintomi 20-1, Futtsu, Chiba 293-8511, Japan. ORCID: https://orcid.org/0000-0002-1175-7303. Email: hiroshima.kp9.satoru@jp.nipponsteel.com
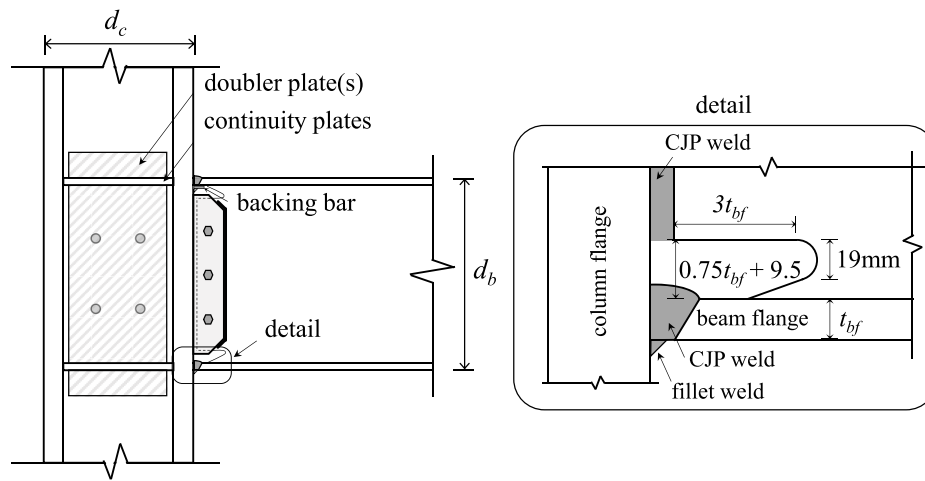
Fig. 1. Illustration of typical welded unreinforced flange-welded web connection detailing.

welded unreinforced flange-welded web (WUF-W) connection. While similarities in the structural detailing and fabrication of today's prequalified WUF-W connections hold true worldwide, the primary focus of this paper is on WUF-W connections according to the North American seismic design and fabrication standards (AISC 2016a; AWS 2016).

The typical WUF-W connection (Fig. 1), features improved weld specifications (Chi et al. 1997), an optimized access hole geometry (Lu et al. 2000; Mao et al. 2001; Ricles et al. 2000, 2002a, b, 2003), continuity plates, when necessary, to transfer the beam flange forces due to flexure in the beam, and doubler plates to satisfy the targeted panel zone design requirements (Lee et al. 2005a, b). Moreover, after completing the CJP groove weld at the bottom beam flange-to-column face joint, it is imperative to remove the conventional backing bar, while the weld root should be back-gouged. Fillet weld reinforcement should be placed at the same location to close potential defects in the beam flange outer fiber. Prequalified WUF-W connections should also be inspected with nondestructive ultrasonic testing (UT) in accordance with AWS (2016). While necessary, the foregoing detailing is time and resource consuming (FEMA 2000; Miller 2017; Popov et al. 1998).

Structural detailing simplifications for column splices (e.g., Shaw et al. 2015; Stillmaker et al. 2016) and for continuity and doubler plate weld details of WUF-W connections (Reynolds and Uang 2022) have emerged. These rely on advancements in weld specifications and practice as well as today's quality control in fabrication.

Motivated by the foregoing, Skiadopoulos and Lignos (2022a) proposed a customized beveled backing bar configuration for welded connections by enabling finite element simulation-assisted design. The advantage of the beveled backing bar is that its removal is not imperative after the completion of the CJP groove welds at the beam flange-to-column flange location. Skiadopoulos and Lignos (2022a) demonstrated through continuum finite element simulations that the beveled backing bar configuration shifts the fracture-critical location away from the backing bar location. However, these simulations have not been validated by experimental testing.

Experimental research (Engelhardt et al. 2000; Lee et al. 2005a; Ricles et al. 2002b; Shin 2017; Zhang and Ricles 2006) has shown that fully restrained welded moment connections generally meet the prequalification requirements of AISC (2016b) when inelastic deformations concentrate in the steel beams. Fig. 2(a) shows such an example, where the inelastic panel zone shear distortion did not exceed $2\gamma_y$ (Shin 2017) while loading the WUF-W connection with a symmetric cyclic loading history. On the other hand, structural repairs are deemed imperative in this case due to inelastic local buckling near the beam ends [Fig. 2(b)] even at modest lateral drift demands (Uang and Bruneau 2018), particularly when the beam profiles are near the limits for highly ductile members according to AISC (2016b). This results in increased column twist demands, which could be detrimental when deep columns are utilized in the seismic design of steel MRFs (Chi and Uang 2002; Ricles et al. 2004).
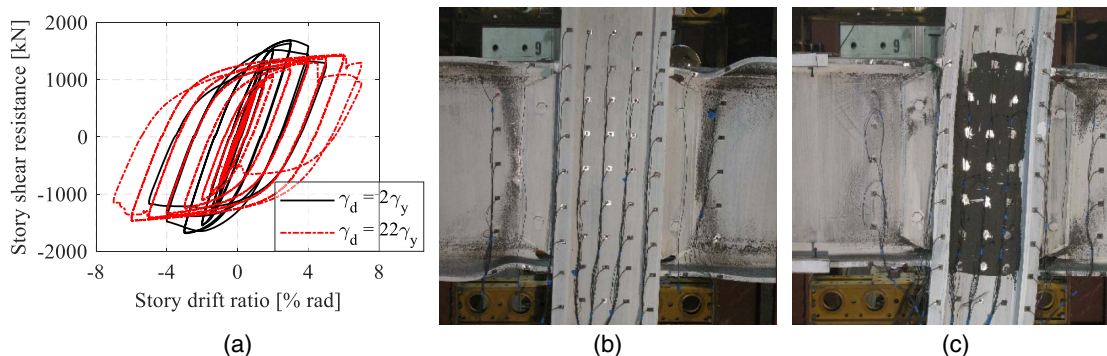

Fig. 2. (a) Hysteretic responses of welded unreinforced flange-welded web beam-to-column connections with variable design panel zone distortions, γ_d; (b) deformed shapes for the $2\gamma_y$ (at 4% rad lateral drift demand); and (c) the $22\gamma_y$ (at 4% rad lateral drift demand) cases. (Reprinted with permission from Shin 2017.)

When balancing inelastic deformations between the beam ends and the panel zone in welded connections, local buckling in the former only occurs at large lateral drift demands (Kim and Lee 2017; Lee et al. 2005a; Rahiminia and Namba 2013; Ricles et al. 2002b; Shin 2017). For instance, Fig. 2(a) illustrates the cyclic response of a WUF-W connection, which was designed with a targeted shear strength-to-demand ratio of 0.5 (Shin 2017). In this case, the use of doubler plates was not imperative, which reduced the associated fabrication costs in comparison to its strong panel zone counterpart. Moreover, Figs. 2(a and c) suggest that the WUF-W connection exhibits a stable hysteretic response up until a lateral drift of 6% rad. Arguably, at this drift level, the global stability of steel MRFs is governed by P-Δ effects (Elkady and Lignos 2015; Gupta and Krawinkler 2000). In a more recent study, Skiadopoulos and Lignos (2022b) demonstrated through extensive system-level simulations that at the maximum considered earthquake event (i.e., 2% probability of exceedance over a 50-year building life expectancy), residual story drift ratios reduce by half when the targeted panel zone distortions shift from $4\gamma_y$ (i.e., allowable limit) to $10\gamma_y$. This is particularly important from a building demolition standpoint (FEMA 2012).

In cases where the column flanges are subjected to highly inelastic strain demands due to panel zone kinking (Krawinkler et al. 1971; Lee et al. 2005b), stricter flange through-thickness (i.e., Z-direction) material requirements may be imperative to prevent lamellar tearing and/or divot fractures. Such fracture types, which are mostly common in columns with thick flanges [i.e., higher than 38 mm, as per AISC (2016b)], were reported in post-Northridge WUF-W connection tests (Lin et al. 2000). For the same reasons, CEN (2004) requires increased Z-direction quality class steel materials. The same applies for columns with flange thicknesses larger than 38 mm (AISC 2016b). Such toughness requirements in North America may be respected by enabling A913 steels (Bouchard and Axmann 2000).

Motivated by the foregoing, this paper introduces a new welded moment connection that defies the current design paradigm of pre-qualified WUF-W connections. The novelty of the proposed connection is threefold. First, beveled backing bars are employed and intentionally left in place after the completion of the CJP groove welds in the beam flange-to-column face joint; second, the connection design allows for highly dissipative panel zones; and third, steel columns are designed with minimum through thickness properties to prevent divot fracture, as well as the early onset of cracks due to ultra-low-cycle fatigue at the so-called kink location. The hysteretic behavior of the proposed connection is characterized by means of full-scale physical testing of two interior beam-to-column subassemblies. The effect of loading history on the global and local performance criteria is quantified. Implications for prospective seismic design of steel MRFs along with limitations of the present work are also discussed.

Test Objectives and Anticipated Performance of the Welded Connections

The proposed connection design exploits the beneficial aspects of shear yielding in a beam-to-column web panel zone by assuming a panel zone resistance-to-demand ratio, $R_{n,pl}/R_u$, that equals 0.8 [$R_{n,pl}$ is calculated per the Skiadopoulos et al. (2021) panel zone model at $4\gamma_y$]. According to Skiadopoulos and Lignos (2022b), steel MRFs featuring welded moment connections with a panel zone strength-to-demand ratio that ranges from 0.75 to 0.85 show reduced seismic collapse risk and expected structural repairs when compared with conventionally designed welded connections.

Therefore, in the presented experimental program, a panel zone strength-to-demand ratio of 0.80 is adopted. For this design value, at a design-basis earthquake (10% probability of exceedance over 50 years), the steel beams are expected to exhibit only flexural yielding and no local geometric instabilities, while the panel zone inelastic shear distortions are expected to be as much as $8\gamma_y$ (Skiadopoulos and Lignos 2022b). During a maximum-considered earthquake (2% probability of exceedance over 50 years) it is anticipated that panel zone distortions should be as much as $15\gamma_y$ provided that a stocky column is employed, whereas local buckling should not occur in the steel beam ends. While past studies have proposed targeted panel zone design distortions of up to $10\gamma_y$ (El Jisr et al. 2019; Skiadopoulos and Lignos 2021, 2022b) for the same purpose, herein, at maximum considered earthquake (MCE), the targeted inelastic shear distortion of $15\gamma_y$ is selected so as to conservatively impose increased strain demands to the anticipated panel zone kinking locations. The increased inelastic deformation demands within the beam-to-column web panel can result in reduced fabrication costs due to the anticipated reduction in doubler plates.

With the foregoing performance targets in mind, the overarching goal is that the welded connections achieve a non-degrading hysteretic response up to a lateral drift demand of 5% rad. Within such a context, structural repairs at the connection level would be minimized in the aftermath of design-basis earthquakes. Moreover, such a connection design would guarantee a sufficient reserve capacity of a steel MRF so as to minimize the risk of earthquake-induced collapse in a typical mainshock/aftershock earthquake series (Fig. 2).

Additional economic benefits of the proposed design are anticipated through the use of a beveled backing bar (Skiadopoulos and Lignos 2022a) that is intentionally left in place after the completion of the on-site CJP welds at the beam-flange-to-column face joints. To prevent divot fracture due to the expected high strain demands in the column through-thickness direction, a high notch toughness material in the Z-direction is enabled for the steel column material.

Overview of the Test Program

Test Specimens and Experimental Apparatus

Fig. 3 provides an overview of the test apparatus after the installation of the subject interior WUF-W connection. The test configuration consisted of two nominally identical beam-loaded test specimens. The steel beams were subjected to lateral loading through two 5,000 kN displacement-controlled servo hydraulic actuators. These actuators transferred the load from the test specimen to the reaction wall through a spreader steel beam. A pinned connection was realized in the column north end, while the shear and axial reaction forces were transferred to the reaction wall through the spreader beam.

The axial force in the column was applied through a 10,000 kN servo hydraulic actuator in force control. Therefore, a roller connection in the north-south direction was realized (Fig. 3). The movement in the east-west direction was restrained by a rigid support beam that reacted against the strong wall through a spreader beam. Pantographs were also clamped to the steel beams at 1,000 mm distance from the beam ends to restrain beam twisting and provide lateral restraint to the beam. Secondly, an additional lateral support system was designed according to the stability bracing requirements of AISC (2016b, c). This lateral support system, which is illustrated in Fig. 3, featured beams that consisted of a pair of C10 × 90 × 300 and columns that employed four L19 × 150 × 150.

Fig. 3. Overview of the test setup (unit: mm).

The test specimens featured HY650 × 300 × 16 × 25 steel beams (equivalent to a W24 × 131 in North America) with web and flange local slenderness ratios, $h/t_w = 35.9$, and $b/2t_f = 6$, respectively (where h is the clear flange distance minus the fillet radii, t_w is the web thickness, b is the flange width, and t_f is the flange thickness of the cross section). This profile meets the requirements for highly ductile members according to AISC (2016b). The steel columns featured an H498 × 432 × 45/70 (i.e., $h/t_w = 7.0$, and $b/2t_f = 3.1$), which is equivalent to a stocky W14 × 398 in North America. The flange thickness of the selected column cross section was equal to 70 mm. The foregoing member sizes and the connection geometry reflect the current seismic design practice in North America (Elkady and Lignos 2015; NIST 2010; Skiadopoulos and Lignos 2022b). The steel beams and columns were made of SN490B (JIS-G3136) and SM490A (JIS-G3106), respectively. Both structural steel materials had a nominal yield stress $f_y = 325$ MPa. The columns in both specimens were from the same steel heat. The same applied for the steel beams.

The beam-to-column connection designs intentionally violated the doubler plate requirements and the beam flange-to-column face weld detail as per AISC-358-16 (AISC 2016a). The former allows for a balanced inelastic deformation design between the steel beams and the panel zone. The clear span-to-beam depth ratio, L_c/d, equals 11.6, which meets the minimum requirement for special moment frames (AISC 2016a). Continuity plates were not imperative in the connection design, because the column flange and web thicknesses are able to accommodate the concentrated beam flange force demands (AISC 2016b). The strong column-weak beam (SCWB) ratio was larger than two. Therefore, the column was expected to remain elastic throughout the imposed lateral loading

history. This SCWB ratio was adopted due to the geometric limitations of the experimental setup. However, complementary CFE analyses (Skiadopoulos and Lignos 2022a) demonstrate that the proposed concept works with other SCWB ratios.

Test Specimen Fabrication

The fabrication process of the test specimens aimed at simulating realistic field weld conditions. For this purpose, the construction sequence was performed with the test specimens in the upright position. The shear tabs were shop-welded to the column face with double bevel CJP weld of YGW-18 weld electrode, as shown in Fig. 4, Detail 1. Two M24 prestressed erection bolts (AISC 2016b, c) of F10T material (equivalent to A490 in the US) were used for positioning the steel beams in place and for satisfying a perpendicular alignment between the two beams and the column. The beveled backing bars were then tack-welded at the top and bottom beam flanges. The geometry of the backing bars (Fig. 4, Detail 2), was designed according to the recommendations by Skiadopoulos and Lignos (2022a) for WUF-W connections. The access hole geometry (Fig. 4, Detail 3) met the design specifications (AISC 2016a; AWS 2016).

Runoff tabs were used for a smooth start and termination of the welding process [Fig. 5(a)]. Prior to the CJP weld execution, a preheat was applied at 50°C in accordance with AIJ (2018b). The CJP welds were then performed for both the top and bottom beam flanges and for the beam web by using YGW-18 and T49J0T1-1CA-UH5 weld electrodes, respectively (Fig. 4, Detail 1), which satisfy the requirements for demand critical welds of AISC (2016b). In this case, the minimum Charpy V-notch toughness of these welds was 70 J at 0°C. All CJP field welds were performed
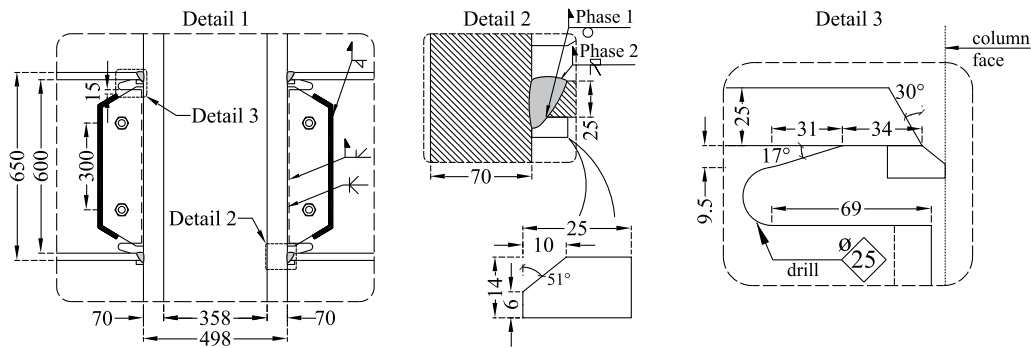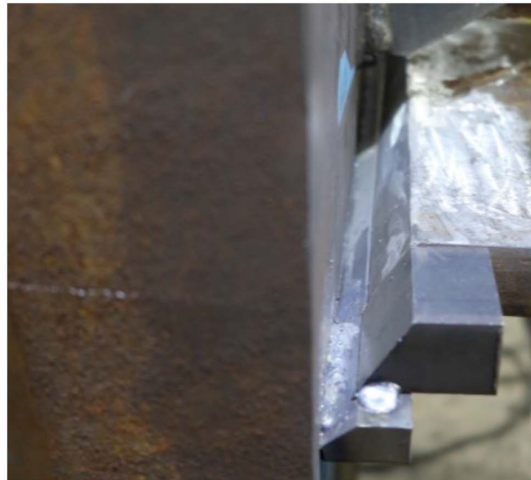
Fig. 4. Overview of the beam-to-column connection detailing (unit: mm).

(a)

(b)

Fig. 5. Fabrication of the beam-to-column connection: (a) beveled backing bar and weld runoff tab prior to CJP welding; and (b) removal of weld runoff tab after execution of the CJP welding.

by the gas metal arc welding (GMAW) process. The maximum heat input was 30–40 kJ/cm and the maximum permissible temperature between passes was 250°C –350°C. Noteworthy, the CJP weld electrode diameters were 1.2 mm, regardless of the weld detail and weld pass. Although this diameter lies in the upper bound of available electrode diameters, the relatively tight welded joint between the

beveled backing bars and the column face intersection was filled with the molten metal without any trace of discontinuity. The runoff tabs were removed and grinded to ensure a smooth surface, according to AISC (2016a), as shown in Fig. 5(b), after the execution of the CJP welds. The shear tabs were then fillet-weld reinforced by using a T49J0T1-1CA-UH5 weld electrode, as per AISC (2016a).

After welding, UT was performed in all demand critical CJP welds (AISC 2016b; AWS 2016) to ensure that potential discontinuities were below the established limits of current practice (AIJ 2018a). The UT confirmed that Specimen 1 had no traceable discontinuities, while Specimen 2 had two discontinuities at the west beam flange-to-column face connection. One discontinuity was located at the shear tab-to-column weld mid-height location, adjacent to the shear tab, and was 2 mm deep and 10 mm long. The other discontinuity was found at the bottom beam flange CJP weld, adjacent to the beam flange, and was positioned at the beam web centerline, where the welding process was interrupted at the access hole location. This discontinuity was 1 mm deep and 10 mm long. The foregoing discontinuities were within the allowable limits of (AIJ 2018a); therefore, no weld repairs were executed.

Instrumentation Plan and Deduced Measurements

Each test specimen employed 171 channels of instrumentation. These comprised 72 strain gauges in the beams and the columns, five rosette gauges in the panel zone and four near the access hole region, 58 linear variable differential transformers (LVDTs) in the panel zone and the pinned connections, four potentiometers in the panel zone kinking locations, and 10 string potentiometers at the actuator locations. The instrumentation at the panel zone bottom and top sides is illustrated in Figs. 6(a and b), while the instrumentation immediately before starting the test is depicted in Fig. 6(c) for the panel zone top side.

The story drift ratio, θ_{tot}, was calculated by considering a correction due to rigid body motion rotation, θ_{RB}, as per Eq. (1):

$$\theta_{tot} = \frac{\delta_{act,y,W} - \delta_{act,y,E}}{L_b} - \theta_{RB}$$

$$\theta_{RB} = \frac{\delta_{RB,x,N} - \delta_{RB,x,S}}{H_{c,RB}} \tag{1}$$

where $\delta_{act,y,W}$ and $\delta_{act,y,E}$ are the west and east actuator displacements in the y-direction; $\delta_{RB,x,N}$ and $\delta_{RB,x,S}$ are the LVDT displacements in the x-direction at the north and south column ends at the adapter plate mid-height location, respectively; $H_{c,RB}$ is the
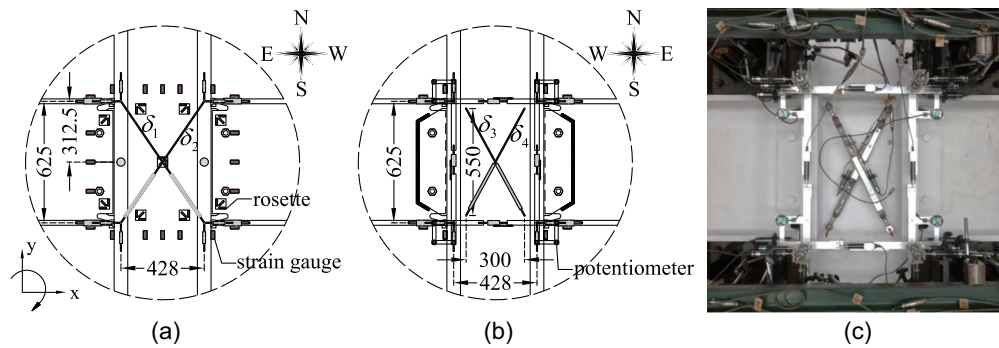
Fig. 6. Overview of the instrumentation plan at the panel zone region (unit: mm).

distance between these LVDTs, which equals 3,490 mm (Fig. 3); and L_b is the distance between the displacement-control actuator centerlines, which equals 8,000 mm.

The panel zone shear distortion, γ, was calculated based on the displacements of the diagonal pair of LVDTs that were mounted at the column flanges [Fig. 6(a), δ_1 and δ_2] as

$$\gamma = \frac{(\delta_1 - \delta_2) \cdot \sqrt{b_{pz}^2 + d_{pz}^2}}{2 \cdot b_{pz} \cdot d_{pz}} \tag{2}$$

where b_{pz} and d_{pz} are the width and the depth of the panel zone as defined by the points the LVDTs were attached to. More details on the panel zone distortion measurements as well as the deduction of the beam and column chord rotations are found in Skiadopoulos (2022).

Ancillary Tests

Ancillary tests were performed to infer the material properties of the steel beams and columns. The yield stress, $f_{y,m}$, the ultimate stress, $f_{u,m}$, and the elongation at fracture were determined according to standard tensile coupon testing (ASTM 2016). The average values based on five coupons with thickness, t, are reported in Table 1 for the web and flange plates. The specified minimum

yield, f_y, and ultimate stresses, f_u, are 325 MPa and 490 MPa, respectively, for the steel beams, whereas for the steel columns the corresponding f_y is 295 MPa because of the column web and flange thicknesses (i.e., larger than 40 mm). As for SN490B, the results indicate that the measured-to-nominal yield strength ratio, $f_{y,m}/f_y$, equals 1.13 and the measured-to-nominal ultimate strength ratio, $f_{u,m}/f_u$, equals 1.08, on average. Similar values are found for SM490A. These values are consistent with prior reports on relevant Japanese steel materials (Fujisawa et al. 2013) and correspond to similar values for A992 Gr. 50 steel (i.e., $f_y = 345$ MPa), as per AISC (2016b).

The chemical composition of the structural steel materials is summarized in Table 2. The carbon equivalent (CEV) that is a function of the chemical composition of steels (AWS 2010) is also reported. The CEV values indicate that the structural steel employed in the test specimens provides good weldability; hence, there is decreased potential for cracking near the heat affected zone (HAZ), as discussed in AWS (2010). According to Table 2, the sulfur content (denoted as "S") for the column is 0.004% of the total mass. At this level of sulfur content, the brittleness decreases, the weldability increases, and the steel anisotropy is practically eliminated (ASTM 2018; Miller 2017). Therefore, the through-thickness material strength and CVN toughness are fairly similar to those in the longitudinal direction, which is consistent with current material standards (ASTM 2018). The foregoing were also confirmed with

Table 1. Specified and measured material properties of the test specimens

| Section | t (mm) | Steel grade designation | Nominal material properties | Measured material properties | | | $\dfrac{f_{y,m}}{f_y}$ | $\dfrac{f_{u,m}}{f_u}$ |
				$f_{y,m}$ (MPa)	$f_{u,m}$ (MPa)	Elongation (%)		
Beam	25	SN490B	$f_y = 325$ MPa	Flange: 363	Flange: 509	Flange: 31.4	1.13	1.08
	16		$f_u = 490$ MPa	Web: 398	Web: 525	Web: 26.6	1.12	1.08
Column	70	SM490A	$f_y = 295$ MPa[a]	Flange: 368	Flange: 531	Flange: 36.0	1.12	1.04
	45		$f_u = 490$ MPa	Web: 363	Web: 528	Web: 33.7	1.22	1.07

[a]The lower value of f_y is attributable to the column web and flange thicknesses, which exceed 40 mm.

Table 2. Chemical composition of steel materials

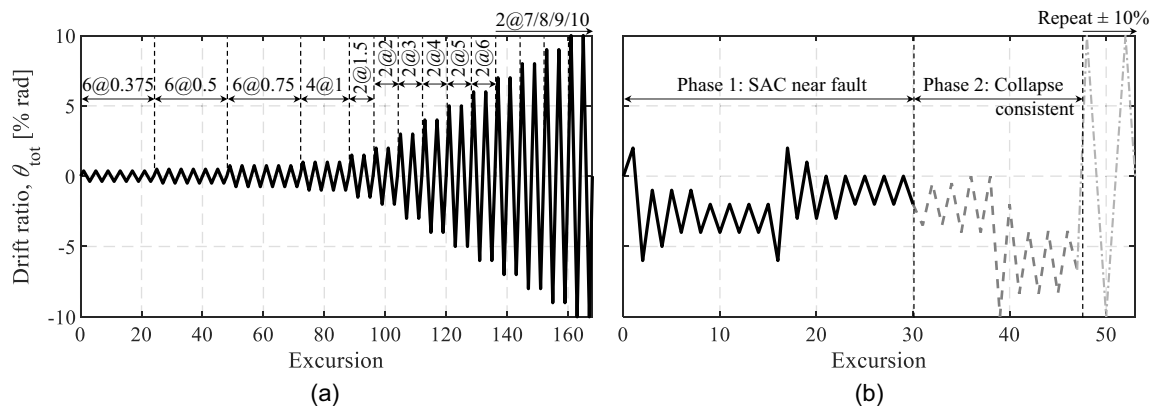| Material | Chemical composition (% mass) | | | | | | | | | | | | | | |
	C	Si	Mn	P	S	Cu	Ni	Cr	V	Nb	Mo	Ti	Al	N	CEV
Beam	0.18	0.34	1.07	0.019	0.008	NR	0.01	0.05	0.000	NR	0.010	NR	0.016	NR	0.37
Column	0.16	0.30	1.40	0.017	0.004	NR	NR	NR	NR	NR	NR	NR	0.032	NR	0.41

Fig. 7. Loading protocols for the beam-to-column connection test specimens: (a) Specimen 1; and (b) Specimen 2.

conventional CVN tests according to ASTM (2021) but are not shown herein for brevity.

Applied Loading Protocols

Specimen 1 was subjected to a standard symmetric cyclic loading protocol (AISC 2016b), as per Fig. 7(a). This protocol was considered so that the connection performance is contrasted with the AISC (2016a) prequalification requirements. For Specimen 2, three loading phases were implemented [Fig. 7(b)]: Phase 1 employed the SAC near-fault asymmetric loading protocol (Krawinkler et al. 2000), whereas Phase 2 featured the collapse-consistent loading protocol (Suzuki and Lignos 2020). In Phase 3, the specimen was loaded cyclically at $\pm 10\%$ rad drift ratio intervals. Phase 1 was employed because pulse-like near-fault ground motions with forward directivity are found to be considerably damaging compared with ordinary ground motions (Alavi and Krawinkler 2004). Phase 2 was employed to acquire representative experimental data at large deformations associated with global collapse of steel MRFs (Lignos et al. 2011; Suzuki and Lignos 2021). Phase 3 was employed until the loss of at least 50% of the lateral load carrying capacity of the test specimen, so as to characterize experimentally its ultimate failure modes and compare them with those of Specimen 1.

Prior to the imposition of the previously-mentioned loading protocols, a compressive axial load was applied to the steel column of each test specimen. This load was kept constant throughout loading. The magnitude of the applied axial force was $P_c = 5,000$ kN, which

corresponds to $0.2P_{y,n}$. ($P_{y,n}$ is the column axial yield strength, based on nominal material properties.) This value is representative for mid- to high-rise steel MRFs (Skiadopoulos and Lignos 2022b).

Experimental Results and Discussion

Qualitative Summary of Experimental Behavior

In this section, the results from both experiments are discussed in a qualitative manner. Emphasis is given on the story shear resistance, V_{col}, versus story drift ratio, θ_{tot} (Fig. 8), and on the panel zone shear force, V_{pz}, versus the normalized shear distortions, γ/γ_y (Fig. 9). The discussion is facilitated with informative illustrations, which demonstrate the overall performance of the welded connections.

Figs. 8(a and b) show the hysteretic responses of Specimens 1 and 2, respectively. Superimposed are key damage states throughout loading. Both test specimens remained elastic until a lateral drift demand of 0.75%–1% rad, where panel zone yielding occurred [Fig. 8(a)]. The lateral elastic stiffness of both test specimens is almost identical (i.e., $8.34 \cdot 10^4$ kN/rad). At a lateral drift demand of 2% rad, which is representative of a design-basis earthquake (DBE), the beams in both test specimens yielded in flexure (Fig. 8). The inelastic shear distortion in the panel zones reached $4\gamma_y$ at this point. Interestingly, the beam-to-column connections did not indicate any sign of visual damage.
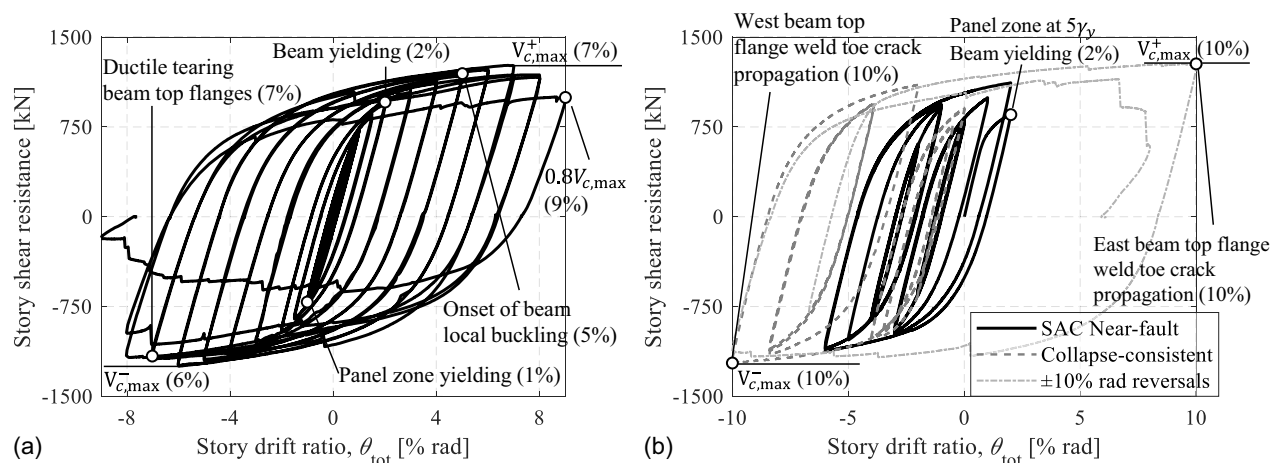

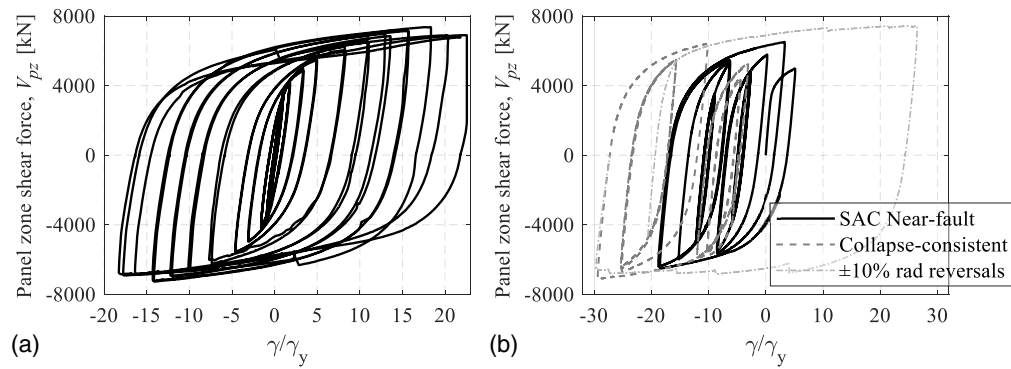**Fig. 8.** Story shear resistance versus story drift ratio: (a) Specimen 1; and (b) Specimen 2.

Fig. 9. Panel zone shear force versus normalized panel zone shear distortion: (a) Specimen 1; and (b) Specimen 2.
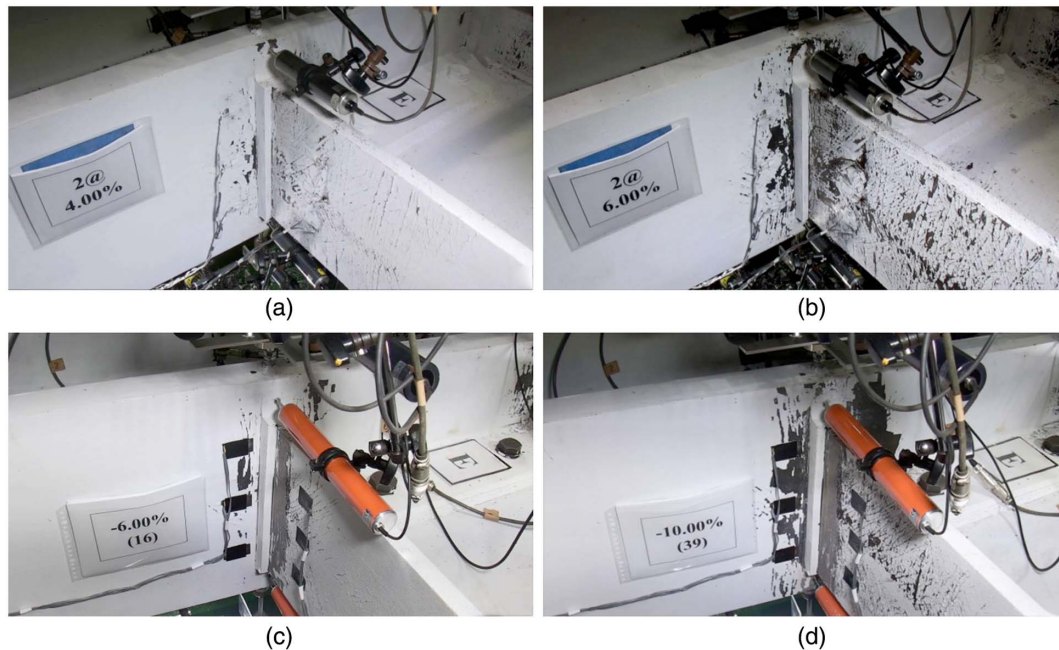

Fig. 10. Bottom beam flanges at characteristic loading excursions: (a) Specimen 1 at 4% rad; (b) Specimen 1 at 6% rad; (c) Specimen 2 at 6% rad (near fault loading protocol); and (d) Specimen 2 at 10% rad (collapse consistent loading protocol).

Regarding Specimen 1, at a lateral drift demand of 3% rad, flexural yielding in the beams progressed without any indication of local buckling. Referring to Fig. 9(a), the panel zone shear distortion reached $8\gamma_y$. At about 4% rad (that is, a representative lateral drift demand in steel MRFs when subjected to an MCE) the backing bar region did not exhibit any visual damage, as illustrated in Fig. 10(a). The panel zone shear distortions at this drift amplitude were nearly $10\gamma_y$. Fig. 11(a) depicts the shear yield pattern in the panel zone at the same lateral drift demand.

Upon further loading (5%–6% rad), the beam flanges exhibited mild local buckling that was barely visible [Fig. 10(b)]. Moreover, the anticipated panel zone shear distortion design target ($15\gamma_y$) was reached at 6% rad. The panel zone kinking effect at the four corners where the beam flanges joined the column flanges was more evident [Fig. 11(b)]. This led to the formation of ductile microcracks at the beam top flange-to-column face joint near the weld toes. These microcracks grew in a stable manner due to ultra-low-cycle fatigue. The bottom beam flange backing bar did not exhibit any visible damage. At the first loading excursion of the 7% rad lateral drift amplitude, the story shear resistance reached its peak value (1,265 kN).

During 7% rad, ductile tearing propagated slightly through the thickness of the column flange at the CJP weld toe of the west and east beam top flanges. Up until this lateral drift amplitude, the story shear resistance of Specimen 1 did not exhibit softening and cyclic deterioration. The associated deteriorating mechanisms (i.e., steel beam local buckling and crack initiation and propagation in the column flanges) had practically no influence on the hysteretic behavior of the connection [Fig. 8(a)]. At the first negative loading excursion of 8% rad, a ductile crack initiated at the weld root between the backing bar and the column flange of the east beam bottom flange. At the positive excursion of 9% rad, a 20% loss of the maximum achieved story shear resistance was observed due to the propagation of the existing ductile cracks. At the negative excursion of the same lateral drift amplitude, the connection lost more than 80% of its lateral load resistance due to crack propagation in the column flange near the west top and east bottom beam flanges. Prior to the test termination, the panel zone reached $23\gamma_y$ [Fig. 9(a)].

Specimen 2 exhibited a very stable hysteretic response during the near-fault loading protocol [Fig. 8(b)]. Visual inspection of the steel beams and the beveled backing bars did not reveal any noticeable
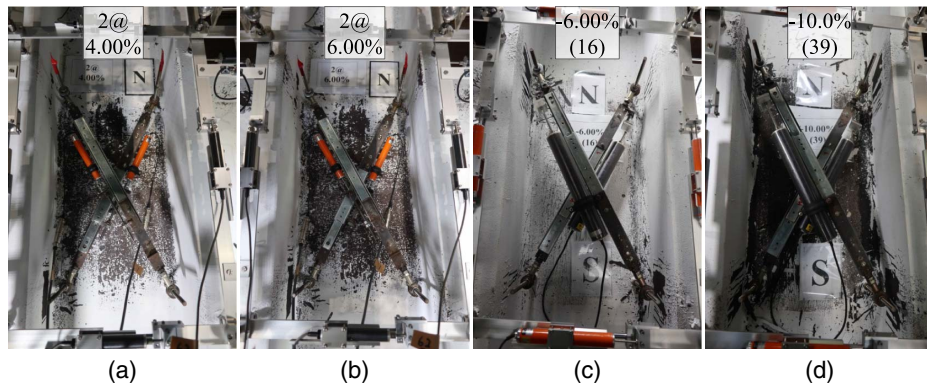
Fig. 11. Panel zone deformation at characteristic loading excursions: (a) Specimen 1 at 4% rad; (b) Specimen 1 at 6% rad; (c) Specimen 2 at 6% rad (near fault loading protocol); and (d) Specimen 2 at 10% rad (collapse consistent loading protocol).

damage [Fig. 10(c)] besides flexural yielding in the beam flanges. The panel zone shear distortions reached $18\gamma_y$ [Fig. 9(b)] at the second peak lateral drift excursion of the near-fault protocol (−6% rad), which led to localized yielding in the column flanges due to panel zone kinking [Fig. 11(c)]. Ductile microcracks of a nature similar to those in Specimen 1 became visible on both weld toes near the top flanges of the beams adjacent to the column flange surface.

At the peak lateral drift excursion of the collapse-consistent protocol (−10% rad), the cracks of the west beam top flange weld fusion propagated slightly towards the column width and thickness direction. At this excursion, the welded connection reached its negative maximum story shear resistance (−1,223 kN). The observed cracks were ductile, because they propagated slowly and did not compromise the overall hysteretic behavior of the welded connection [Fig. 8(b)]. Moreover, the panel zone shear distortion reached $30\gamma_y$ [Fig. 9(b)]. The shear yielding in the panel zone was the primary energy dissipation mechanism [Fig. 11(d)]. Specimen 2 exhibited a stable hysteretic response until the end of the collapse-consistent loading protocol. Moreover, no crack initiated from the customized beveled backing bars [Fig. 10(d)]. The overall response was dominated by cyclic hardening of the steel material.

From this point forward, lateral drift reversals of ±10% rad were performed. While lateral drift reversals of this amplitude in steel MRFs are very unlikely even during extreme earthquake loading, these load reversals were still conducted to determine the ultimate failure mode of the welded connection. During the second loading excursion of this loading phase, the ductile crack of the CJP weld toe of the west beam top flange propagated through the column flange thickness, thereby indicating a consistent failure mode between test specimens regardless of the employed loading history. The test was terminated once Specimen 2 lost at least 50% of its story shear resistance. The ultimate failure modes as determined after conducting scanning electron microscopy (SEM) to systematically characterize the crack initiation and propagation at the foregoing locations are further discussed in the subsequent sections.

The targeted panel zone shear distortions were exceeded in both test specimens at a lateral drift demand of about 6% rad. The experimental program demonstrated that the proposed WUF-W connections can sustain panel zone shear distortions that are substantially higher than the targeted design values. This is an important finding, considering that epistemic uncertainties (e.g., material variability, the presence of a floor system in steel MRFs) could potentially influence the extent of inelastic shear distortion in the panel zone.

Quantitative Assessment of the Test Results

This section discusses in a quantitative manner the experimental results for both test specimens. Emphasis is put on the beam-to-column connection prequalification criteria according to AISC (2016b), the assessment of the balanced design, and the measured column flange localized deformations.

Prequalification Limits

According to AISC (2016b), beam-to-column connections under a symmetric cyclic loading history should sustain beam end moment demands higher than $0.8M_{pl}$ (M_{pl} is the beam's plastic moment resistance based on the nominal material properties) at the second cycle of a lateral drift demand of 4% rad. Both beams of Specimen 1 exceeded M_{pl} at 2% rad and reached nearly $1.4M_{pl}$ at 8% rad. The computed peak connection strength factor, C_{pr}, equals nearly 1.20 for both test specimens, versus the 1.4 that is currently assumed for WUF-W connections as per AISC (2016a). Collectively, after assessing the results from this and nearly 100 connection tests with dissipative panel zones (Skiadopoulos and Lignos 2021), AISC-358-16 (AISC 2016a) seems to overestimate the influence of strain hardening on WUF-W connections.

Balanced Design of WUF-W Connections

Fig. 12 shows for both test specimens the moments at the beam ends at the column face location versus the beam chord rotations. The associated chord rotations are calculated over the beam length (i.e., from the column face to the load application point). The results are reported until the last loading excursion for which the decomposition of deflections was deemed to be accurate (6% rad for Specimen 1 and 49th excursion for Specimen 2). From this figure, it is evident that the steel beams did not exhibit cyclic deterioration in flexural strength, although they did experience modest flange local buckling. This observation is important from a repairability standpoint in the aftermath of earthquakes.

Fig. 13 depicts the contribution of the beams, the panel zone, and the column to the total story drift ratio, θ_{tot}, for both test specimens. Referring to Fig. 13(a), once inelastic deformations concentrated in the panel zone (i.e., after 1% rad), its contribution increased from 40% to 50% and stabilized up until the onset of mild flange local buckling in the beams at 5%–6% rad. Referring to Fig. 13(b), the panel zones of Specimen 2 contributed nearly 10% more to θ_{tot} than did Specimen 1. This is due to the influence of the loading protocol on the onset of beam flange local buckling.
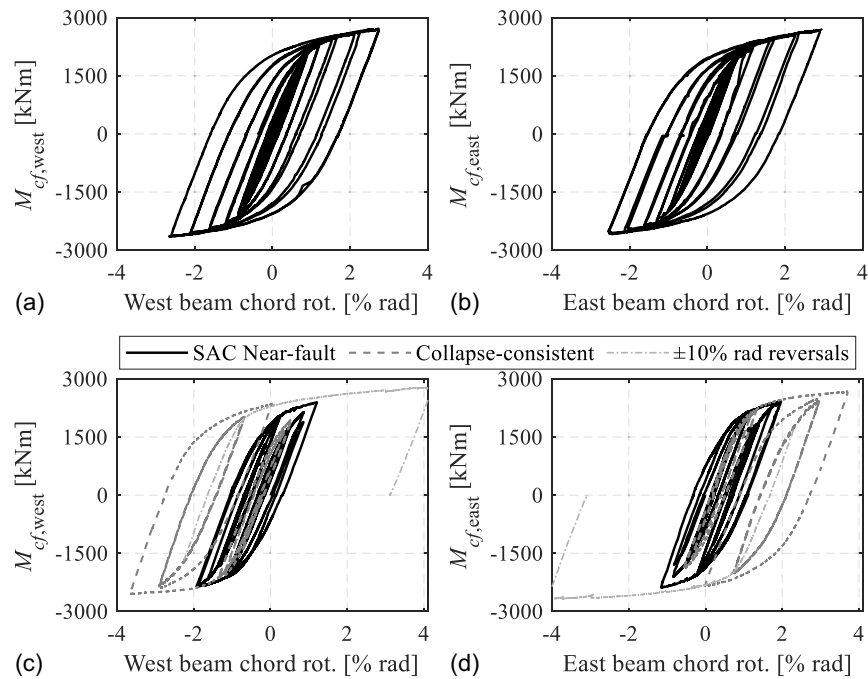
Fig. 12. Moments at the beam ends at the column face location versus beam chord rotations: (a and b) Specimen 1; and (c and d) Specimen 2.
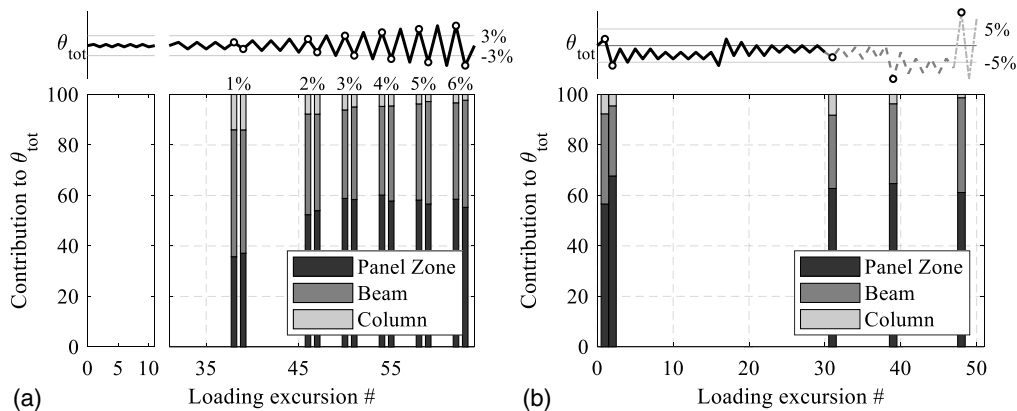

Fig. 13. Contributions of the panel zone, beams and column to the story drift ratio at characteristic lateral loading excursions: (a) Specimen 1; and (b) Specimen 2.

It can be concluded that the overall connection design was well-balanced between the panel zone and the steel beams, regardless of the employed loading history.

Column Flange Local Deformations

In both test specimens, a cantilever-like deformation mode was observed in the panel zone kinking locations, causing column flange localized yielding [Fig. 14(a)]. This deformation mode, which is schematically illustrated in Figs. 14(b and c) is more prominent when continuity plates are not deemed imperative. El-Tawil (2000) found that this mode increases the fracture potential of beam-to-column connections under cyclic loading near the beam web center-line due to the resultant stress distribution over the flange width [Fig. 14(b)].

To quantify the column flange local deformations, a horizontal pair of LVDTs was placed at each kinking location [Fig. 6(c)] to compute the rotation at the column flange extremity, $\theta_{cf,local}$. Moreover, the displacement at the panel zone kinking locations, $\delta_{cf,local}$

[Fig. 14(b)], was deduced from $\theta_{cf,local}$, by conservatively assuming that the column flange cantilever was under uniform load.

Fig. 14(d) depicts in a dual plot the computed peak $\theta_{cf,local}$ and $\delta_{cf,local}$ at characteristic lateral loading excursions for Specimen 1. Due to symmetry, the response in the northwest (NW) and southeast (SE) panel zone kinking locations is nearly identical. Similar findings hold true for the northeast (NE) and southwest (SW) locations. Therefore, the peak values of these pairs (NW-SE and NE-SW) are shown herein. The average of the two flange plate rotations per kinking location is considered in the computations. Positive values of $\theta_{cf,local}$ and $\delta_{cf,local}$ correspond to column flanges being pulled by the adjacent beams [i.e., NE-SW in Fig. 14(c)].

Referring to Fig. 14(d), the column flange local deformations are consistent at both NW-SE and NE-SW locations, while their amplitudes are, qualitatively, proportional to the imposed lateral drift demands. At 2% rad and 4% rad lateral drift demands, $\theta_{cf,local}$ equals nearly 0.5% rad and 1.0% rad, accordingly. The maximum
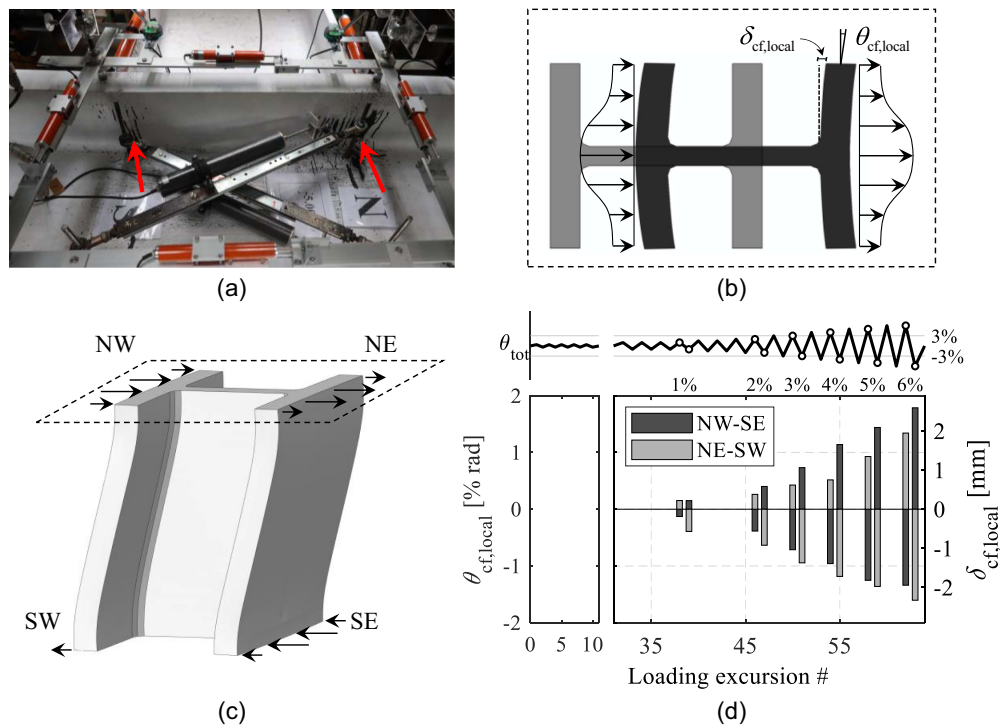
Fig. 14. (a) Column flange yield pattern; (b) schematic illustration of column flange local deformations; (c) locations of column flange local deformation calculation; and (d) column flange local deformations at characteristic lateral loading excursions of Specimen 1.

measured $\delta_{cf,local}$ equals 2.5 mm and is achieved at 6% rad. The results confirm that the column flange local deformations remained relatively minor due to the flange thickness ($t_{cf} = 70$ mm) of the employed column cross section; hence the AISC (2016b) requirements for continuity plates are deemed to be satisfactory. Similar findings hold true for Specimen 2 but are not shown here due to brevity.

Performance of Beveled Backing Bars

In this section, the performance of the beveled backing bars is assessed. Current prequalification requirements allow for top flange backing bars to remain in place (AISC 2016a). The test results confirmed that this location did not experience any notable damage at lateral drift demands associated with DBE and MCE events. Similar observations hold true for the bottom beam flange beveled backing bars, except for the east beam of Specimen 1, which

experienced ductile crack propagation at 8% rad lateral drift demands. This remarkable bottom beam flange backing bar performance was confirmed by macro-etching examination near the beam web centerline, which is considered as the location with the highest fracture potential.

Fig. 15(a) shows the deformed configuration of Specimen 2 after testing. Macro-etching results extracted from the east beam bottom flange near the beam web centerline are highlighted in Fig. 15(b). The results indicate that there was no crack initiating from the weld root of the beveled backing bars, even at lateral drift demands of 10% rad. By beveling the backing bar, potential flaws that emerge during the welding process are kept away from the critical beam flange region. Therefore, the beam can sustain its probable moment carrying capacity, because the beam flange area is not reduced. Moreover, the stress concentration near the backing bar physical notch tips is substantially reduced by beveling the backing
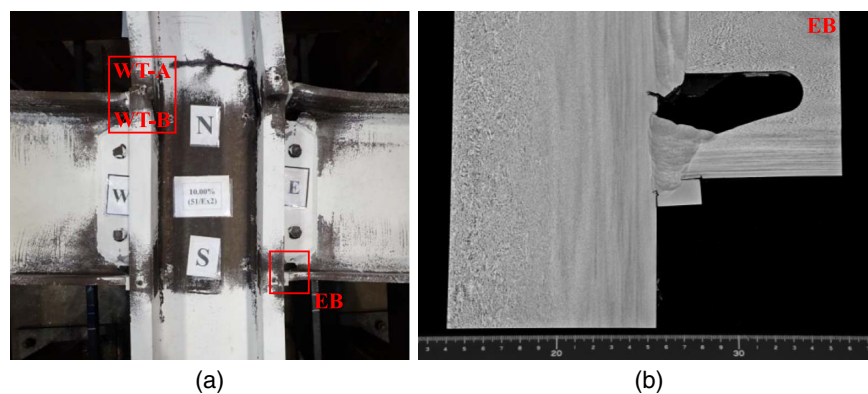

Fig. 15. Fractographic analyses of Specimen 2: (a) overview of the examined locations; and (b) macro-etching results at the east beam bottom flange backing bar location.

bar, because of the stress flow interruption. The stress concentration near the backing bar-to-column face and the backing bar-to-beam flange notch tips can be optimized based on the selected bevel angle (Skiadopoulos and Lignos 2022a).

Effect of Loading History and Implications on Predictive Modeling and Structural Collapse

Prior work (Krawinkler 1996, 2009; Lignos et al. 2011) has stressed the influence of the loading history on the evaluation of seismic demand and capacities of structural components. The same issue has also been stressed for the development of acceptance criteria for collapse prevention when assessing the seismic performance of existing structures (Maison and Speicher 2016; Suzuki and Lignos 2021). While the AISC symmetric cyclic loading protocol is generally conservative for structural component qualification at lateral drift demands higher than 2% rad (Krawinkler 2009), the experimental results suggest that the welded connections tested herein exhibit a stable hysteretic response until a lateral drift demand of about 8% rad.

The seismic performance of steel MRFs during low probability of occurrence earthquakes tends to become asymmetric due to ratcheting prior to structural collapse (Ibarra and Krawinkler 2005; Lignos et al. 2011). In formal collapse risk assessment methodologies [e.g., FEMA (2009)] as well as system level simulation studies, the dynamic stability of steel MRFs is governed by global P-Δ effects at lateral drift demands of 5% rad and above. Fig. 8(b) suggests that even in cases where seismic demands become asymmetric due to ratcheting, the welded connections exhibit a non-degrading hysteretic behavior even at a lateral drift demand of 10% rad.

Ibarra and Krawinkler (2005) pointed out the role of strength and post-peak strength deterioration (i.e., softening) of structural components on the earthquake-induced collapse risk of MRFs. In that respect, the testing program demonstrates that the welded connections with highly inelastic panel zones remain stable throughout the employed loading histories. Therefore, unlike steel MRFs with elastic panel zone designs, the global collapse of steel MRFs featuring welded connections with highly dissipative panel zones such as those discussed in this paper is mostly controlled by the destabilizing effects of the gravity load and not by component deterioration. In that respect, Fig. 12 implies that simple bilinear models suffice in this case for simulating the steel beam behavior even at large lateral drift demands associated with collapse; hence, the influence of modeling uncertainties in component modeling at large deformations, where the validity of currently available deterioration models (e.g., Ibarra et al. 2005) may be questionable (Krawinkler and Deierlein 2013), becomes negligible.

Ultimate Failure Modes

The experimental program highlighted that at 6% rad, the column flanges started exhibiting localized yielding due to kinking near their intersection with the beam flanges. The yielding zone progressed in an elliptical manner and maximized near the column flange mid-width location, as illustrated in the finite element model of Fig. 16(a) and in the east beam bottom flange of Specimen 1 of Fig. 16(b). This localized yielding pattern, which is associated with increased strain demands due to panel zone kinking, led to ductile crack initiation and propagation that became evident at 7%–8% rad. The cracks at the CJP weld toe of the east beam bottom flange initiated at the column flange, near the bottom backing bar at the beam web centerline and propagated towards the column thickness and longitudinal direction [Figs. 16(c and d)]. This ultimate failure mode, which is described by ultra-low-cycle fatigue of the CJP weld toes at
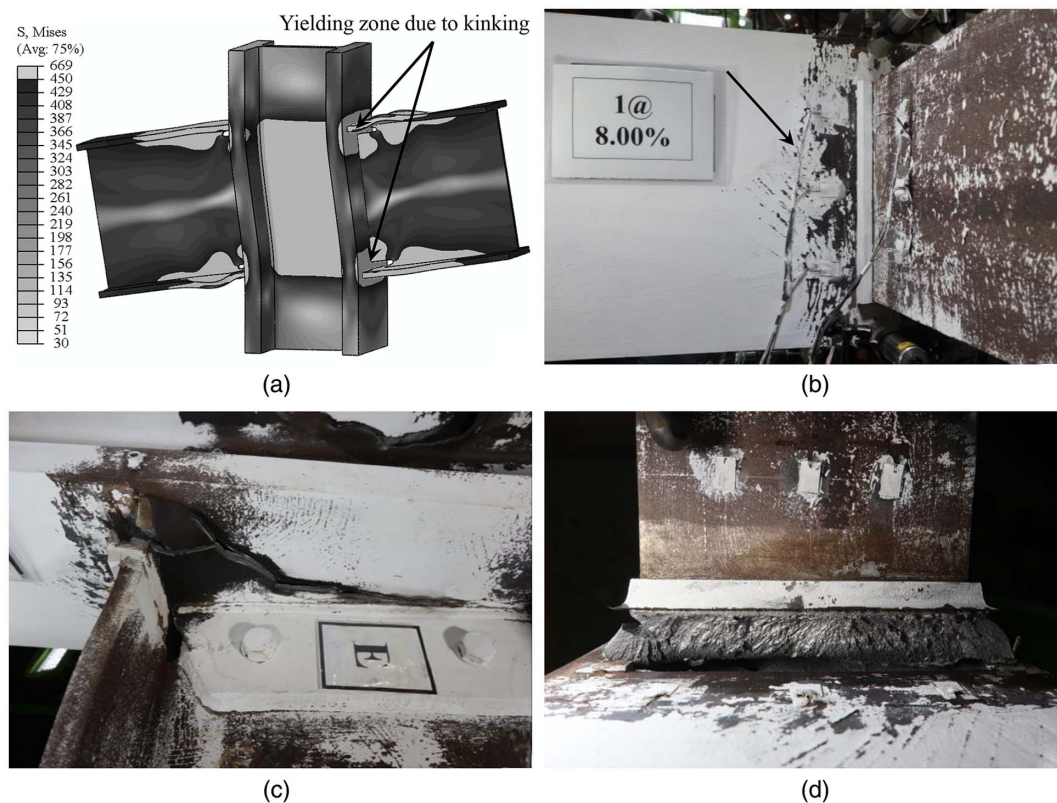

Fig. 16. Kinking at the east beam bottom flange of Specimen 1: (a) illustration though finite element modeling; (b) localized yielding due to kinking at 8% rad and crack pattern due to kinking at 9% rad; (c) side view; and (d) bottom beam flange view.
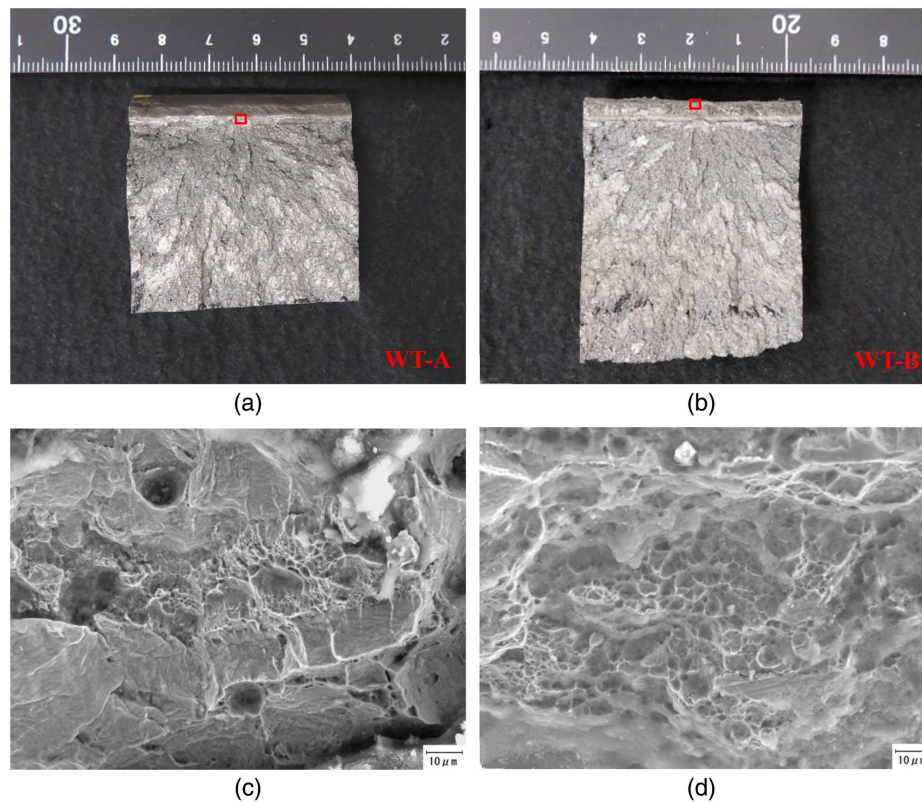
Fig. 17. Fractographic analyses of Specimen 2 west beam top flange-to-column face location: (a) sample extracted from the column flange mid-width; (b) sample extracted from the beam flange mid-width; (c) scanning electron microscopy results at the column flange; and (d) scanning electron microscopy results at the beam flange.

the beam flange to column face connection, was also characteristic at the beam top flange locations in both test specimens.

To identify the nature of this failure mode, fractographic analysis was conducted with SEM at selected fracture surfaces of both test specimens. Indicatively, Fig. 15(a) shows one of these locations (see WT-A and WT-B). Fig. 17 shows characteristic SEM fractography images from the fracture location near the west beam top flange (WT) of Specimen 2. Referring to Figs. 17(a and b), the SEM samples were extracted from the column flange in the beam web center-line where the fracture initiated and propagated throughout the loading cycles. Location WT-A refers to the sample extracted from the surface on the column side, whereas WT-B refers to the sample extracted from the surface on the beam side. While the original shape of the dimples cannot be accurately determined due to the loading cycles that succeeded the fracture initiation, it is observed that the dimples were of oblate shape [Figs. 17(c and d)], which is characteristic of microvoids and coalescence (Kanvinde 2017). This suggests that the origin of the ultimate failure mode observed in both test specimens was indeed ductile crack initiation due to ultra-low-cycle fatigue. Moreover, from the same SEM fractography images, it appears that the direction of dimples is downward at WT-A [Fig. 17(c)], whereas an upward direction appears at WT-B [Fig. 17(d)]; hence, the crack growth is attributed to a localized shear force due to column flange secondary bending at the kinking locations [Figs. 16(a and b)], i.e., the presence of stress gradients.

Conversely, near the crack tip, the SEM fractography images depict cleavage fracture that led to the loss of the load carrying capacity of both test specimens during the final lateral loading excursions in both test specimens. However, in both test specimens, cleavage was preceded by large-scale plastic flow and ductile crack growth as discussed earlier.

The experimental results reveal that the ultimate failure modes were consistent in both test specimens. While cracks did initiate due to ultra-low-cycle fatigue, they were deemed to be stable and did not compromise the overall stability of the welded connections until large amplitude lateral drift demands (i.e., above 7% rad). Evidently, from the point of noticeable crack initiation to the point of loss of at least 50% of the lateral load carrying capacity of both connections, these dissipated about one third of the total dissipated energy.

Limitations of the Present Study

The present work comes with a number of limitations that should be addressed in future studies. In particular, the presence of the concrete slab raises the strain demands on the bottom beam flange, thereby increasing the fracture potential at the beam flange-to-column face welded connection (Hajjar et al. 1998; Kim and Lee 2017; Leon et al. 1998). In such case, the balanced design could consider the maximum probable moment of the composite beam, depending on the degree of composite action. Another aspect that may lead to increased strain demands in the beam flange-to-column face welded connection is the increased beam depth. However, continuum finite element studies demonstrated that, contrary to the level of panel zone inelastic deformations, the use of deeper sections does not greatly affect the fracture potential when the proposed concept is adopted (Skiadopoulos and Lignos 2022a).

All CJP welds were performed based on the GMAW. This welding process, which is similar to gas-shielded flux-cored arc welding (FCAW-G), is sensitive to the wind speed under which the welds are performed. It is usually prohibited for field welds when

wind speeds exceed 5 km/h (AWS 2016). A more typical welding process for field welds is self-shielded flux-cored arc welding (FCAW-S), which provides less arc action than FCAW-G. In Japan, the current practice in field welding features GMAW. In this case, both the welder and the welded connection are typically covered, to minimize the influence of wind conditions during field welding.

Another issue to be stressed is the challenge of tracing discontinuities through UT in welded connections when backing bars are left in place. This is a concern especially in the beam web centerline location (FEMA 2000; Paret 2000). On the other hand, Skiadopoulos and Lignos (2022a) showed via continuum finite element simulations that uncertainty in potential weld root discontinuities would not compromise the connection performance in such a case. Also, the beveled backing bar may be an interesting alternative to minimize the fracture potential at the top beam flange-to-column face joints.

Finally, in the present study, the geometric tolerances during alignment of beams and columns, of beam flange groove angles, and of the backing bar geometry, were fully respected. The backing bar groove angle may not always coincide precisely with the groove angle of the beam flange. This issue should be further investigated.

Summary and Conclusions

This paper investigates experimentally the cyclic performance of welded connections with highly dissipative panel zones and simplified weld details. Contrary to today's prequalified beam-to-column connections, the novel aspects of the explored welded connections were: (1) a beveled backing bar configuration that was intentionally kept in place after the completion of the top and bottom beam flange-to-column face CJP welds, (2) the exploitation of the stable hysteretic response of panel zones in an effort to make welded connections resilient to local buckling until a lateral drift demand of at least 5% rad, and (3) the utilization of a column steel material with minimum notch toughness requirements in the through-thickness direction to prevent divot fracture in the column flange. Within such a context, two nominally identical welded connections were tested at full-scale with two loading histories. The first one was a reversed cyclic symmetric loading protocol (AISC 2016b). The second was a near-fault loading protocol (Krawinkler et al. 2000), which was followed by a collapse-consistent protocol (Suzuki and Lignos 2020) to benchmark the seismic performance of the welded connection at incipient collapse, as well as excessive loading cycles of 0.2 rad range to determine the ultimate failure modes of the connection. The main findings are summarized as follows:

- At seismic demands representative of a design-basis earthquake event (i.e., lateral drift demands of 2% rad), the welded connections experienced shear yielding in the panel zone and flexural yielding in the beams. No visual signs of nonlinear geometric instabilities, i.e., local buckling, were observed in the beam-to-column connections. The panel zone shear distortions reached $4\gamma_y$ at 2% rad, as intended.
- At lateral drift demands representative of a maximum-considered earthquake event (i.e., 3%–4% rad), the panel zone shear distortions remained below $10\gamma_y$. Panel zone kinking led to mild localized yielding in the column flanges near the four panel zone corners without compromising the connection's performance. The test results confirmed that the prequalification requirements of AISC (2016b) were satisfied, because none of the welded connections exhibited strength deterioration. From a repairability standpoint, no visual structural damage was observed in the welded connections at the same drift amplitude, regardless of the employed loading protocol.

- Mild local buckling in the steel beams became visible after 6% rad under a symmetric cyclic loading protocol. At the same lateral drift amplitude, the panel zones reached their targeted inelastic shear distortions ($15\gamma_y$). The onset of local buckling in the steel beams did not cause in-cycle strength/stiffness deterioration to the connection. Local buckling in the steel beams was further delayed in the case of the nonsymmetric lateral loading history. Despite the severity of the symmetric cyclic loading history, at a lateral drift ratio of 6% rad no cracks were observed in the welded connections.
- The experimental results suggest that the ultimate failure modes were consistent in both test specimens regardless of the employed lateral loading protocol. At 7%–10% rad lateral drift demands, ductile cracks initiated due to ultra-low-cycle fatigue mostly at the column face, near the beam flange CJP weld root. While this fracture mode mostly controlled the connection's ultimate behavior, this was superior up until 9%–10% rad.
- The beveled backing bars did not exhibit any visible sign of structural damage, even at lateral drift demands of 8% rad. This is attributable to the optimal bevel angle design that minimized the fracture potential near the backing bar notches. Another important reason was that the notch tip was kept away from the beam flanges.
- For the panel zone resistance-to-demand design ratio, $R_{n,pl}/R_u = 0.8$, the panel zone and the beams participated nearly equally in the energy dissipation of the welded connections throughout the imposed lateral loading history. The experimental program demonstrated that, at a lateral drift amplitude of 10% rad, the welded connections can sustain panel zone shear distortions of nearly $30\gamma_y$.
- The experiments indicate that the absence of the continuity plates did not lead to appreciable column flange local deformations due to the concentrated beam flange load. The column cross section with 70 mm flange thickness did not allow for column flange relative deformations higher than 2–4 mm at 10% rad lateral drift demands.
- Although deeper beam sections may increase the fracture potential in the welded connection, the fact that the selected beam sizes were well below the current compactness limits for highly ductile members is deemed critical for the CJP welds. The early occurrence of beam local buckling in case of deep and slender beam cross sections would localize the inelastic cyclic strain demands within the dissipative zone of the beam(s), thereby reducing the demands in the CJP welds.

In the authors' opinion, the experiments presented herein as well as the overall research program demonstrate a tremendous potential to further advance the associated technology of welded connections for seismic applications in steel MRFs along with simplifications that promote a more economic fabrication and simplicity in their design process while ensuring superior energy dissipation capabilities.

Data Availability Statement

Some or all data, models, or code that support the findings of this study are available from the corresponding author upon reasonable request.

Acknowledgments

References

AIJ (Architectural Institute of Japan). 2018a. *Standard for the ultrasonic inspection of weld defects in steel structures*. [In Japanese.] Tokyo: AIJ.

AIJ (Architectural Institute of Japan). 2018b. *Technical recommendations for steel construction for buildings Part1: Guide to steel-rib fabrications*. [In Japanese.] Tokyo: AIJ.

AISC. 2016a. *Prequalified connections for special and intermediate steel moment frames for seismic applications*. ANSI/AISC 358-16. Chicago: AISC.

AISC. 2016b. *Seismic provisions for structural steel buildings*. ANSI/AISC 341-16. Chicago: AISC.

AISC. 2016c. *Specification for structural steel buildings*. ANSI/AISC 360-16. Chicago: AISC.

Alavi, B., and H. Krawinkler. 2004. "Behavior of moment-resisting frame structures subjected to near-fault ground motions." *Earthquake Eng. Struct. Dyn.* 33 (6): 687–706. https://doi.org/10.1002/eqe.369.

ASTM. 2016. *Standard test methods for tension testing of metallic materials*. ASTM E8/E8M-16a. West Conshohocken, PA: ASTM.

ASTM. 2018. *Standard specification for through-thickness tension testing of steel plates for special applications*. A770/A770M-03. West Conshohocken, PA: ASTM.

ASTM. 2021. *Standard test methods and definitions for mechanical testing of steel products*. ASTM A370-21. West Conshohocken, PA: ASTM.

AWS (American Welding Society). 2010. *Structural welding code—Steel*. ANSI/AWS D1.1:2010. Miami: AWS.

AWS (American Welding Society). 2016. *Structural welding code-seismic supplement*. AWS D1.8/D1.8M:2016. Miami: AWS.

Bouchard, S., and G. Axmann. 2000. "ASTM A913 grades 50 and 65: Steels for seismic applications." In *Proc., 3rd Int. Conf. on Behavior of Steel Structures in Seismic Areas (STESSA)*, 11–17. Montreal: CRC Press.

CEN (European Committee for Standardization). 2004. *Eurocode 3: Design of steel structures—Part 10: Material toughness and through-thickness properties*. EN 1993-1-10. Brussels, Belgium: CEN.

Chi, B., and C.-M. Uang. 2002. "Cyclic response and design recommendations of reduced beam section moment connections with deep columns." *J. Struct. Eng.* 128 (4): 464–473. https://doi.org/10.1061/(ASCE)0733-9445(2002)128:4(464).

Chi, W. M., G. G. Deierlein, and A. Ingraffea. 1997. *Finite element fracture mechanics investigation of welded beam-column connections*. SAC Background Documents, Rep. No. SAC/BD-97/05. Sacramento, CA: SAC Joint Venture.

Chi, W.-M., G. G. Deierlein, and A. Ingraffea. 2000. "Fracture toughness demands in welded beam-column moment connections." *J. Struct. Eng.* 126 (1): 88–97. https://doi.org/10.1061/(ASCE)0733-9445(2000)126:1(88).

El Jisr, H., A. Elkady, and D. G. Lignos. 2019. "Composite steel beam database for seismic design and performance assessment of composite-steel moment-resisting frame systems." *Bull. Earthquake Eng.* 17 (6): 3015–3039. https://doi.org/10.1007/s10518-019-00564-w.

Elkady, A., and D. G. Lignos. 2015. "Effect of gravity framing on the over-strength and collapse capacity of steel frame buildings with perimeter special moment frames." *Earthquake Eng. Struct. Dyn.* 44 (8): 1289–1307. https://doi.org/10.1002/eqe.2519.

El-Tawil, S. 2000. "Panel zone yielding in steel moment connections." *Eng. J.* 37 (3): 120–131.

El-Tawil, S., E. Vidarsson, T. Mikesell, and S. K. Kunnath. 1999. "Inelastic behavior and design of steel panel zones." *J. Struct. Eng.* 125 (2): 183–193. https://doi.org/10.1061/(ASCE)0733-9445(1999)125:2(183).

Engelhardt, M. D., M. J. Venti, G. T. Fry, S. L. Jones, and S. D. Holliday. 2000. *Behavior and design of radius cut reduced beam section connections*. Rep. No. SAC/BD-00/17. Sacramento, CA: SAC Joint Venture.

FEMA. 2000. *State of the art report on connection performance*. Rep. No. FEMA-355D. Washington, DC: FEMA.

FEMA. 2009. *Effects of strength and stiffness degradation on seismic response*. Rep. No. FEMA-P440A. Washington, DC: FEMA.

FEMA. 2012. *Seismic performance assessment of buildings*. Rep. No. FEMA-P-58-1. Washington, DC: FEMA.

Fujisawa, K., Y. Ichinohe, M. Sugimoto, and M. Sonoda. 2013. "Statistical study on mechanical properties and chemical compositions of SN Steels." In *Proc., Summary of Technical Papers of Annual Meeting*, 699–700. Tokyo: Architectural Institute of Japan.

Gupta, A., and H. Krawinkler. 2000. "Dynamic P-delta effects for flexible inelastic steel structures." *J. Struct. Eng.* 126 (1): 145–154. https://doi.org/10.1061/(ASCE)0733-9445(2000)126:1(145).

Hajjar, J. F., R. T. Leon, M. A. Gustafson, and C. K. Shield. 1998. "Seismic response of composite moment-resisting connections. II: Behavior." *J. Struct. Eng.* 124 (8): 877–885. https://doi.org/10.1061/(ASCE)0733-9445(1998)124:8(877).

Han, S. W., G. U. Kwon, and K. H. Moon. 2007. "Cyclic behaviour of post-Northridge WUF-B connections." *J. Constr. Steel Res.* 63 (3): 365–374. https://doi.org/10.1016/j.jcsr.2006.05.003.

Ibarra, L. F., and H. Krawinkler. 2005. *Global collapse of frame structures under seismic excitations*. Rep. No. 152. Stanford, CA: The John A. Blume Earthquake Engineering Research Center, Dept. of Civil Engineering, Stanford Univ.

Ibarra, L. F., R. A. Medina, and H. Krawinkler. 2005. "Hysteretic models that incorporate strength and stiffness deterioration." *Earthquake Eng. Struct. Dyn.* 34 (12): 1489–1511. https://doi.org/10.1002/eqe.495.

Kanvinde, A. M. 2017. "Predicting fracture in civil engineering steel structures: State of the art." *J. Struct. Eng.* 143 (3): 03116001. https://doi.org/10.1061/(ASCE)ST.1943-541X.0001704.

Kim, S.-Y., and C.-H. Lee. 2017. "Seismic retrofit of welded steel moment connections with highly composite floor slabs." *J. Constr. Steel Res.* 139 (Dec): 62–68. https://doi.org/10.1016/j.jcsr.2017.09.010.

Krawinkler, H. 1995. "Earthquake design and performance of steel structures." In *Proc., Pacific Conf. on Earthquake Engineering, PCEE 95*. Richmond, VIC, Australia: Australian Earthquake Engineering Society.

Krawinkler, H. 1996. "Cyclic loading histories for seismic experimentation on structural components." *Earthquake Spectra* 12 (1): 1–12. https://doi.org/10.1193/1.1585865.

Krawinkler, H. 2009. "Loading histories for cyclic tests in support of performance assessment of structural components." In *Proc., 3rd Int. Conf. on Advances in Experimental Structural Engineering*. San Francisco: Pacific Earthquake Engineering Research Center.

Krawinkler, H., G. Akshay, R. Medina, and M. Luco. 2000. *Development of loading histories for testing of steel beam-to-column assemblies*. Stanford, CA: Dept. of Civil and Environmental Engineering, Stanford Univ.

Krawinkler, H., V. V. Bertero, and E. P. Popov. 1971. *Inelastic behavior of steel beam-to-column subassemblages*. Rep. No. 71/07. Berkeley, CA: Univ. of California.

Krawinkler, H., and G. G. Deierlein. 2013. "Chapter 1: Challenges towards achieving earthquake resilience through performance-based earthquake engineering." In *Performance-based seismic engineering: Vision for an earthquake resilient society*, edited by M. Fischinger. New York: Springer.

Lee, D., S. C. Cotton, J. Hajjar, R. J. Dexter, and Y. Ye. 2005a. "Cyclic behavior of steel moment-resisting connections reinforced by alternative column stiffener details I. Connection performance and continuity plate detailing." *Eng. J.* 42 (4): 189–214.

Lee, D., S. C. Cotton, J. F. Hajjar, R. J. Dexter, and Y. Ye. 2005b. "Cyclic behavior of steel moment-resisting connections reinforced by alternative column stiffener details II. Panel zone behavior and doubler plate detailing." *Eng. J.* 42 (4): 215–238.

Leon, R. T., J. F. Hajjar, and M. A. Gustafson. 1998. "Seismic response of composite moment-resisting connections. I: Performance." *J. Struct. Eng.* 124 (8): 868–876. https://doi.org/10.1061/(ASCE)0733-9445(1998)124:8(868).

Lignos, D. G., H. Krawinkler, and A. S. Whittaker. 2011. "Prediction and validation of sidesway collapse of two scale models of a 4-story steel moment frame." *Earthquake Eng. Struct. Dyn.* 40 (7): 807–825. https://doi.org/10.1002/eqe.1061.

Lin, K. C., K. C. Tsai, S. L. Kong, and S. H. Hsieh. 2000. "Effects of panel zone deformations on cyclic performance of welded moment connections." In *Proc., 12th World Conf. on Earthquake Engineering (WCEE)*. Auckland, New Zealand: New Zealand National Society for Earthquake Engineering.

Lu, L. W., J. M. Ricles, C. Mao, and J. W. Fisher. 2000. "Critical issues in achieving ductile behaviour of welded moment connections." *J. Constr. Steel Res.* 55 (1–3): 325–341. https://doi.org/10.1016/S0143-974X(99)00092-9.

Mahin, S., J. Malley, and R. Hamburger. 2002. "Overview of the FEMA/SAC program for reduction of earthquake hazards in steel moment frame structures." *J. Constr. Steel Res.* 58 (5–8): 511–528. https://doi.org/10.1016/S0143-974X(01)00088-8.

Maison, B. F., and M. S. Speicher. 2016. "Loading protocols for ASCE 41 backbone curves." *Earthquake Spectra* 32 (4): 2513–2532. https://doi.org/10.1193/010816EQS007EP.

Malley, J. O. 1998. "SAC steel project: Summary of Phase 1 testing investigation results." *Eng. Struct.* 20 (4–6): 300–309. https://doi.org/10.1016/S0141-0296(97)00033-3.

Mao, C., J. Ricles, L. W. Lu, and J. Fisher. 2001. "Effect of local details on ductility of welded moment connections." *J. Struct. Eng.* 127 (9): 1036–1044. https://doi.org/10.1061/(ASCE)0733-9445(2001)127:9(1036).

Miller, D. K. 2017. *Design guide 21: Welded connections—A primer for engineers*. 2nd ed. Chicago: American Institute of Steel Construction.

NIST. 2010. *Evaluation of the FEMA P-695 methodology for quantification of building seismic performance factors*. Gaithersburg, MD: NIST.

Paret, T. F. 2000. "The W1 Issue. II: UT reliability for inspection of T-joints with backing." *J. Struct. Eng.* 126 (1): 19–23. https://doi.org/10.1061/(ASCE)0733-9445(2000)126:1(19).

Popov, E. P., T.-S. Yang, and S.-P. Chang. 1998. "Design of steel MRF connections before and after 1994 Northridge earthquake." *Eng. Struct.* 20 (12): 1030–1038. https://doi.org/10.1016/S0141-0296(97)00200-9.

Rahiminia, F., and H. Namba. 2013. "Joint panel in steel moment connections, part 1: Experimental tests results." *J. Constr. Steel Res.* 89 (Oct): 272–283. https://doi.org/10.1016/j.jcsr.2013.07.002.

Reynolds, M., and C.-M. Uang. 2022. "Economical weld details and design for continuity and doubler plates in steel special moment frames." *J. Struct. Eng.* 148 (1): 04021246. https://doi.org/10.1061/(ASCE)ST.1943-541X.0003203.

Ricles, J. M., J. W. Fisher, L.-W. Lu, and E. J. Kaufmann. 2002a. "Development of improved welded moment connections for earthquake-resistant design." *J. Constr. Steel Res.* 58 (5–8): 565–604. https://doi.org/10.1016/S0143-974X(01)00095-5.

Ricles, J. M., C. Mao, L. W. Lu, and J. W. Fisher. 2003. "Ductile details for welded unreinforced moment connections subject to inelastic cyclic loading." *Eng. Struct.* 25 (5): 667–680. https://doi.org/10.1016/S0141-0296(02)00176-1.

Ricles, J. M., C. Mao, L.-W. Lu, and J. W. Fisher. 2000. *Development and evaluation of improved details for ductile welded unreinforced flange connections*. SAC Background Documents, Rep. No. SAC/BD-00/24. Sacramento, CA: SAC Joint Venture.

Ricles, J. M., C. Mao, L.-W. Lu, and J. W. Fisher. 2002b. "Inelastic cyclic testing of welded unreinforced moment connections." *J. Struct. Eng.* 128 (4): 429–440. https://doi.org/10.1061/(ASCE)0733-9445(2002)128:4(429).

Ricles, J. M., X. Zhang, L.-W. Lu, and J. W. Fisher. 2004. *Development of seismic guidelines for deep-column steel moment connections*. ATLSS Rep. No. 04-13. Bethlehem, PA: Lehigh Univ.

Shaw, S. M., K. Stillmaker, and A. M. Kanvinde. 2015. "Seismic response of partial-joint-penetration welded column splices in moment-resisting frames." *Eng. J.* 52 (2): 87–108.

Shin, S. 2017. "Experimental and analytical investigation of panel zone behavior in steel moment frames." Ph.D. dissertation, Dept. of Civil, Architectural and Environmental Engineering, Univ. of Texas at Austin.

Skiadopoulos, A. 2022. "Welded moment connections with highly dissipative panel zones for enhanced seismic performance of steel moment frames." Ph.D. thesis, Dept. of Architecture, Civil and Environmental Engineering, École Polytechnique Fédérale de Lausanne.

Skiadopoulos, A., A. Elkady, and D. G. Lignos. 2021. "Proposed panel zone model for seismic design of steel moment-resisting frames." *J. Struct. Eng.* 147 (4): 04021006. https://doi.org/10.1061/(ASCE)ST.1943-541X.0002935.

Skiadopoulos, A., and D. G. Lignos. 2021. "Development of inelastic panel zone database." *J. Struct. Eng.* 147 (4): 04721001. https://doi.org/10.1061/(ASCE)ST.1943-541X.0002957.

Skiadopoulos, A., and D. G. Lignos. 2022a. "Proposed backing bar detail in welded beam-to-column connections for seismic applications." *J. Struct. Eng.* 148 (8): 04022102. https://doi.org/10.1061/(ASCE)ST.1943-541X.0003374.

Skiadopoulos, A., and D. G. Lignos. 2022b. "Seismic demands of steel moment resisting frames with inelastic beam-to-column web panel zones." *Earthquake Eng. Struct. Dyn.* 51 (7): 1591–1609. https://doi.org/10.1002/eqe.3629.

Stillmaker, K., A. Kanvinde, and C. Galasso. 2016. "Fracture mechanics-based design of column splices with partial joint penetration welds." *J. Struct. Eng.* 142 (2): 04015115. https://doi.org/10.1061/(ASCE)ST.1943-541X.0001380.

Stojadinović, B., S. C. Goel, K.-H. Lee, A. G. Margarian, and J.-H. Choi. 2000. "Parametric tests on unreinforced steel moment connections." *J. Struct. Eng.* 126 (1): 40–49. https://doi.org/10.1061/(ASCE)0733-9445(2000)126:1(40).

Suzuki, Y., and D. G. Lignos. 2020. "Development of collapse-consistent loading protocols for experimental testing of steel columns." *Earthquake Eng. Struct. Dyn.* 49 (2): 114–131. https://doi.org/10.1002/eqe.3225.

Suzuki, Y., and D. G. Lignos. 2021. "Experimental evaluation of steel columns under seismic hazard-consistent collapse loading protocols." *J. Struct. Eng.* 147 (4): 04021020. https://doi.org/10.1061/(ASCE)ST.1943-541X.0002963.

Tremblay, R., P. Timler, M. Bruneau, and A. Filiatrault. 1995. "Performance of steel structures during the 1994 Northridge earthquake." *Can. J. Civ. Eng.* 22 (2): 338–360. https://doi.org/10.1139/l95-046.

Uang, C.-M., and M. Bruneau. 2018. "State-of-the-art review on seismic design of steel structures." *J. Struct. Eng.* 144 (4): 03118002. https://doi.org/10.1061/(ASCE)ST.1943-541X.0001973.

Whittaker, A., A. Gilani, and V. Bertero. 1998. "Evaluation of pre-Northridge steel moment-resisting frame joints." *Struct. Des. Tall Build.* 7 (4): 263–283. https://doi.org/10.1002/(SICI)1099-1794(199812)7:4<263::AID-TAL118>3.0.CO;2-B.

Zhang, X., and J. M. Ricles. 2006. "Experimental evaluation of reduced beam section connections to deep columns." *J. Struct. Eng.* 132 (3): 346–357. https://doi.org/10.1061/(ASCE)0733-9445(2006)132:3(346).